UNIVERSITY OF OKLAHOMA

GRADUATE COLLEGE

INTELLIGENT CONDITION MONITORING AND PROGNOSTIC METHODS

WITH APPLICATIONS TO DYNAMIC SEALS IN THE OIL & GAS INDUSTRY

A DISSERTATION

SUBMITTED TO THE GRADUATE FACULTY

in partial fulfillment of the requirements for the

Degree of

DOCTOR OF PHILOSOPHY

By

MADHUMITHA RAMACHANDRAN
Norman, Oklahoma
2019

INTELLIGENT CONDITION MONITORING AND PROGNOSTIC METHODS
WITH APPLICATIONS TO DYNAMIC SEALS IN THE OIL & GAS INDUSTRY

A DISSERTATION APPROVED FOR THE
SCHOOL OF INDUSTRIAL AND SYSTEMS ENGINEERING

BY THE COMMITTEE CONSISTING OF

Dr. Randa Shehab, Chair

Dr. Zahed Siddique, Co-chair

Dr. Yingtao Liu

Dr. Charles Nicholson

Dr. Kash Barker

Dr. Raghu Madhavan

I would like to dedicate this dissertation to my late maternal grandfather, V.R. Ramachandran. My grandfather was the biggest source of inspiration in my life, although he is not here to give me strength and support, I always feel his motivation and inspiration to strive to achieve my goals in life.

Acknowledgements

I wish to express my deep sense of thanks and gratitude to my advisors Drs. Randa Shehab and Zahed Siddique. Since my first day at OU, Dr. Shehab believed in me like nobody else and gave me endless support. Dr. Zahed Siddique is someone you will instantly love and never forget for his great personality. He has been very supportive and has provided me various opportunities to grow as an independent researcher, mentor and teacher. I would give him most of the credit for becoming the kind of researcher I am today. I will always be grateful for all his advice and support.

Besides my advisors, I would like to thank my committee members Drs. Charles Nicholson, Kash Barker, Raghu Madhavan and Yingtao Liu. I have thoroughly enjoyed Dr. Nicholson's Intelligent data analytics and Advanced analytics and metaheuristics course. His class has offered me an opportunity to expand my knowledge in advanced analytics and has equipped me with the knowledge and skillset to address my dissertation research. Dr. Barker is an energetic, enthusiastic, fun and funny professor. He has always inspired me by his passion for teaching. If I ever become a professor someday, I would be happy if I am half energetic as he is during his lectures. It has always been nice to meet and talk with Dr. Liu in copy room.

My special thanks to Dr. Raghu Madhavan, industry collaborator from Schlumberger for his great mentorship and guidance during his visits to OU and over phone. He has exposed me to challenges in the oil & gas industry due to components failure. My appreciation also goes to other collaborators from Schlumberger: Dr. Chunnong Wang, Paulo Soares and Sandra Roth. This dissertation would not have been possible without their intellectual contribution.

These past several years has not been an easy ride, both academically and personally. I thank almighty for providing me the strength and perseverance to pursue my dreams in each phase of my life.

Table of Content

List of Tables

List of Figures

Abstract

The capital-intensive oil & gas industry invests billions of dollars in equipment annually and it is important to keep the equipment in top operating condition to help maintain efficient process operations and improve the rate of return by predicting failures before incidents. Digitalization has taken over the world with advances in sensor technology, wireless communication and computational capabilities, however oil & gas industry has not taken full advantage of this despite being technology centric.

Dynamic seals are a vital part of reciprocating and rotary equipment such as compressor, pumps, engines, etc. and are considered most frequently failing component. Polymeric seals are increasingly complex and non-linear in behavior and have been the research of interest since 1950s. Most of the prognostic studies on seals are physics-based and requires direct estimation of different physical parameters to assess the degradation of seals, which are often difficult to obtain during operation. Another feasible approach to predict the failure is from performance related sensor data and is termed as data-driven prognostics. The offline phase of this approach is where the performance related data from the component of interest are acquired, pre-processed and artificial intelligence tools or statistical methods are used to model the degradation of a system. The developed models are then deployed online for a real-time condition monitoring. There is a lack of research on the data-driven based tools and methods for dynamic seal prognosis. The primary goal in this dissertation is to develop offline data-driven intelligent condition monitoring and prognostic methods for two types of dynamic seals used in the oil & gas industry, to avoid fatal breakdown of rotary and reciprocating equipment.

Accordingly, the interest in this dissertation lies in developing models to effectively evaluate and classify the running condition of rotary seals; assess the progression of degradation from its incipient to failure and to estimate the remaining useful life (RUL) of reciprocating seals.

First, a data-driven prognostic framework is developed to classify the running condition of rotary seals. An accelerated aging and testing procedure simulating rotary seal operation in oil field is developed to capture the behavior of seals through their cycle of operation until failure. The diagnostic capability of torque, leakage and vibration signal in differentiating the health states of rotary seals using experiments are compared. Since the key features that differentiate the health condition of rotary seals are unknown, an extensive feature extraction in time and frequency domain is carried out and a wrapper-based feature selection approach is used to select relevant features, with Multilayer Perceptron neural network utilized as classification technique. The proposed approach has shown that features extracted from torque and leakage lack a better discriminating power on its own, in classifying the running condition of seals throughout its service life. The classifier built using optimal set of features from torque and leakage collectively has resulted in a high classification accuracy when compared to random forest and logistic regression, even for the data collected at a different operating condition.

Second, a data-driven approach to predict the degradation process of reciprocating seals based on friction force signal using a hybrid Particle Swarm Optimization - Support Vector Machine is presented. There is little to no knowledge on the feature that reflects the degradation of reciprocating seals and on the application of

SVM in predicting the future running condition of polymeric components such as seals. Controlled run-to-failure experiments are designed and performed, and data collected from a dedicated experimental set-up is used to develop the proposed approach. A degradation feature with high monotonicity is used as an indicator of seal degradation. The pseudo nearest neighbor is used to determine the essential number of inputs for forecasting the future trend. The most challenging aspect of tuning parameters in SVM is framed in terms of an optimization problem aimed at minimizing the prediction error. The results indicate the effectiveness and better accuracy of the proposed approach when compared to GA-SVM and XGBoost.

Finally, a deep neural network-based approach for estimating remaining useful life of reciprocating seals, using force and leakage signals is presented. Time domain and frequency domain statistical features are extracted from the measurements. An ideal prognostic feature should be well correlated with degradation time, monotonically increasing or decreasing and robust to outliers. The identified metrics namely: monotonicity, correlation and robustness are used to evaluate the goodness of extracted features. Each of the three metric carries a relative importance in the RUL estimation and a weighted linear combination of the metrics are used to rank and select the best set of prognostic features. The redundancy in the selected features is eliminated using Kelley-Gardner-Sutcliffe penalty function-based correlation-clustering algorithm to select a representative feature from each of the clusters. Finally, RUL estimation is modeled using a deep neural network model. Run-to-failure data collected from a reciprocating set-up was used to validate this approach and the findings show that the

proposed approach can improve the accuracy of RUL prediction when compared to PSO-SVM and XGBoost regression.

This research has important contribution and implications to rotary and reciprocating seal domain in utilizing sensors along with machine learning algorithms in assessing the health state and prognosis of seals without any direct measurements. This research has paved the way to move from a traditional fail-and-fix to predict-and-prevent approach in maintenance of seals. The findings of this research are foundational for developing an online degradation assessment platform which can remotely monitor the performance degradation of seals and provide action recommendations on maintenance decisions. This would be of great interest to customers and oil field operators to improve equipment utilization, control maintenance cost by enabling just-in-time maintenance and increase rate of return on equipment by predicting failures before incidents.

Chapter 1: Introduction

1.1 Background

In oil & gas industry, rotary and reciprocating equipment such as compressors, pumps, turbines and engines are required to have high reliability and long lifetime to meet the demand from oil field. Since oil & gas requires large capital-investments, it is important to keep the equipment in top operating condition to help maintain efficient process operations.

A seal is a torus or doughnut- shaped object widely used to retain fluid inside while preventing the passage of mud, dirt, dust, water, etc. Seals operate by holding pressure against a counter surface to close the gap between two components in contact. Seals are generally made of soft and compliant material such as elastomer which displays high flexibility and elasticity, to conform to the contacting surface. They can also be made in Polytetrafluoroethylene (PTFE), other plastic materials, and metals (hollow and solid). Based on the nature of their application, they are classified into static or dynamic seals. Dynamic seals such as rotary and reciprocating seals act as a barrier between the moving parts in applications involving rotating shafts and moving pistons.

Dynamic seals are a vital part of rotary and reciprocating equipment and are considered most frequently failing component. Although it is relatively less expensive, when compared to the overall machinery, failure of seals could result in expensive downtime, contamination and potential danger to human health and safety. For example, when a seal in rotary machinery fail, the contaminants from outside enter the cavity which will affect the performance of bearing that support the shaft in operating

conditions. The performance degradation in bearing will result in excessive shaft run-out due to increased vibration which will be transferred to other components in the machinery resulting in costly down.

In many applications, replacing a seal after failure can be extremely expensive, while replacing the seal early may lead to lower life utilization. Therefore, assessing the early degradation of rotary seals is important for better maintenance decision making. In existing literature, the degradation of seal is characterized only by measuring the physical properties, as an example degradation of seals under the effect of temperature, hydraulic oil and compressive stress are characterized by measuring the chemical and mechanical properties of seal materials [1]. In another study, the degradation of seals exposed to air at different temperature under the compressed state are characterized using mechanical properties such as weight loss, tensile strength and elongation at break [2]. Tensile mechanical properties, volume swell, compression set and chemical properties are measured to estimate the degradation of seals in hydraulic oil at different temperatures and immersion times [3].

In recent times, prognostics have gained importance in oil & gas industry because of the need to increase the system utilization, safety and reliability. Prognostics is the use of predictive maintenance practices and tools to assess the performance degradation of systems and estimate the remaining useful life of equipment. The key aspects of prognostics include improving equipment availability by minimizing equipment downtime, preventing catastrophic failure, improving rate of return on equipment by predicting failures before incidents, reducing operational risk of critical equipment and enabling appropriate timely and maintenance decisions. Failure prognostics is commonly

classified into model based and data-driven based prognostic methods [4]. Model-based prognostic (physics based/ behavioral model) is a set of algebraic and differential equations to represent the behavior (degradation) of systems under many operating conditions using laws of physics. In a study by Guo et al., constant temperature oil bath is used to age seals to measure the change in material properties and seal performance [5]. The performance of seals characterized by leakage and friction torque are computed through numerical simulations using a mixed Elastohydrodynamic (EHL) model. Similarly, the effect of heat and oxygen on the change in material properties and performance of seals is investigated using an air oven aging test and the performance characteristic are computed using a mixed EHL model [6]. Data-driven prognostics methods use artificial intelligence tools or statistical methods to model the degradation of a system and to predict future health without the knowledge of physics associated with the system. Literature shows the success of data-driven prognostics approach for monitoring the health condition of bearings in rotating machinery through accelerometer and vibration transmitters [7-9]. One of the main reasons for the deterioration of bearings is the failure of seals and hence it is important to develop a prognostics approach to monitor the health of seals.

Dynamic seals has been the research of interest since 1950s and many researchers have investigated physics-based prognostics methods which require estimation of material, mechanical and seal properties [5, 6, 10]. During operation, it is extremely difficult for users to monitor the change in physical parameters of seal to assess their performance. With advances in sensor technology, wireless communication

and computational capabilities, there is a radical shift in the way to monitor the health of mechanical equipment and its components.

1.2 Aim and Goals

Polymeric seals are increasingly complex and non-linear in behavior. Most of the prognostic studies on seals are physics-based approach where they model the life based on mechanical, material and seal measurements which are often difficult to obtain during operation. The primary aim of this dissertation is to introduce data-driven intelligent condition monitoring and prognostic approaches for two types of dynamic seals used in oil & gas industry, to avoid fatal breakdown of equipment. To achieve this, the first step is to acquire performance data from the component of interest. For the below mentioned reasons, most data used to validate the prognostic models are always acquired from accelerated degradation test set-ups instead of historic performance data acquired from industrial assets:

1. Degradation from nominal to failure might take several months or years and it would be time consuming and expensive to capture the degradation process

2. In industrial settings, machineries are maintained periodically even before they breakdown and acquiring run-to-failure data from such instances would be impossible

3. There is little to no knowledge on the right set of sensors that are specific in capturing seal performance degradation

Accordingly, the interest in this research is to *develop models to evaluate the health state of seals, assess the progression of seals degradation from its incipient to failure*

and to estimate the remaining useful life of seals. To achieve this goal, the following research tasks has been performed:

1. To develop a testing procedure that would capture the behavior of seals through their cycle of operation until failure

2. To investigate the diagnostic capability of different sensor signals in differentiating the health state of seals

3. To identify the methods to transforms raw sensor/monitoring data into meaningful and most responsive features

4. To identify metrics to evaluate the goodness of extracted features for accurate prognosis of dynamic seals

5. To choose modeling methods and algorithms that improve the accuracy of predicting seal's health state, degradation and remaining useful life.

This research has important contribution and implications to rotary and reciprocating seal domain in utilizing sensors along with machine learning algorithms to assess the health state and prognosis of seals without any direct measurements. The findings of this research are foundational for developing an online degradation assessment which can remotely monitor the performance degradation of seals and provide action recommendations on maintenance decisions. This would be of great interest to oil field operators to improve equipment utilization, control maintenance cost by enabling just-in-time maintenance, and increase rate of return on equipment by predicting failures before incidents.

1.3 Organization of Dissertation

The remaining dissertation is organized as follows. In chapter 2, a data-driven prognostic framework is developed to classify the health state/ condition of rotary seals. An accelerated aging and testing procedure simulating rotary seal operation in oil field is developed to capture the behavior of seals through their cycle of operation until failure. The diagnostic capability of torque, leakage and vibration signal in differentiating the health states of rotary seals using experiments are compared. Since the key features that differentiate the health condition of rotary seals are unknown, an extensive feature extraction in time and frequency domain is carried out and a wrapper-based feature selection approach is used to select relevant features, with Multilayer Perceptron neural network utilized as classification technique. This approach is validated by testing the approach on an unseen data collected at different temperature and comparing the performance of MLP with random forest and logistic regression.

In chapter 3, a data-driven approach to predict the degradation process of reciprocating seals based on friction force signal using a hybrid Particle Swarm Optimization - Support Vector Machine is developed. There is little to no knowledge on the feature that reflects the degradation of reciprocating seals and on the application of SVM in predicting the future running condition of polymeric components such as seals. Controlled run-to-failure experiments are designed and performed, and data collected from a dedicated experimental set-up is used to develop the proposed approach. A degradation feature with high monotonicity is used as an indicator of seal degradation. Phase space reconstruction is used to determine the essential number of inputs for forecasting the future trend. The most challenging aspect of tuning parameters in SVM

is framed in terms of an optimization problem aimed at minimizing the prediction error. Finally validated the proposed approach by comparing the performance of PSO-SVM with GA-SVM and XGBoost regression.

In chapter 4, a deep neural network-based approach for estimating remaining useful life of reciprocating seals, using force and leakage signals is presented. Time domain and frequency domain statistical features are extracted from the measurements. An ideal prognostic feature should be well correlated with degradation time, monotonically increasing or decreasing and robust to outliers and therefore after feature extraction, features are selected based on three important metrics namely: monotonicity, correlation and robustness, which makes it easier to model the trends in features overtime that lead to better RUL estimation. Each of the three metric carries a relative importance in the RUL estimation and a weighted linear combination of the metrics are used to rank and select the best set of prognostic features. The redundancy in the selected features is eliminated using KGS penalty function-based correlation-clustering algorithm to select a representative feature from each of the clusters. Finally, RUL estimation is modeled using a deep neural network model. The proposed approach is validated by comparing the performance of DNN with PSO-SVM and XGBoost regression.

Finally, in chapter 5, a summary of this study conclusions, implications and future work is presented.

Chapter 2: Degradation Assessment of Rotary Seals Using Multi-Sensor-Based Neural Network Model

2.1 Introduction

2.1.1 Rotary Seal

Rotating machinery is the most widely used mechanical equipment in oil and gas industry and keeping rotary drilling equipment in top operating condition is a key activity that helps maintain efficient process operations in oil and gas plants. Rotary machinery is a complex system consisting of hydraulic oil, radial lip seals, bearings, shaft, gear and sealing groove. The radial lip seal failure is one of the foremost causes of breakdown in rotary machinery, and such failure can be catastrophic, resulting in costly downtime and large expenses.

The rotary lip seal consists of an elastomeric lip and the shaft. The rotary lip seal is mounted on a rotary shaft with an interference fit. Figure 1 illustrates the cross-sectional area of an elastomeric lip located on the rotary shaft. An elastomeric sealing lip has a sealing edge, which is pressed against the counterface surface of the shaft, creating the most important functional area of a rotary seal.
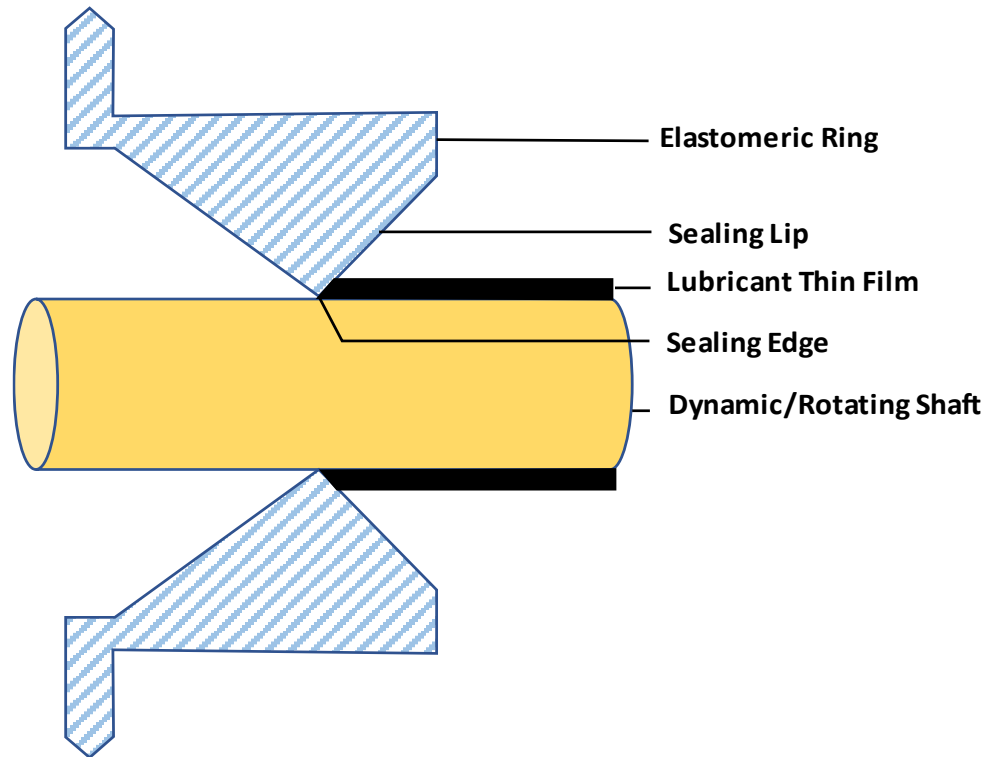
Figure 1: Cross-Section of an Elastomeric Lip on a Rotary Shaft

The lip seals can be spring less or spring-loaded. The primary reason of having a spring is to provide a consistent load on the shaft throughout the seal life. It also aids in keeping the lip in contact with the shaft at higher shaft speeds and also to overcome the compression set and wear on lip material. There are several types of spring that are used to energize the lip. Garter or wound spring, cantilever, canted-coil and helical coil are some of the most commonly used springs. Each type has a different spring characteristic based on the displacement/load ratio.

2.1.1 Mechanisms Related to Performance of Rotary Seal

The performance of rotary seals on a rotating shaft are explained through three mechanisms: the lubrication, sealing and pumping. Lubrication mechanism creates a thin lubricant film between the seal lip and shaft which lubricates the seal lip-shaft interface [11]. This film between the lip and shaft helps in the reduction of wear, friction and leakage. Sealing is the primary function of seals which aid in the retention of lubricant inside and contaminants outside the system [12]. The pumping mechanism is responsible for pumping the fluid from the air side towards the lubricant side to compensate for any leakage [13].

In 1957, Jagger demonstrated an experiment which showed a continuous fluid film separating the lip from shaft under typical operating conditions [11]. This film between the lip and shaft helps in the reduction of wear, friction and leakage. He observed the formation of a lubricant meniscus in the airside to be responsible for sealing mechanism and the retention of oil inside the film is due to surface tension of the oil.

Later investigators demonstrated that sealing mechanism that prevents fluid within lubricating film from leaking out of the seal is related to the phenomena of reverse pumping [12-16]. They showed that a non-leaking successful seal is able to pump the liquid from the air side back to the lubricant side when the air side is flooded with liquid. This counteracts the pressure-induced leakage through the seal.

Experimental studies have showed that the surface roughness of the seal is responsible for sealing mechanism[17-19]. This is expected as the asperity height is of same order as the lubricant film thickness and would definitely have an effect on the flow

field within the film. Horve, 1991 found that the seal with a large number of asperities on the lip surface will have high pumping when compared to the seals with a few asperities [14].

In 1969, Kuzma showed that asperities on the lip surface in the sealing zone is responsible for sealing and load support mechanism [20]. According to this study, rotary lip seals have asperities or microundulations on the sealing surface and under dynamic conditions the shear forces generated within the fluid film deforms the lip surface and the asperities. The deformed asperities act as viscous shear pump which produces a net pumping when the fluid is dragged over them by the rotating shaft.

Later studies gave a detailed description of viscous shear pump mechanism for a seal with microundulations on the sealing surface [13, 21] Under dynamic conditions, due to shear deformation of the elastomeric seals in the circumferential direction, the asperities are deformed into vane like shapes which pumps liquid from the airside to the liquid side. A successful non-leaking seal will have the maximum shear deformation of the lip surface closer to the liquid side and will be pumping fluid from air-side toward the liquid-side. This is the basis of viscous pump mechanism and has been verified experimentally by several investigators.

Gabelli, 1989 and Gabelli and Poll, 1992 developed the first numerical model of a lip seal to investigate the load support mechanism [22, 23]. Asperities were represented as a uniform distribution using two-dimensional sinusoid and finite difference techniques were used to solve the Reynolds equation to predict the pressure distribution in the lubricating film and the results demonstrated the hydrodynamic effects produced by the asperities to maintain the integrity of the lubricating film.

Salant, 1992 put forward the hydrodynamic model of the lip surface to study the reverse pumping mechanism [24]. The results showed that sufficiently high reverse pumping rates are generated to prevent leakage through the seal.

2.1.3 Physics-Based Rotary Seal Prognostics Models

In the following years, many literatures have been published on elastohydrodynamic model to predict the seal performance characteristics. This model considers hydrodynamic analysis of the flow in the lubricant film and the elastic deformation of the lip. In 1994 elastohydrodynamic model was developed to study the surface of the lip with microundulations [25]. The model showed that the elevated pressure within the film is sufficiently high to lift the lip off the shaft to maintain the film in addition to the high reverse pumping rates generated to prevent leakage through the seal. In 1995, the elastohydrodynamic model has been expanded to study the lip with microasperities and similar results were observed as seals with microundulations except for the lower reverse pumping rates [26]. In [27], a mixed elastohydrodynamic model was developed to accurately predict the seal performance characteristics over the range of shaft speeds. This model takes into account the contact mechanics between the elastic lip and the shaft and considers both the shear and normal deformations of the elastic surface unlike the elastohydrodynamic model which neglects the normal deformation of the elastic surface. The inclusions made in this model are necessary as they influence the reverse pumping action.

In the following year, a mixed elastohydrodynamic model was developed for the seal with quasi-random sealing surface [28]. In the previous numerical models, asperities were represented by regular periodic structures but the actual distribution on the seals are

found to be random [23] Therefore Salant and Shi incorporated the quasi-random surface into the mixed elastohydrodynamic model to study the sealing and local support mechanism of the seal.

2.1.4 Modes of Rotary Seal Failure

There are different factors responsible for a typical seal failure including incompatibility between the seal material and the fluid it is to seal, improper seal size, improper use or installation, improper gland design, not enough seal lubrication, abrasion, compression set, and chemical and thermal degradation [29]. Like any other material, the biggest problem with elastomers is that it is more prone to aging under the influence of heat, UV radiation, oxygen, ozone, extended exposure to oil, dust, mud, etc. In rotary equipment, elastomeric seals are exposed to harsh environment including high temperature, contaminants such as dust, mud, dirt, etc. [5]. The aging of elastomeric material changes the lip surface microtopography, the sealing lip profile, and the interface between the seal and shaft which causes the leakage of fluid. The change in lip surface microtopography directly affects the pumping action while the change in sealing lip profile and interference also affects the pumping action by changing the contact temperature and contact characteristics of the seal lip-shaft interface. An extended exposure of rotary seals to such an environment will gradually reduce the elastic modulus and hardness of seals [30]. This will lower the interference between shaft and seals, leading to excessive leakage and lower friction torque. Hence friction torque and leakage are considered good indicators of seal degradation.

2.1.5 Multi-Sensor-Based Rotary Seal Prognostics

Replacing a seal after its failure can be extremely expensive while replacing the

seal before its failure may lead to lower life utilization. Thus, evaluating seal

degradation and severity estimation are very important for making maintenance

decision. In the available literature, the degradation of seal is characterized only by

measuring the physical properties. Although literature review shows the development of

numerical models to predict the behavior (degradation) of seals, these models are based

on the laws of physics governing them. In real world, it is quite not possible for users to

keep track of the change in material and mechanical properties of seals to assess the

performance of seals. The performance indicators (friction torque and leakage) of rotary

seals itself usually change with the process of degradation which can be measured using

sophisticated sensors and computerized components. The data collected from the

sensors can be remotely monitored and analyzed to know about the seals' running

conditions. The innovative tools and methods to evaluate early seal degradation would

be of great interest to users, for maintenance decision making and there is a pressing

need for this research in rotary seal domain [10, 31]. Thus, we propose a data-driven

based degradation assessment approach to study the performance of seals with aging

time.

The first step in assessing the performance degradation of rotary seal is to

extract and select the meaningful and most relevant features from raw performance

signal [8]. Extracting meaningful and sensitive features from raw signal is a challenging

task of degradation assessment. There are different feature extraction techniques: time

domain, frequency domain and time-frequency domain. Various statistical time domain

features can be extracted from the raw time series data. The statistical time domain features show the change in amplitude, energy and distribution of a signal overtime [8]. Mean, root mean square (RMS), standard deviation, skewness and kurtosis are the commonly used time domain features. In recent times, non-dimensional features such as margin factor, shape factor, crest factor and impulse factor are also used to assess the performance degradation [32]. For signal processing in frequency domain, Fast Fourier Transform (FFT) is often applied to transform a time series into frequency spectrum to analyze the signal characteristics in the frequency domain. The statistical frequency domain features show the change in amplitude, energy and the position change of main frequencies which are dominant in the frequency domain [8].

Estimating the relevance of the feature is an important step in the degradation assessment. Inaccurate and less sensitive features reduce the accuracy of predicting the seals actual running condition. Domain experts can select the sensible set of features, but this can be a difficult, tedious and time-consuming task, especially when the dataset is big, and the behavior of the data is not well known.
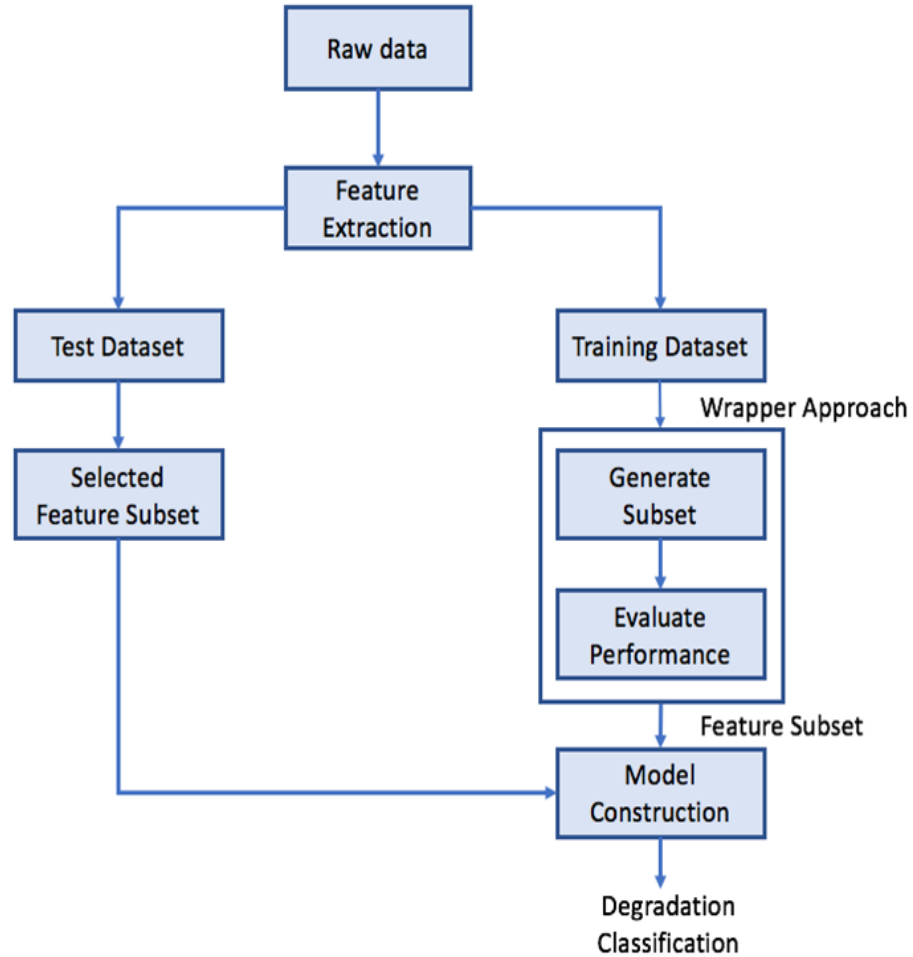
Figure 2: Flowchart Showing the Proposed Approach

Finally, a classification technique (classifier) is used to build a classification

model using the selected features to estimate the health condition of rotary seals. The

technique employs a learning algorithm to build a model that best fits the relationship

between the selected features and the class label (health state of seals) associated with

the data. Once the model is built, it is then used to predict the class labels of new,

unknown data. Some common classifiers include decision tree classifiers [33], neural

networks [7, 34] and support vector machines [8]. Multilayer Perceptron (MLP) is a

class of feed-forward artificial neural network widely used because of universal

function approximation and non-linear classification. MLP has shown to be a powerful classifier in classifying the health condition of shaving tool [34], classifying faults in induction motor [35], gas turbine bearings [36], rotary machine elements [7] etc. Owing to its interesting characteristics and successful classification in other domains, MLP is employed in this study to build a classification model that can predict the running condition of rotary seals. In the last 10 years, different combinations of feature extraction, feature selection and classification techniques are implemented in various domains such as bearings [7, 8], diesel engines [37], electric motors [35, 38], shaving tool [34, 39] etc. to assess their performance degradation.

For the first time, data-driven prognostics approach is used to study the performance degradation of rotary seals. Figure 2 shows the flowchart of proposed approach presented in this study. The remainder of this chapter is structured as follows: The methods and techniques used for data collection, pre-processing, feature extraction, selection and classification are explained in detail in methodology section; results of our approach are discussed in results and discussion section and finally, study conclusions are summarized.
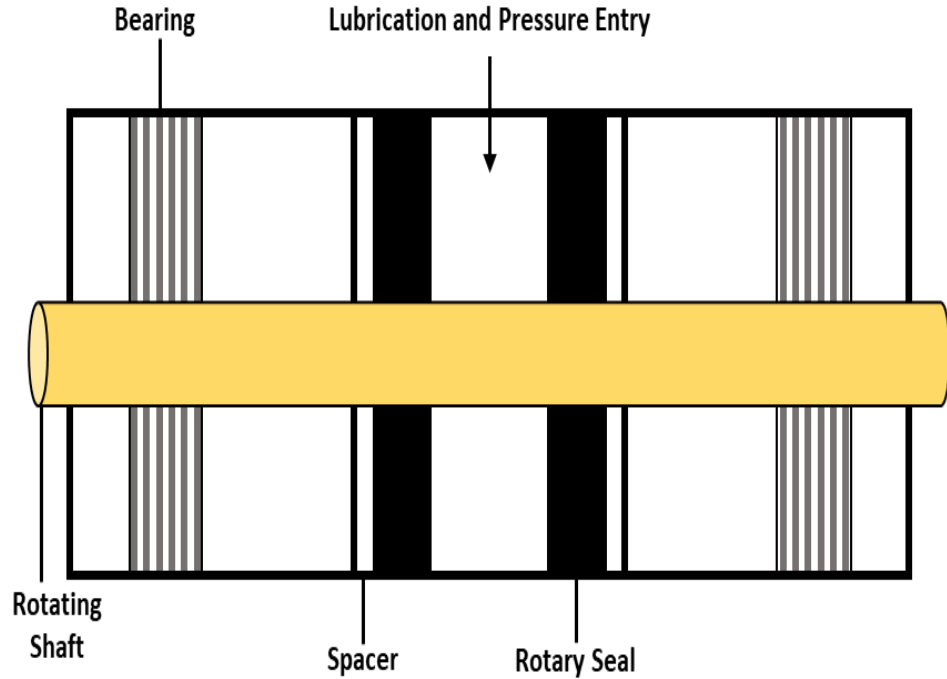
Figure 3: Illustration of Seal Housing with Seals installed on Rotary Shaft

2.2 Methodology

2.2.1 Test Set-up

An experimental test set-up is designed and manufactured to capture the performance of rotary seals in terms of torque (inch-pound) and fluid leakage (milliliter). Seals made of fluoroelastomer (FKM) with a nominal inside diameter of 10 mm is tested in this study. Two identically sized seals are placed in the seal housing at opposite sides of the lubrication inlet. The seals are assembled onto a rotating shaft along with bearings and rotary shaft and placed in a seal housing. Figure 3 shows the cross-sectional view of seal housing. The bearings aid in the rotation of shaft and spacers keep the seals in place while the system is under pressure. The seal housing along with the rotary shaft is then inserted into a seal cavity and retained by end-caps. The seal cavity is designed in the way it can house four heating rods, which is used to heat the seal cavity. The shaft is connected

to the torque meter via a coupling and the motor is connected to the torque meter via another coupling. There is a fluid storage tank below the seal cavity from where the fluid is pumped to the fluid reservoir using a vacuum pump. A vacuum pump connected to the top of fluid reservoir is used to fill the set-up with fluid and to ensure no air remains in the test set-up. The above-mentioned main components of the test set-up can be seen in Figure 4.
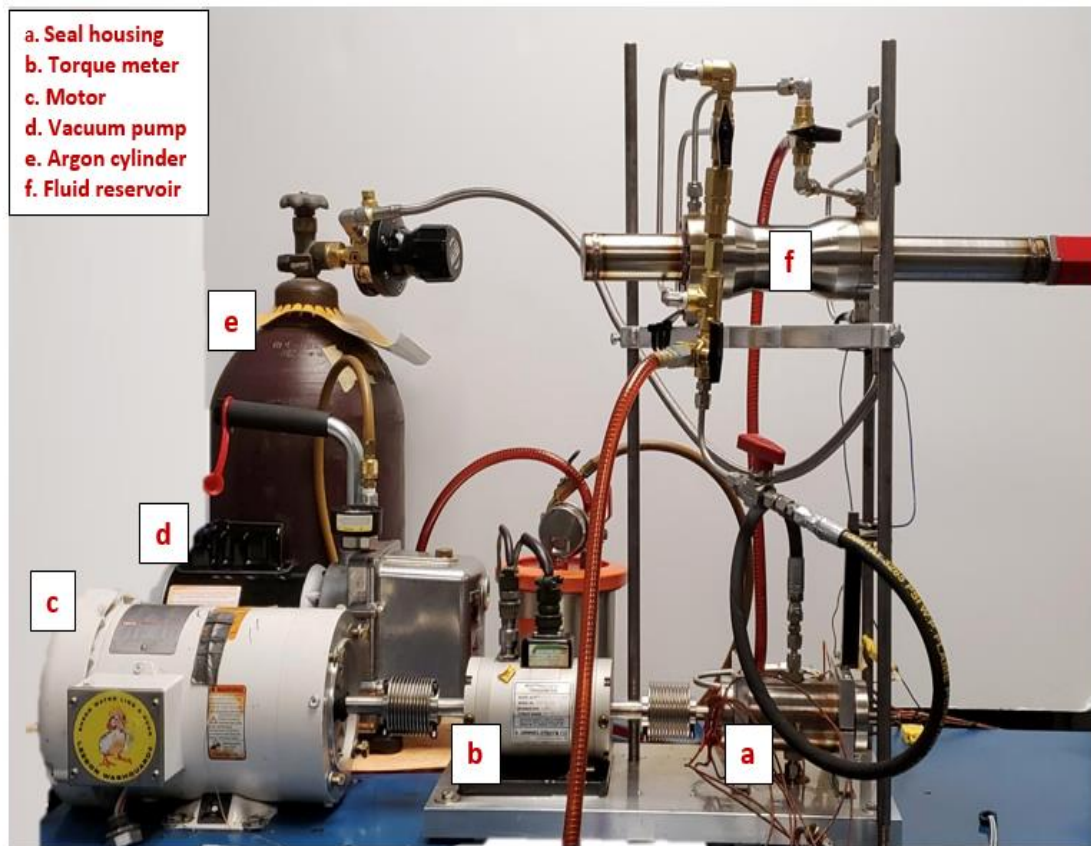
Figure 4: Experimental Test Set-up to Test Rotary Seals

The layout of the test set-up along with the flow of fluid and pressure through the system is illustrated in Figure 5. A Linear Variable Differential Transformer (LVDT) sensor located in the fluid reservoir is used to measure the fluid leakage. The pipeline in blue (in Figure 5) shows the movement of fluid when the system is being filled and the

red pipeline shows the movement of fluid while the system is leaking or being drained. The system is pressurized using an argon cylinder that is connected to the fluid reservoir. Pressure is monitored with pressure transducers to ensure the operating pressure criteria is met.
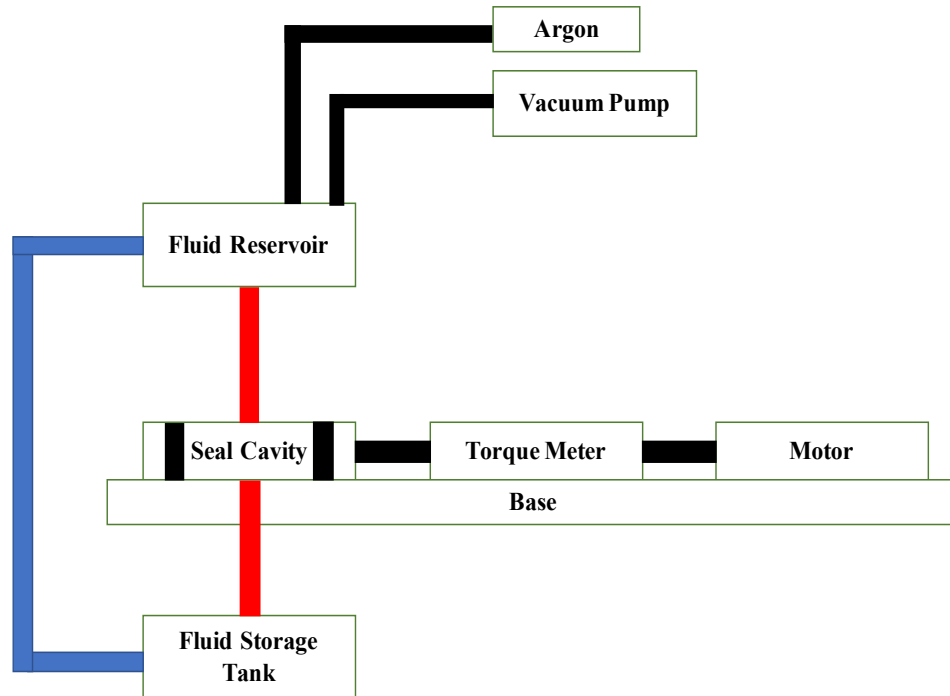
Figure 5: Schematic of the Set-up to Test Rotary Seals

2.2.2 Aging Procedure

To study the performance degradation of rotary seals throughout its lifetime, seals are aged in an aggressive fluid found in the oil field which mainly consists of amines, acids, silica and barite. An aging fixture which is a replicate of seal housing is designed and manufactured to house the seals and rotary shaft. Aging fixture along with seals and rotary shaft are placed in an aging cylinder containing aging fluid which is then placed in an oven pre-heated to 175°C. Figure 6 shows the cross section of aging cylinder with

aging fixture and aging fluid. Seals are tested in the test platform after aging right from their healthy/nominal state.
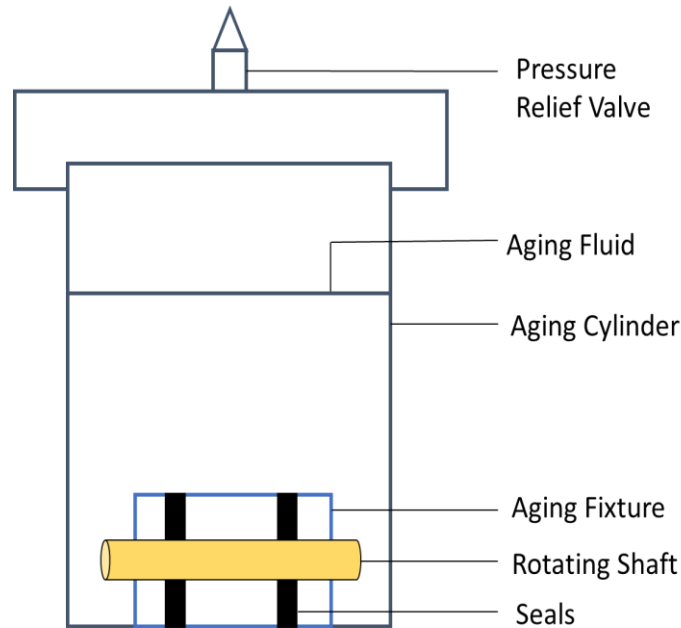
Figure 6: Cross-Section of Seal Aging Cylinder with Aggressive Aging Fluid and Aging Fixture

2.2.3 Data Collection Procedure

A National Instruments data acquisition unit is used to collect data at the rate of 10 KHz with 1280 data points sampled per second. The seals are tested at 1500 RPM, 175°C (because the maximum operating temperature of FKM is 200°C) and 100 PSI (so as to replicate the differential pressure located underground) The motor and the heating rods are controlled in real-time using a custom LabVIEW code with the torque, pressure, vibration and leak monitored continuously. LabVIEW records and stores them in TDMS format. Once the assembly is completed, the motor is turned on for 5 seconds and then turned off for the next 5 minutes to maintain a constant dwell time (the period that the

system is idle). Five-minute dwell is standard for each run as the difference in dwell time affects the total torque required to start the test set-up. After 5 minutes of dwell time, the motor is turned on again. This run is automated using a custom LabVIEW code where 6 seconds of data are collected every 5 minutes. In total, 72 seconds of data are collected in a 60 minutes run. Figure 7 shows the timeline of data collection procedure. This procedure is designed in a way to eliminate the problem of data storage.
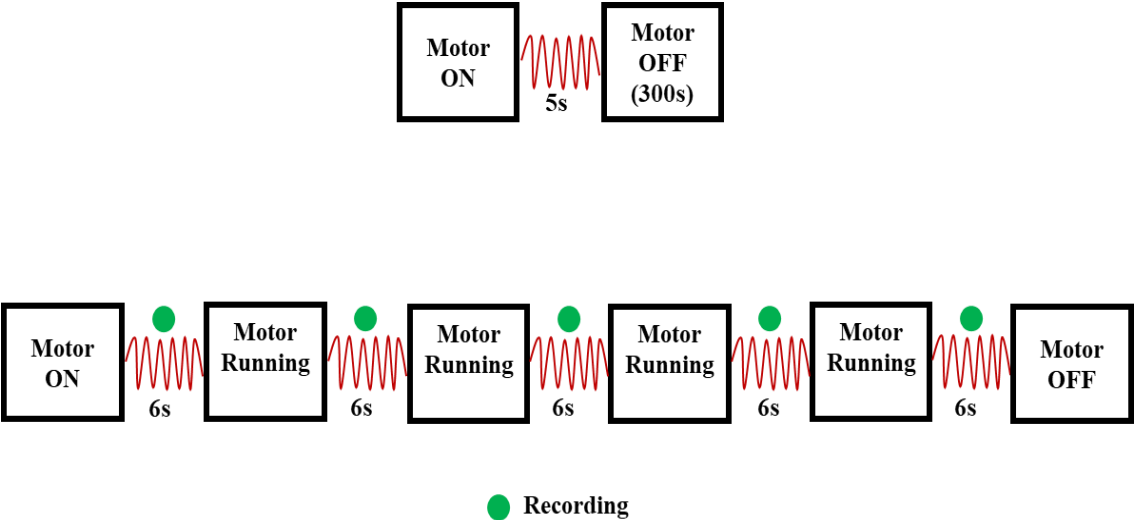
Figure 7: Data Collection Procedure: Dwell Time Procedure (Top) and Timeline of Data Collection (Bottom)

2.2.4 Data Preparation

Torque signal gives information on breakout and steady state torque. Breakout torque is the total torque required to initiate relative rotation between a rotary shaft and seals, and steady state torque is the torque while the system maintains a constant speed. Figure 2.8 illustrates the breakout and steady state torque in the signal. The signal is pre-processed using a 6th order Butterworth filter with a cutoff frequency of 7 Hz to reduce the noise in the signal.
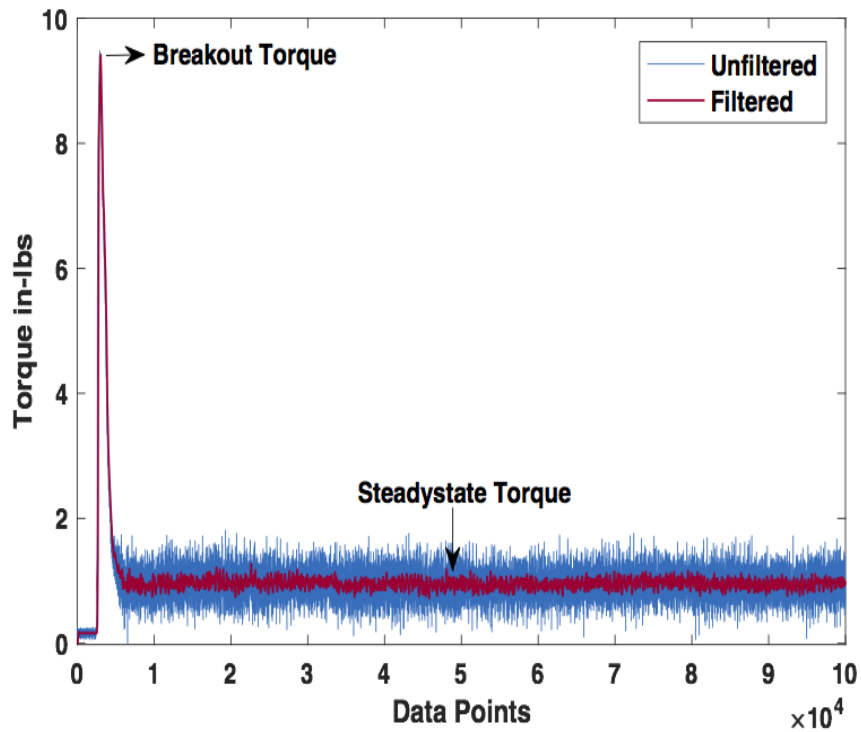
Figure 8: Illustration of Filtered Torque Signal Using Butterworth Filter

In Figure 8, the red line shows the filtered torque while the blue line shows the unfiltered torque. It is clearly seen that the filter applied can capture the critical breakout and steady state data points in the raw torque signal. Leakage signal is pre-processed using a 10th order median filter, a kind of smoothing technique to remove the narrow spikes in the signal that are uncharacteristic of the signal. Figure 9 shows the filtered leakage signal using median filter. In Figure 9, the blue line shows the unfiltered signal with narrow spikes which has been removed using median filter and the red line shows the filtered leak signal.
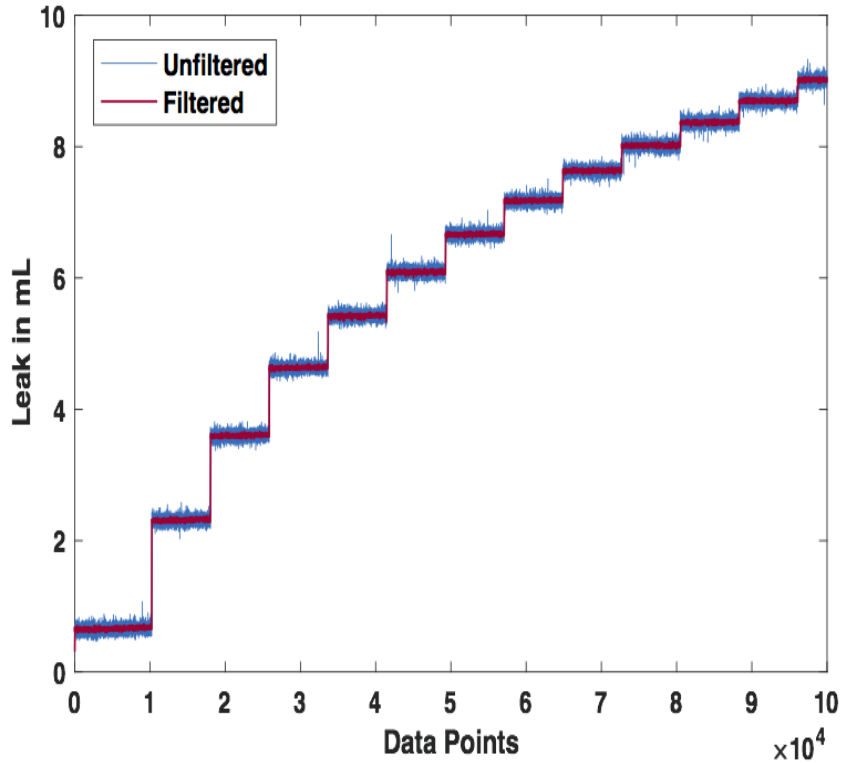
Figure 9: Illustration of Filtered Leakage Signal Using Median Filter

2.2.5 Feature Extraction Methods

In this study, time domain features are extracted from the raw friction torque obtained using test set-up. For time series x with a length of N, 11 different statistical features are calculated from raw torque signal. The most common time domain feature extraction method is to calculate the descriptive statistics, which measures the energy, amplitude and distribution of a signal over time [38, 40]. Table 2.1 shows the equation of time domain features that are used in this study and definitions can be found in [41]. Features f_1, f_2, f_3 & f_7 show the change in amplitude and energy of a signal over time while f_4- f_6 & f_8- f_{11} show the change in distribution of a signal

Table 1: Statistical Time Domain Feature Equations

Feature	Formula	Feature	Formula
Mean	$f_1 = \dfrac{1}{N}\sum_{i=1}^{N} x_i$	Squared Mean Rooted Absolute Amplitude (SRA)	$f_7 = \left[\dfrac{1}{N}\sum_{i=1}^{N} \sqrt{|x_i|}\right]^2$
Root Mean Square (RMS)	$f_2 = \sqrt{\dfrac{1}{N}\sum_{i=1}^{N} |x_i|^2}$	Margin Factor	$f_8 = \dfrac{x_{rms}}{f_7}$
Maximum	$f_3 = max\{|x_i|\}$	Standard Deviation	$f_9 = \sqrt{\dfrac{1}{N-1}\sum_{i=1}^{N} (x_i - \bar{x})^2}$
Impulse Factor	$f_4 = \dfrac{x_{max}}{|\bar{x}|}$	Kurtosis	$f_{10} = \dfrac{\sum_{i=1}^{N}(x_i - \bar{x})^4}{(N-1)f_9^4}$
Crest Factor	$f_5 = \dfrac{x_{max}}{x_{rms}}$	Skewness	$f_{11} = \dfrac{1}{N}\sum_{i=1}^{N} \dfrac{(x_i - \bar{x})^3}{f_9^3}$
Shape Factor	$f_6 = \dfrac{x_{rms}}{|\bar{x}|}$		

overtime with aging. Since leakage signals are dynamic in nature, i.e. leakage increases with time, frequency domain features are used to extract information from leakage signals. Table 1 shows the common statistical features in frequency domain. First, FFT is applied to the raw torque data to transform time domain into its corresponding frequency coefficients. Then, absolute values are calculated from the complex frequency coefficients. Features listed in Table 2 are extracted using the absolute values which represent the strength of corresponding frequency coefficients in the time domain data. In Table 2, $s(i)$ is a spectrum for $i= 1, 2, 3, ..., I$ where I is the number of spectrum lines and f_i is the frequency value of the ith spectrum line. Feature F1 the

mean frequency indicates the leak energy in frequency domain; features F2-F4, F6-F7 and F11-F12 shows the convergence of the spectrum power and features F5 and F8-F10 represents the position change of the main frequencies. In addition to the frequency domain features, information on the difference/change in fluid volume every five minutes (in 60 minutes run) is extracted from each run to see how the fluid leakage varies with aging time.

Table 2: Statistical Frequency Domain Feature Equations

Feature	Formula	Feature	Formula
F1	$\dfrac{\sum_{i=1}^{N} s(i)}{N}$	F7	$\sqrt{\dfrac{\sum_{i=1}^{N} f_i^2 s(i)}{\sum_{i=1}^{N} s(i)}}$
F2	$\dfrac{\sum_{i=1}^{N}(s(i) - f_1)^2}{N-1}$	F8	$\sqrt{\dfrac{\sum_{i=1}^{N} f_i^4 s(i)}{\sum_{i=1}^{N} f_i^2 s(i)}}$
F3	$\dfrac{\sum_{i=1}^{N}(s(i) - f_1)^3}{N\left(\sqrt{f_2}\right)^3}$	F9	$\dfrac{\sum_{i=1}^{N} f_i^2 s(i)}{\sqrt{\sum_{i=1}^{N} s(i) \sum_{i=1}^{N} f_i^4 s(i)}}$
F4	$\dfrac{\sum_{i=1}^{N}(s(i) - f_1)^4}{N f_2^2}$	F10	$\dfrac{f_6}{f_5}$
F5	$\dfrac{\sum_{i=1}^{N} f_i s(i)}{\sum_{i=1}^{N} s(i)}$	F11	$\dfrac{\sum_{i=1}^{N}(f_i - f_5)^3 s(i)}{N f_6^3}$
F6	$\sqrt{\dfrac{\sum_{i=1}^{N}(f_i - f_5)^2 s(i)}{N}}$	F12	$\dfrac{\sum_{i=1}^{N}(f_i - f_5)^{\frac{1}{2}} s(i)}{N f_6}$

Inaccurate and less sensitive features reduce the accuracy of predicting the seals actual running condition [9]. A wrapper based Recursive Feature Elimination (RFE) is an iterative backward selection method which uses a classification model as a part of evaluation function to produce a feature subset ranking as opposed to feature ranking. It begins by fitting the model to all the features and at each iteration, it eliminates the feature with least importance [42]. Random forest is used to train the model. For each tree, random forest estimates variable importance by recording the out-of-bag prediction accuracy for every predictor variable permutation. At each iteration, the difference between the model accuracy of prior and the permuted model is averaged over all trees and normalized by the standard error. Ten-fold cross-validation is used to provide a more robust estimate of feature selection.
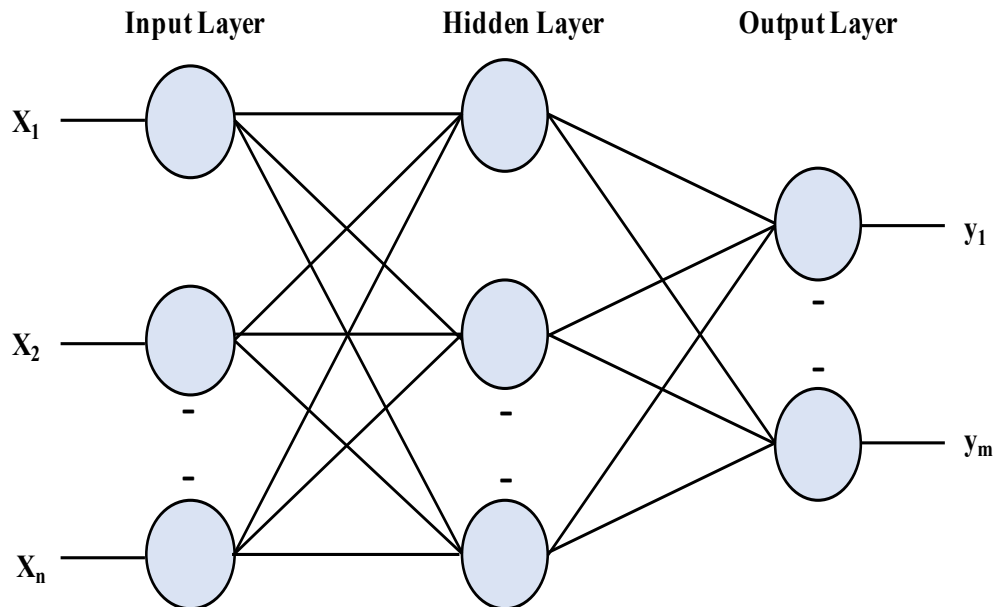
Figure 10: Three-layer Architecture of Multilayer Perceptron Model

2.2.7 Multilayer Perceptron Neural Network

Multilayer Perceptron (MLP) is a class of feed-forward artificial neural network widely used because of universal function approximation and non-linear classification. Owing to its interesting characteristics and successful classification in other domains [7, 34-36], MLP has a three-layer architecture: an input layer that represents the input value, one or more hidden layers that define the activation function and an output layer that represents the output value. Figure 10 shows the three-layer architecture of the MLP network. MLP neural network consists of multiple, non-linear processing units called as neurons that are interconnected through weights. The number of neurons in each layer is problem specific. The number of neurons in the input layer is equal to the number of features in the model; the number of neurons in the hidden layer is the mean of neurons in the input and output layers and output layer has one neuron per class label in the model. Neurons in the hidden layer has a sigmoid activation function which utilizes backpropagation and training algorithm of gradient descent. This work in two stages. First, in feed-forward propagation, output of one layer is propagated to the next layer using current weights and the activation function of that layer. When the output of the neural network is obtained, the error is calculated by comparing the desired output with the forward propagated output. Second, in the backpropagtion, the error signal is propagated backwards from output layer to the input layer, through hidden layers, updating the weights of output layer before updating the weights of hidden and input layers. Thus, the goal of backpropagtion through gradient descent algorithm is to optimize the value of weights through an iterative process to minimize the performance function Mean Square Error (MSE). Learning rate is the amount the weights are updated i.e. it

28

controls the change in weights to control for the error. Momentum provides information about the weight change in previous epoch (one forward and backward pass of all training samples) and is used to slow down the process when the system is close to local minimum.

2.3 Results and Discussion

Rotary seals were aged at an elevated temperature in an aggressive aging fluid consisting of amines and acids to study the performance of seals throughout its lifetime. Exposure of seals to harsh environments including high temperature and chemical contaminants such as amines and acids gradually reduced the elastic modulus and hardness of seals. Seals started to exhibit many signs of aging such as blisters, cracks, reduction in size and discoloration. Figure 11 shows the initiation and development of aging signs with aging time. Aging of seals was stopped, and the seals were characterized as failed when the seals started leaking excessively as soon as the system was pressurized.
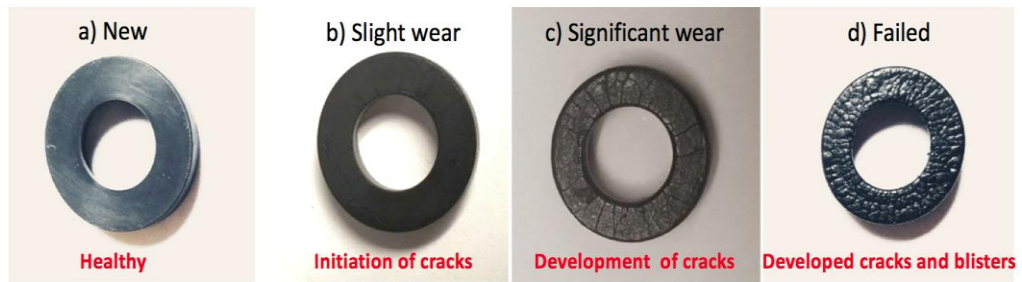
Figure 11: Development of Aging Signs in Rotary Seals During Aging

Reduced elastic modulus and hardness of seals lowered the interference between the shaft and seals, leading to excessive leakage and lower friction torque. Friction torque and leakage were used to measure the performance of seals after every aging cycle.
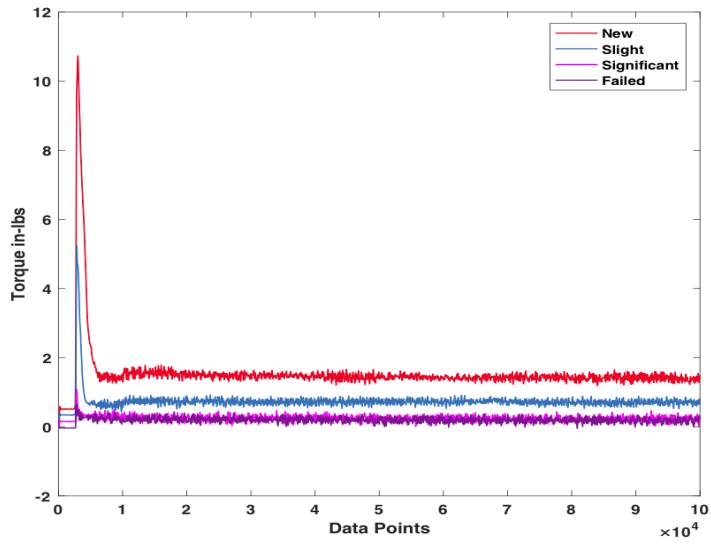
Figure 12: Filtered Torque Vs Running Condition of Rotary Seal
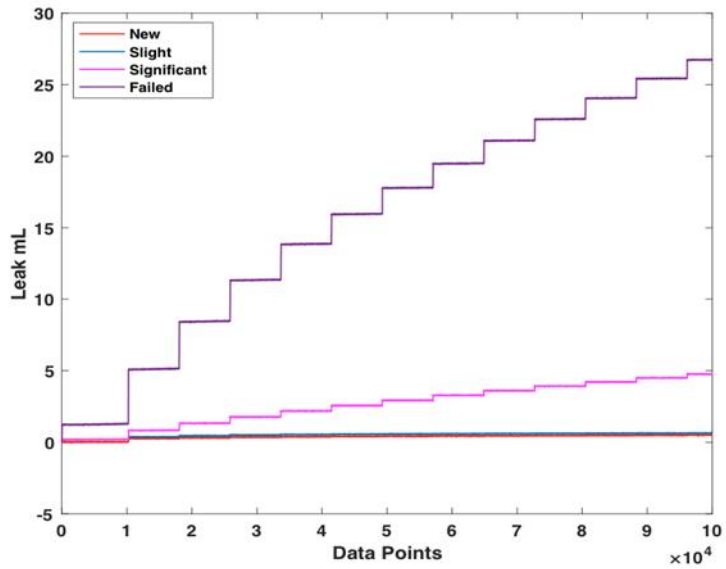
Figure 13: Filtered Leak Vs Running Condition of Rotary Seal

In Figure 12, we can see that as the seals approached failure, there was not much

difference in the friction torque of rotary seal. Figure 13 shows that seals did not leak

30

significantly during its early life, but the leakage increased significantly as the seals approached failure. Vibration has been the sensor of interest for machinery prognostics in the oil & gas industry. To compare the diagnostic capability of friction torque and leakage with vibration signal in rotary seal prognostics, we have illustrated the trend of vibration signal for different running conditions of rotary seal in Figure 14. It is evident from Figure 14 that vibration plays the least role in rotary seal prognostics and this could be because of the polymeric properties of seals. In addition, we test the aged seals in clear fluid whereas in oil field they operate in a contaminated environment and when the seals fail, bearings become the next target and it is when bearings begin to fail, the system starts vibrating due to excessive shaft runout. Therefore, multi-sensor based prognostic model utilizing both friction torque and leakage signals is used for predicting the running condition of rotary seals.
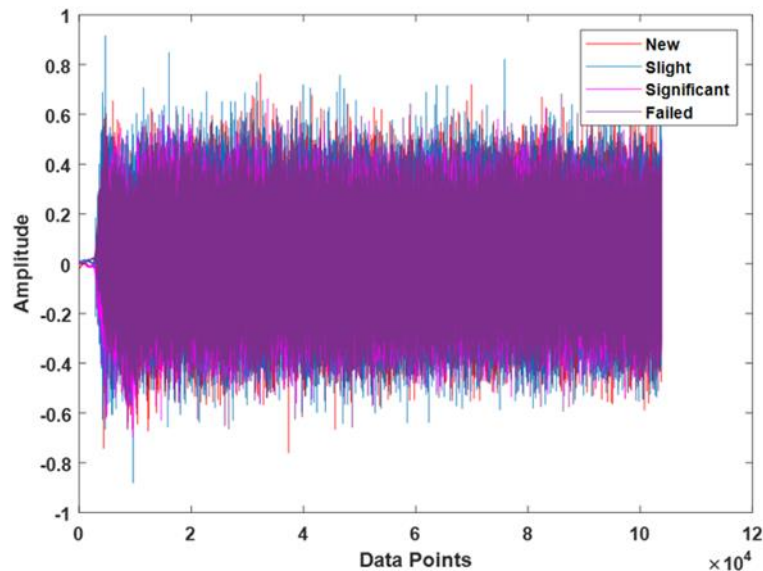
Figure 14: Vibration Vs Running Condition of Rotary Seal

Meaningful and informative features were extracted to reduce the complexity of raw signals and to make the pattern related to the running condition of rotary seals more obvious to the classifier. Time domain features were used to extract information from raw torque signal. Since the torque required to start a machine is always greater than the steady state torque, maximum/peak value is used to measure the breakout torque from the raw signal. It can be observed from Figure 15 that breakout torque reduces with an increase in seal wear due to the reduction of interference between shaft and seals. Eleven other statistical time domain features shown in Table 1 were extracted from the filtered steady state torque signal. The response of some of the extracted features which indicate the change in amplitude of the signal over time are shown in Figure 16. Features such as mean, Root Mean Square (RMS), maximum and squared mean rooted amplitude (SRA) which are related to the amplitude of the signal   decreases with increase in seal wear.
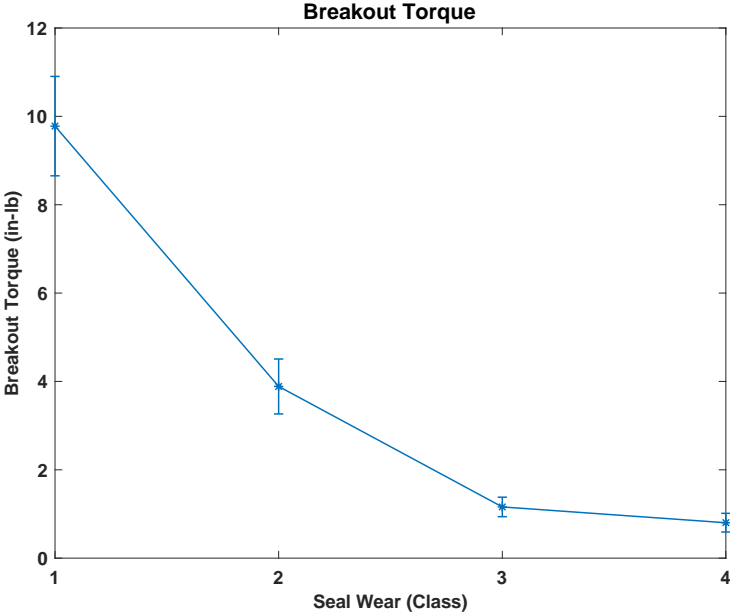
Figure 15: Effect of Seal Wear on the Breakout Torque (Class 1: Healthy, Class 2: Slightly Worn, Class 3: Significantly Worn and Class 4: Failed)

In contrast to the raw steady state torque, raw leakage signals are dynamic in nature (see Figure 13). Hence it is obvious that amplitude and energy of the signal keeps changing with time. Therefore, instead of time domain features, we extracted frequency domain features in addition to the change in fluid volume (every five minutes) to investigate how the change in leakage varies with seal wear. Twelve frequency domain features shown in Table 2 were extracted from the filtered leakage signal. Figure 17 shows the response (increasing or decreasing trend with the wear) of some of the extracted features about the running condition of seals.
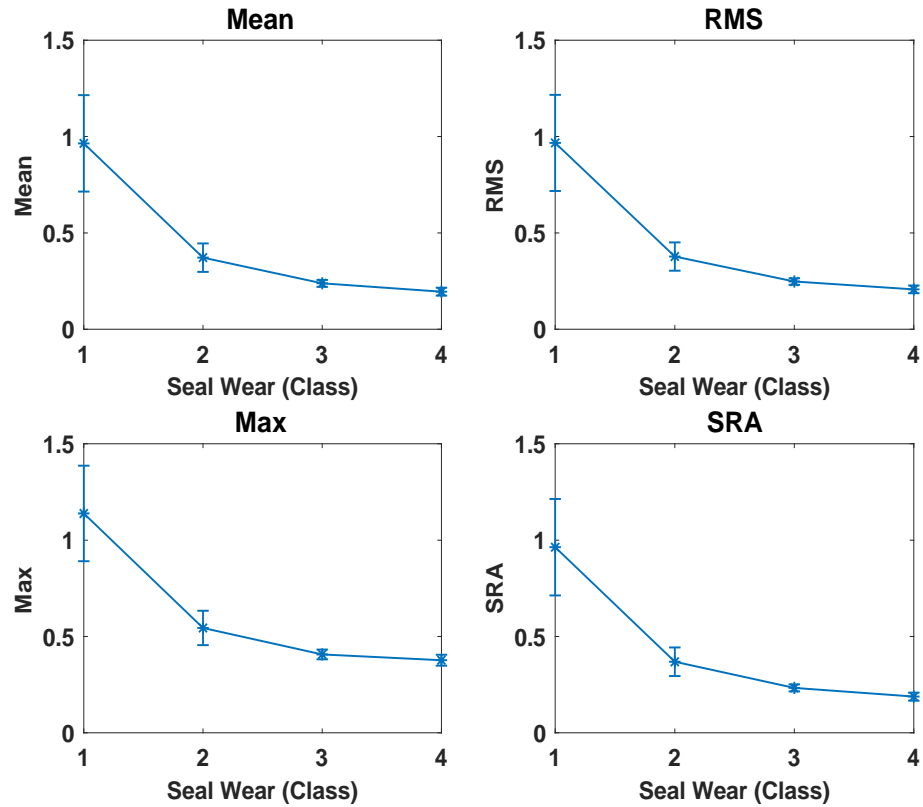
Figure 16: Effect of Seal Wear on Amplitude Related Steady State Torque Features (Class 1: Healthy, Class 2: Slightly Worn, Class 3: Significantly Worn and Class 4: Failed)

Not all the features are relevant and helpful in classifying the running condition of rotary seals, therefore, we performed feature selection using Recursive Feature Elimination search algorithm. To show that features from both torque and leakage signals are needed for effective prediction of seals' running condition we repeated feature selection and classification for 1) torque features, 2) leakage features and 3) torque and leakage features. After feature extraction, the data is randomly split into training (70%) and test data (30%). Features (of the training data) along with the class labels are fed as an input to the RFE search algorithm to select the optimal feature subset. The search algorithm starts with the full set of features and an optimal subset is

34
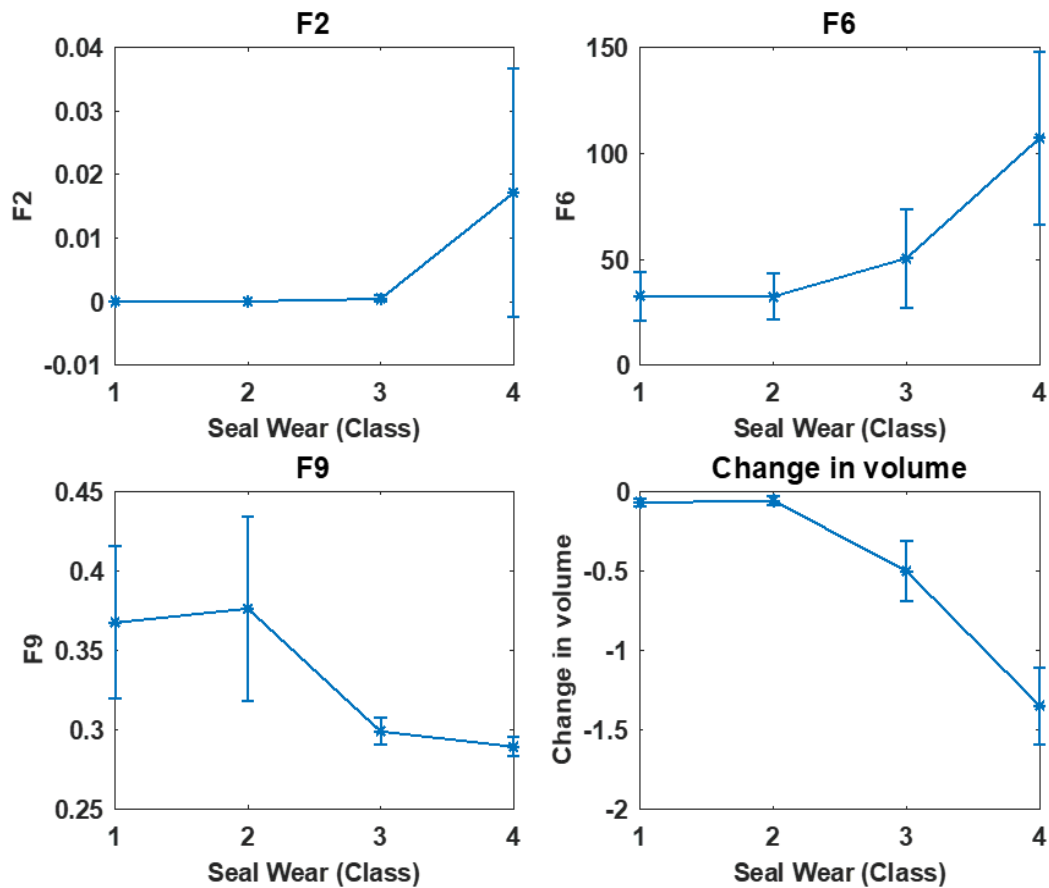
Figure 17: Effect of Seal Wear on Certain Frequency Domain Leakage Features (Class 1: Healthy, Class 2: Slightly Worn, Class 3: Significantly Worn and Class 4: Failed)

selected based on the cross-validation. First, twelve different features extracted from raw torque data along with the class labels were fed into RFE algorithm and the search algorithm ranked mean, RMS, breakout and SRA which are related to the amplitude of torque signal as the optimal torque feature subset. This subset is expected because the torque reduces with the reduction of interference between shaft and seals due to aging. Second, thirteen different features extracted from leakage signal were fed into RFE algorithm and the algorithm ranked the frequency domain features F2, F6 and F9 and the change in fluid volume every five minutes as the optimal leakage feature subset.
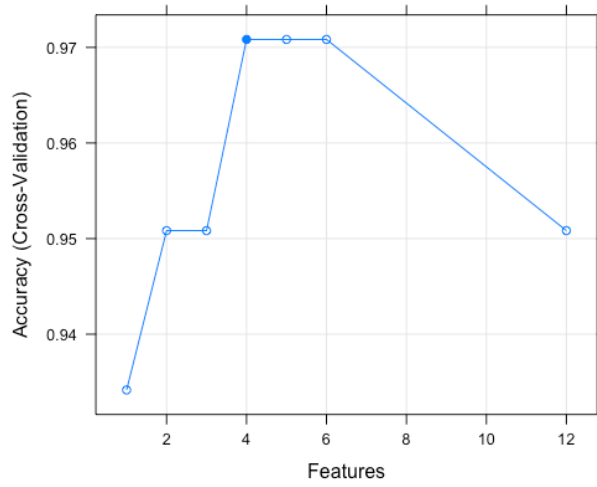
Figure 18: Optimal Feature Subset Selection Using RFE Search Algorithm for Torque Features
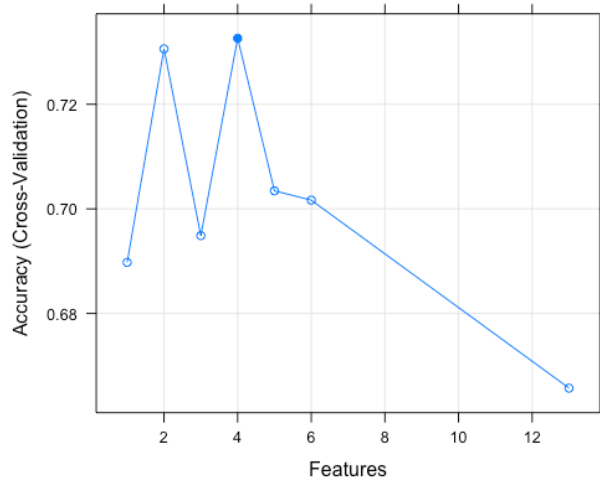
Figure 19: Optimal Feature Subset Selection Using RFE Search Algorithm for Leakage Features
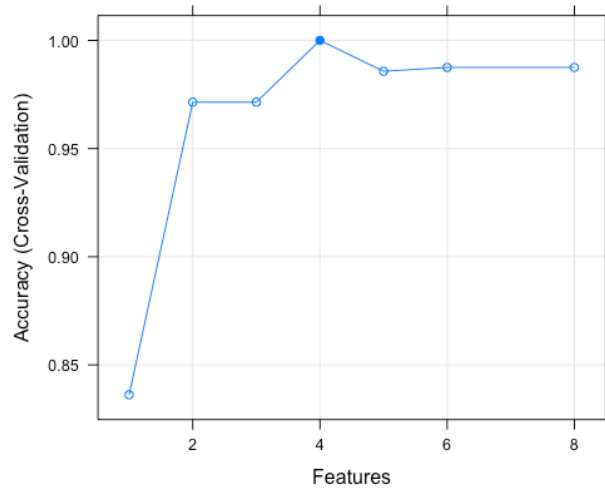
Figure 20: Optimal Feature Subset Selection Using RFE Search Algorithm for Torque and Leakage Features

Third, features extracted from both the torque and leakage signals were fed into the search algorithm and four features such as the mean, RMS, SRA and the change in fluid volume were selected as the optimal set of features from the torque and leakage features. Figure 18-20 shows the performance measure across different subset sizes and the shaded circle indicates the optimal feature subset size for torque, leak, and torque and leak features.

The selected features from training dataset of torque, leakage, and torque and leakage features were used as inputs to MLP and classifiers (for torque, leakage, and torque and leakage features) were built on different partitions of training sets obtained through 10-fold cross-validation. Cross validation randomly divides the entire dataset into training and test data eliminating the biasness while partitioning the dataset. For all the three classifiers, the input layer has 4 neurons (4 inputs), output layer has 4 neurons (4 targets) and the hidden layer has 4 neurons (mean of neurons in the input and output layers). The network was trained until the validation error rises with a learning rate of

37

Table 3: Comparison of Classification Accuracy for Different Performance Signals

Classifier	Cross-validation accuracy	Test accuracy
Torque features	94.12	92.86
Leakage features	83.82	71.43
Torque and leakage features	**99.68**	**97.5**

0.3 and momentum of 0.2. After training, a set of test data, which is not a part of training data, is used to evaluate the classification accuracy of MLP. Table 3 shows the comparison between classification accuracy of three classifiers. The classifier built using the features from both torque and leakage signal has shown to have a 97.5% classification accuracy when tested on an unseen dataset whereas the classifiers built using torque features resulted in 92.86% and leakage features resulted in 71.43%.
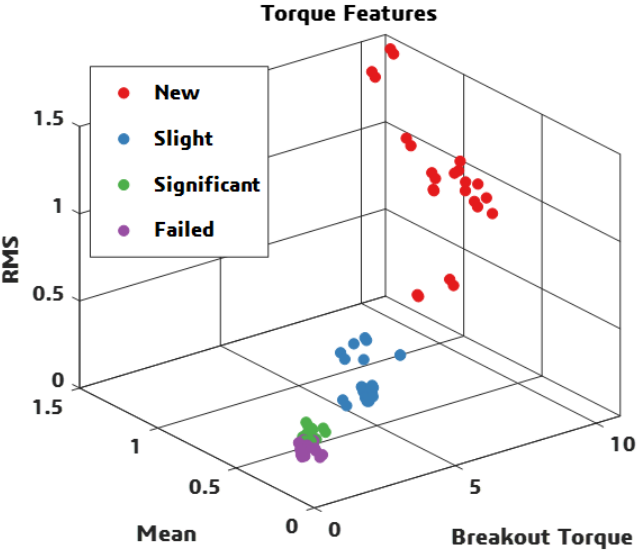
Figure 21: 3D Scatter Plot Showing the Classification Capability of Torque Features
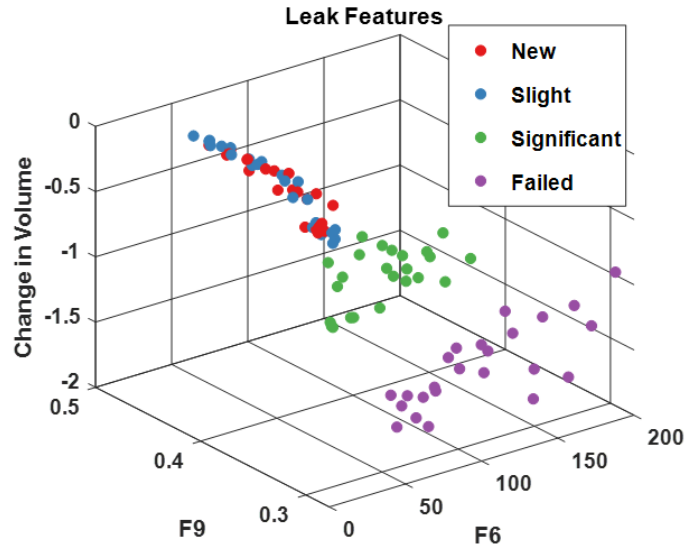
Figure 22: 3D Scatter Plot Showing the Classification Capability of Leakage Features
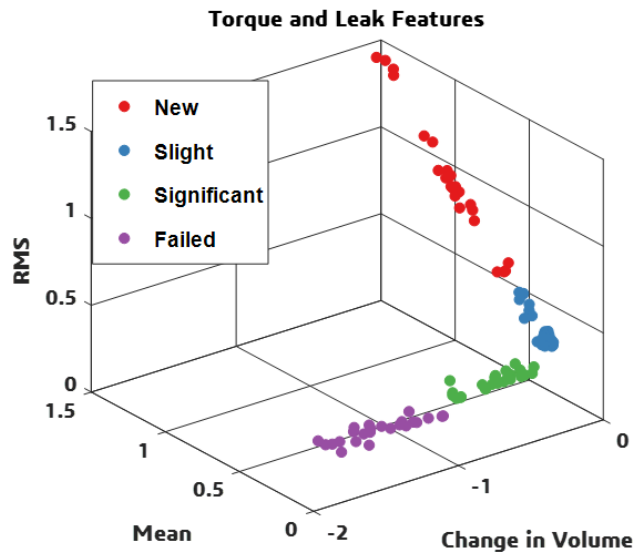
Figure 23: 3D Scatter Plot Showing the Classification Capability of Torque and Leakage Features

To further compare the classification capability of torque and leakage features, we created 3D scatter plots shown in Figure 21-23, to show the capability difference of torque and leakage features in differentiating the health condition of rotary seals. A better separability between class in the feature space shows better classification. Three of the torque features with high classification accuracy was used to construct Figure 21 where there is a distance between each class except for the significant and failure class indicating better classification during seals' early life. Similarly, three of the leak features with high classification accuracy was used to construct Figure 22 where there is no separability between new and slightly worn seal class as the data points are merged with each other in the feature space which indicates poor classification between new and slightly worn seals. Scatter plot in Figure 23, constructed using the top three torque and leakage features shows the expected distance between each class indicating better classification.

Classifier built using torque features incorrectly predicted failed seals as significantly worn as the torque doesn't vary much as it approaches failure whereas the classifier built using leakage features is confused between new and slightly worn seals as the seal doesn't leak significantly during its early life. Since torque features have a better discriminating potential during seals' early life and leakage features have a better discriminating power as the seals approach failure, combining both the torque and leakage features have resulted in a better performing classifier.

To validate the performance of MLP in differentiating the running condition of rotary seals, two other classifiers including logistic regression and random forest were trained and tested on unseen data. MLP showed a better classification (97.5%) when

compared to logistic regression (96.25%) and random forest (96.25%) which can be inferred from Table 4. Also, potential of the proposed approach in classifying the health states of seals operating at different temperature was validated by testing the trained model on data collected at room temperature (data for the trained model was collected at seal's maximum operating temperature) and the approach showed 89.06% classification accuracy while the other two classifiers were about 78%.

Table 4: Comparison of Classification Accuracy of MLP with Different Models

Classifier	Cross-validation accuracy	Test accuracy (175°C)	Room temperature
Multilayer Perceptron	**99.68**	**97.5**	**89.06**
Logistic Regression	98.75	96.25	78.12
Random Forest	98.43	96.25	78.12

2.4 Summary

In this chapter, we have proposed a multi-sensor-based performance degradation assessment approach utilizing friction torque and leakage signals to classify the running/health condition of rotary seals. To make the degradation pattern more obvious to the classifier, statistical time domain features were extracted from raw torque signals and change in fluid volume and frequency domain features were extracted from leakage signals. An optimal feature subset was selected using RFE with MLP neural network utilized as classification algorithm to best fit the relationship between the relevant features and the running condition of rotary seals.

The proposed approach has shown that features extracted from torque and leakage lack a better discriminating power on its own, in classifying the running

condition of seals throughout its service life. Statistical features related to the amplitude of torque signal and the change in fluid volume every five minutes were found to be the optimal set of features using RFE search algorithm. The classifier built using optimal set of features from torque and leakage signals has resulted in a better classification accuracy when tested on an unseen data collected at different temperature. Therefore, the implementation of multi-sensor based prognostic model results in the most reliable performance assessment of rotary seals.

This method can be extended to study the performance degradation of rotary seals by any means, provided the availability of data collected from sensors. In a rotating machinery, failure of rotary seal initiates the degradation of bearings and other inline components and hence this multi-sensor based rotary seal prognostics utilizing torque and leakage can be implemented along with vibration-based bearing prognostics to isolate the defects in rotary machinery.

The potential of the proposed approach in assessing the performance degradation of seals is foundational in developing an online degradation assessment which would be of great interest to end users for making maintenance decisions.

Chapter 3: A Hybrid PSO-SVM-Based Method for Degradation Prediction of Reciprocating Seal

3.1 Introduction

3.1.1 Reciprocating Seal

Dynamic seals such as reciprocating seals are used to separate or retain fluids, pressure and remove contaminants. Reciprocating seals aids in the reciprocating movement which is a linear motion of rod/piston in a cylinder. They are usually found in the piston of a cylinder, plunger entering a chamber and a hydraulic actuator with piston rod anchored. Reciprocating seals are generally made of polymeric materials such as elastomers or thermoplastic materials such as polytetrafluoroethylene, polyurethanes, etc. Leakage from reciprocating cylinder rod contaminates the environment and can lead to catastrophic consequences, resulting in costly downtime and large expenses. Replacing a seal after its failure can be extremely expensive, while replacing the seal much earlier before its failure may lead to lower life utilization.
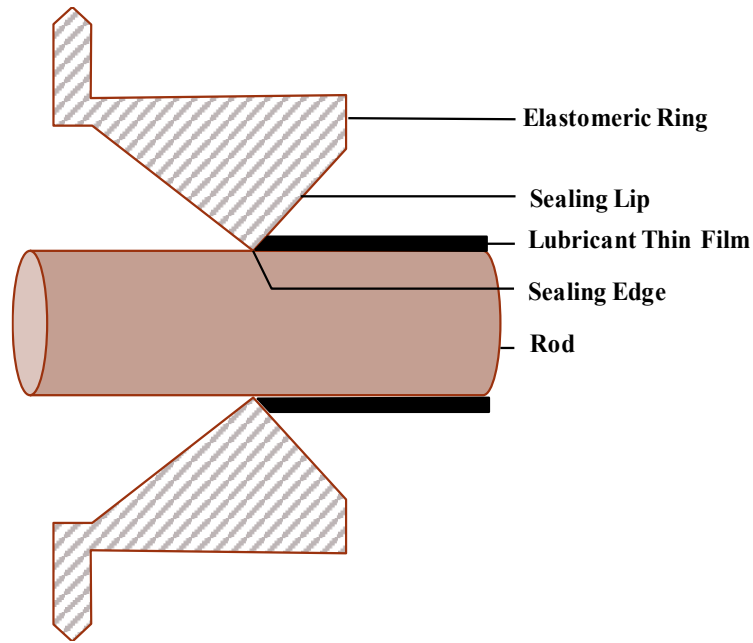
Figure 24: Cross-Section of a Reciprocating Seal on a Reciprocating Rod

3.1.2 Modes of Reciprocating Seal Failure

Reciprocating seals are usually exposed to high velocity, long stroke, high pressure, aggressive environment and rapid and frequent changes of stroke direction. Figure 24 shows the cross-section of reciprocating seal on a rod within reciprocating machines. Material characteristics, amount of seal compression, surface irregularities, inadequate lubrication, fluid contamination, seal size are some of the factors that influence a dynamic seal failure [43]. The seal wear due to friction between the seal and piston/rod results in increased friction force and excessive leakage.

3.1.3 Physics-Based Reciprocating Seal Prognostics Model

Reciprocating seals have been the research of interest since early 1960's beginning with a study to understand the performance of reciprocating seals. In 1974, a model to solve Reynolds equation and elasticity equation was developed to show the

impact of rod speed on the seal leakage [44]. It was showed that in certain operating conditions, asperity contact occurs between seal and rod leading to mixed lubrication in the lip [45]. In [46], surface roughness of the seal in the sealing zone was shown to be affecting the lubrication which in turn affects leakage. The numerical model developed in [47-49] considered mixed lubrication effect and surface roughness to show that sealed pressure and stroking velocity affects the seal leakage, film thickness and friction force.

Literature indicates the development of a numerical model such as mixed lubrication and surface roughness to predict the sealing performance in terms of leakage and friction. Predictive model to estimate the evolution of the future condition of seal will result in reduced downtime and maintenance cost, and improved maintenance and logistic planning. In the last decade, numerous physics-based prediction methods, which demands direct estimation of physical parameters such as material, seal and mechanical properties have been proposed by researchers [50, 51] has been developed to assess the degradation of polymeric seals. Also, physics-based approaches are very specific to the material and geometry of the system and requires a new model with any change in the system. Whereas, data-driven based predictive method utilizes indirect measurements using sensor technology and computational capabilities to monitor the current running condition of seals. This technique is primarily applied to metallic parts such as bearings, gear box, etc. and there is a need for research on data-driven based predictive method that can be applied to engineering systems such as polymeric elastomer seals.

3.1.4 Support Vector Machine for Degradation Prediction

Support Vector Machines has shown to be successful in studying degradation of components because of its performance modeling and generalization attributes, when

compared to widely used methods including neural network [52, 53]. SVM was found to be successful in predicting the degradation of bearing, batteries and other electronic and mechanical components. Dong and Luo [8] developed a PCA based optimized LS-SVM model to predict the degradation process of bearings. Sun, Zhang and He [52] used the SVM-based model to predict bearing degradation by using few failed bearing data. They allocated different weights to different bearings and the information is fused to predict the degaradtion of test bearing. Park and Jeong [54] used recurive SVM to predict the degradation of secondary rechargebale battery. Guo, Ma, Xiao and Tian [55] developed a PSO-SVM model to diagnose faults in electronic system. Xu, Wu, Guo and Hu [56] used LS-SVM to predict the life of barrels of tank guns. According to Huang, Wang, Li, Zhang and Liu [57] applications of SVM in building degradation models are limited to componenets such as bearings and batteries; and they stress the need for research on applications of SVM in predicting the degradation of other key componenets.

The most challenging aspect of SVM is tuning the hyperparameters of SVM during the training phase, which requires solving an optimization problem. In this study, we have implemented phase space reconstruction to determine the input and output vectors of the prediction model and particle swarm optimization, a meta-heuristic approach, to optimize the SVM parameters to improve the prediction accuracy.

The remainder of this chapter is structured as follows: description of experimental test set-up, data collection, phase space reconstruction, particle swarm optimization and support vector machines are explained in detail in methodology section; results of our approach are discussed in results and discussion section; study conclusions are summarized in conclusion section.

3.2 Methodology

3.2.1 Test Set-up

Oscillating seal test fixture mimics the mechanical dynamics of a conventional positive displacement piston pump. Mechanics of interest are isolated to the reciprocating/shuffling motion of a piston or rod within a stationary bore. There exist two common methods of sealing fluids within dynamic reciprocating applications: piston seals and rod seals. Interest here will be to characterize the performance of rod seals. A main pressure chamber encapsulates an interchangeable core. This modular core can be made with many distinct seal geometry gland dimensions for the purpose of testing a variety of polymer seals with differing cross sections. Experimental runs depicted here concern standard AS568, size 214 circular cross section O-rings. Reciprocating through this modular core lies a precision ground rod of desired surface roughness 16RMS. Reciprocating rod is driven by a Baldor 3HP M3611T-9 alternating current three-phase induction motor affixed to a Baldor 10:1 gear reduction transmission whose output shaft turns a cam-arm (as shown in Figure 25). This cam-arm pushes and pulls the rod through one reciprocation for every revolution of gearbox output shaft. Stroke length of reciprocation is fixed at 10.5 inches and is determined by length of cam-arm. Baldor 3HP induction motor is driven by an ABB ACS150-03U-09A8-2 3HP DRIVE. This variable frequency drive gives motor speed and torque control by varying the frequency and voltage supplied to the motor by main power lines. Frequency ranges from 0-60 Hz, for out motor 0 Hz equates to 0RPM and 60 Hz equates to 1750 RPM. This ABB drive also allows for torque boost by pre-energizing induction wound coils of motor and then monitoring rush current of motor upon startup.

This feature has been particularly useful while testing seals with high initial 'break out' forces. That is the force required to start 'stagnant/dormant system'.

Stroke length can be changed, either increased or decreased by replacing the cam-arm. Increasing length of cam-arm allows for a lengthened reciprocating stroke and decreasing length of cam-arm shortens reciprocating stroke. Consequentially if cam-arm is lengthened, stroke lengthens, allowing seals to 'feel' more linear feet of rod travel per some fixed interval of time. Reverse methodology exists if cam-arm is shortened. Stroke length shortens, and seals 'feel' less linear feet of rod traveled per some fixed interval of time.

A fixed motor speed and a fixed cam-arm length will parameterize experimental runs expressed in this study. Motor speed at gearbox output shaft has been fixed at 30 RPM and cam-arm length set to 5.5 inches. Recall that for every separate revolution of the motor gearbox output shaft, the cam-arm moves through one revolution, which translates circular motion into linear motion, hence, the title cam-arm. This means that for every separate revolution, the cam-arm moves a total of 11inches, 5.5 inches of stroke in compression and 5.5 inches of stroke in tension. For our purposes, with the fixed parameters specified above, one reciprocation equates to 330 inches of rod travel per minute.
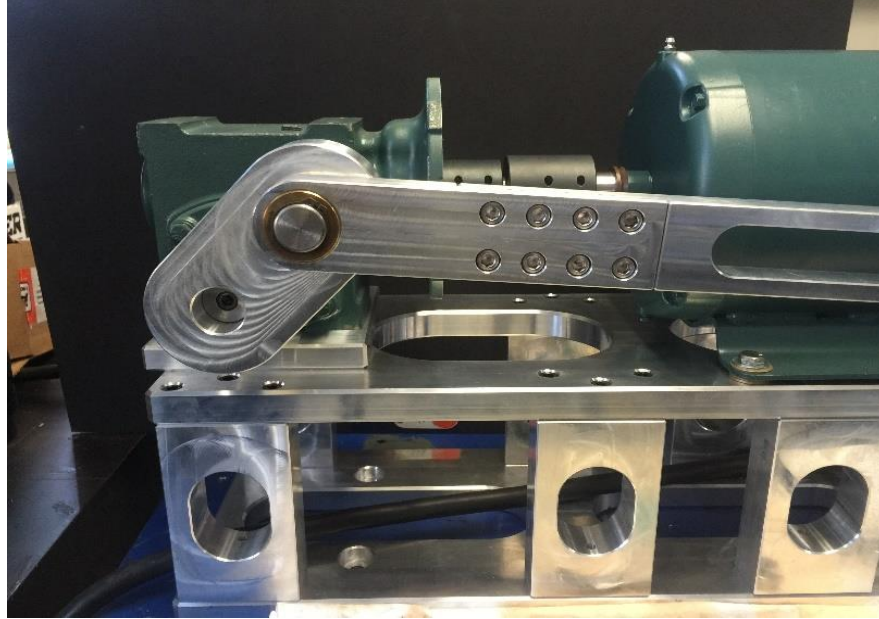
**Figure 25:Test Set-up Showing Induction Motor, Gearbox Cam-Arm Diving
Reciprocating Rod Motion**

To keep linear motion consistent and without binding, Thompson linear guide and

ball bearing carriage are mated to reciprocating rod. As power is transmitted from motor

and cam-arm, opposing end of cam-arm pivots on a shuttle specifically made to accept

power transmission. This shuttle has been designed to transmit cam-arm movement into

an Omega Engineering LC203-1K bi-directional load cell. As shuttle pushes

reciprocating rod through 'compression cycle' and pulls reciprocating rod through

'tension cycle' real time force data is acquired. Overview of reciprocating rod, load cell

and shuttle can be seen in Figure 26.
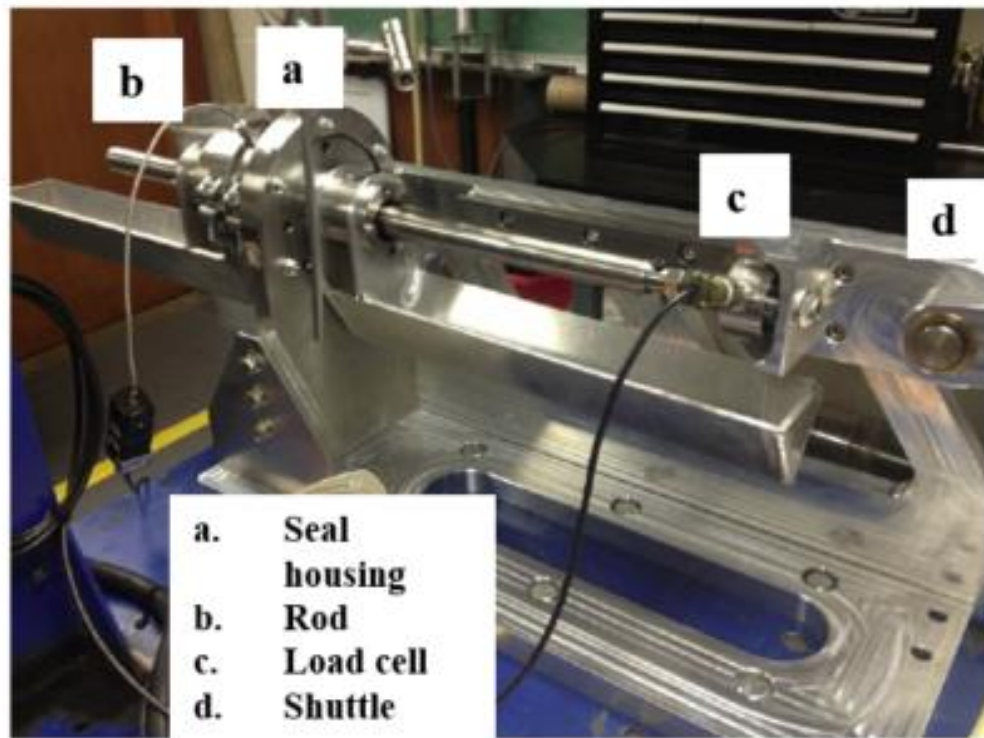
Figure 26:Test Set-up Showing Testing Chamber, Reciprocating Rod, Load Cell and Shuttle

Main pressure chamber and seals are energized through the hydraulic

pressurization of Aero Shell 560 Turbine oil. Considering the 'leak rate' of seals to be

of interest it is required to keep system at a constant pressure elimination one variable in

the experimental run. To counteract the transient effects of mechanical cycling of a

hydraulic pump, a specialty hydraulic piston accumulator with active piston position

feedback is used to transmit high-pressure nitrogen to high-pressure hydraulic oil.

Hydraulic piston accumulator with live piston positioning allows for active

tracking of displaced fluid through system, or 'leaked fluid while system is kept at

constant pressure. The hydraulic piston accumulator accomplishes this by implementing

an MTS GHT0060UFD21V0 liner variable differential transducer to actively track position of piston within bore of accumulator (as shown in Figure 27).
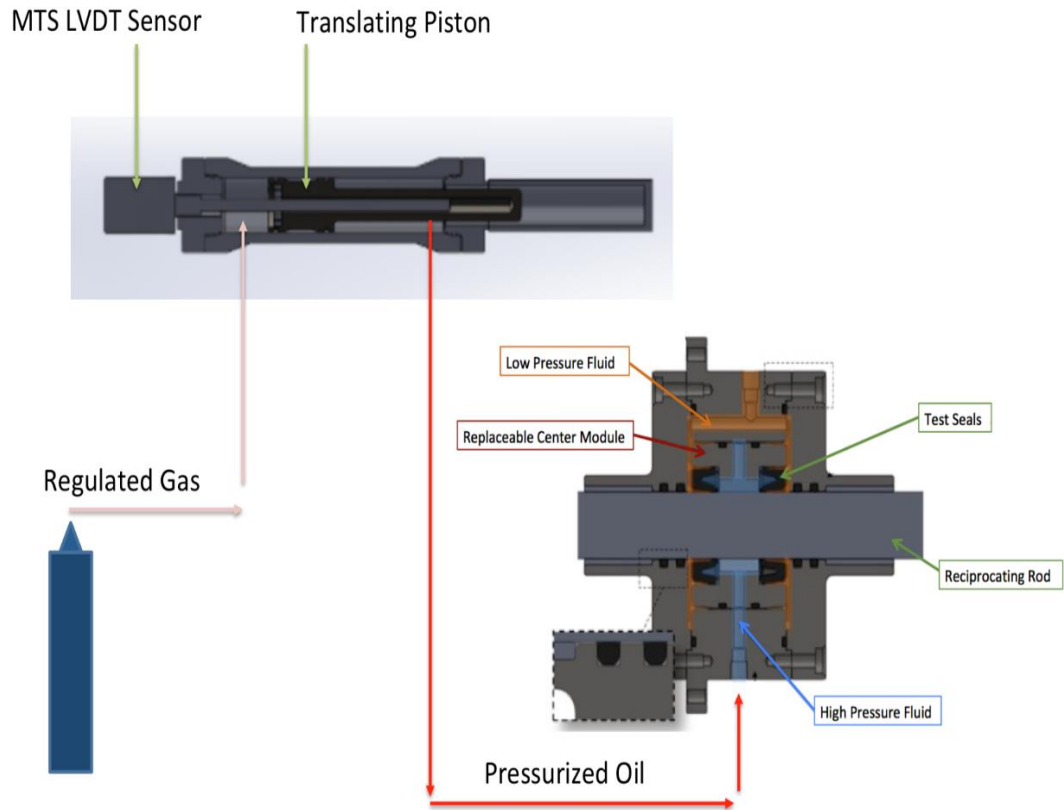
Figure 27: Hydraulic Fluid Pressurization Through Piston Accumulator

Special design of experiment conditions requires simulating real operating conditions of seals within componentry exposed to harsh temperature conditions. Test chamber assembly has been outfitted with large diameter 240volt mica heating bands. Heating bands are controlled with Omega Engineering iSeries programmed proportional integral differential (P.I.D.) temperature controller. This controller allows precise temperature control +/- 1°C for all experimental runs conducted thus far up to 200°C.

Real time data from all transducers is acquired through the utilization and

combination of National Instruments LabVIEW in conjunction with National

Instruments USB X-Series 6341 Multifunction I/O device. Device acquires data through

high speed TDMS streaming and functions as a controller for all peripheral

componentry. Eight run-to-failure tests at 150°C, 1500 PSI are performed to collect

information on the force required to move reciprocating rod some unit length per unit

time. 20 data points are sampled every second. Figure 3.4 shows the run-to-failure test

of seal-1 of data length of 60,370. For a better visualization, a segment of run-to-failure

force signal is shown in Figure 28.
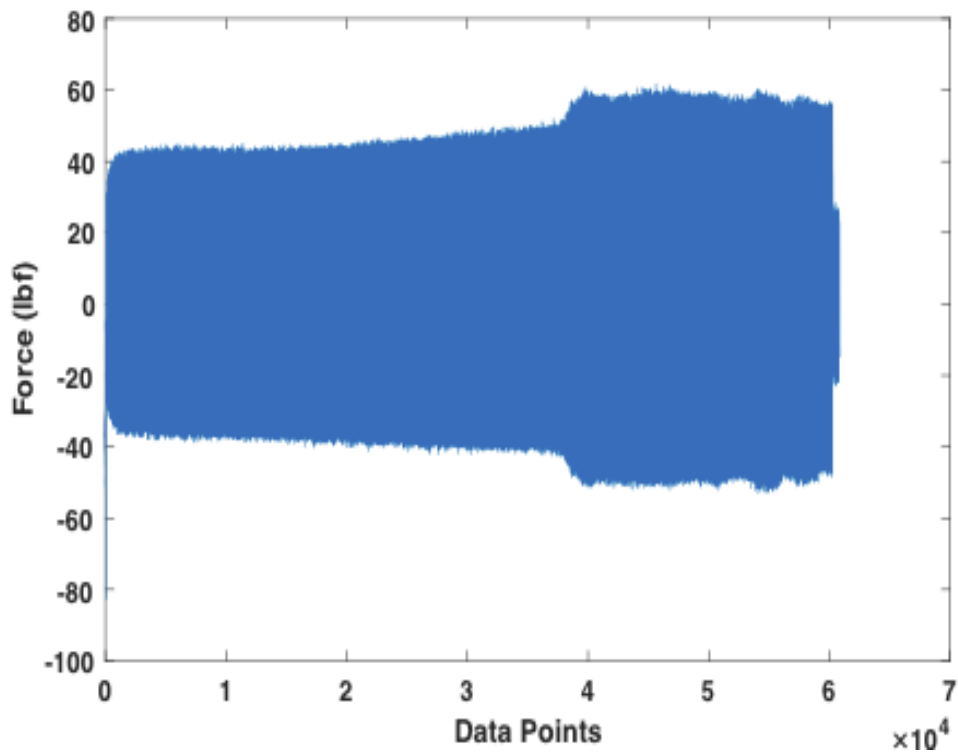
Figure 28: Run-to-Failure Test of Seal-1

52

Figure 29 shows two regions of interest: Region 1 will overview force vs. time while reciprocating rod is in tension and Region 2 will overview Force vs. Time while rod is in compression. Considering these two regions to be mirrors of each other, we will simply limit our discussion to Region 1 knowing that Region 2 is the inverse. Within Region 1 we see a positively oriented parabolic trend from point A-B. If we consider this region to be in simple tension, then we would expect the force graph to be almost perfectly flat therefore why is it not? Experiments have led us to believe the force graph is affected by two things: first is rooted in the mechanics of this system. There exists some small acceleration and deceleration at the leftmost and rightmost limit of the reciprocating stroke. This causes upon switching from tension to compression B-B* or compression to tension A*-A some momentary 'jerk' resulting in a transient spike in force graph. Second comes from the idea of seal wiping. This phenomenon exists when the seal physically wipes excess lubricating film from the reciprocating rod. At leftmost and rightmost stroke limits the seal has less fluid to wipe away resulting in a not fully lubricated seal which in turn increases force seen at stroke limits. It takes around 3.90 seconds to complete a tension and compression cycle.
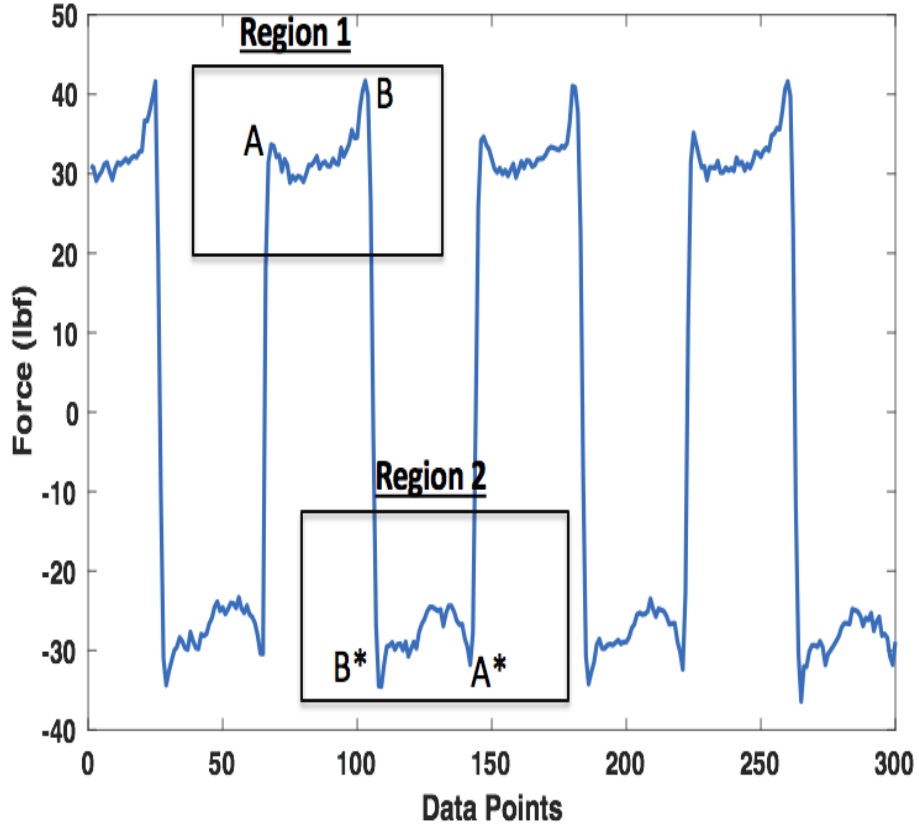
Figure 29: A Segment of Force Signal Showing Tension and Compression Cycle

3.2.3 Phase Space Reconstruction

Following feature extraction, phase space reconstruction based on Takens embedding theorem is used to construct a set of vectors whose components are lagged version of time series [58]. Let $X_t = \{x_1, x_2, ..., x_N\}$ be a univariate time series of length N and $y_{im} = \{x_i, x_{i+\tau}, ..., x_{i+(m-1)\tau}\}$, where $i = 1,2, ..., N_m$, $N_m = N - (m-1)\tau$ is the length of reconstructed vector, τ is the time delay, m is the embedding dimension. In 1986, Fraser and Swinney found the concept of time delay for embedding a univariate time series [59]. The time delay τ is estimated using average mutual information which is a nonlinear generalization of the autocorrelation function. The average mutual

54

information estimates how much a time series $x(t)$ can provide information on another time series $x(t + \tau)$ and is given by:

$$I\big(x(t), x(t + \tau)\big) = \sum_{ij} p_{ij}\,(\tau)\log\left(\frac{p_{ij}(\tau)}{p_i p_j}\right) \tag{1}$$

Where, p_i is the probability that the time series $x(t)$ is in the bin i of the histogram constructed from data points in series $x(t)$, p_j is the probability that the time series $x(t + \tau)$ is in the bin j of the histogram constructed from data points in series $x(t + \tau)$ and p_{ij} is the probability that the time series $x(t)$ is in the bin i and $x(t + \tau)$ is in the bin j. The optimal time delay is estimated using the position of the first minimum of average mutual information function.

The embedding dimension m is determined using CAO method [60] and is defined as:

$$a(i, m) = \frac{\| y_i\,(m + 1) - y_i^{nn}(m + 1) \|}{\| y_i\,(m) - y_i^{nn}(m) \|} \tag{2}$$

Where, $\|\cdot\|$ is the Euclidean distance given by the maximum norm. $y_i(m)$ is the ith reconstructed vector and $y_i^{nn}(m + 1)$ is the nearest neighbor of $y_i(m)$ in embedding dimension m. The mean value of all $a(i, m)$ is defined as:

$$E(m) = \frac{1}{N - m\tau} \sum_{i=1}^{N - m\tau} a(i, m) \tag{3}$$

E(m) depends on dimension *m* and lag time τ and its variation from *m* to *m+1* is given by a parameter E_1:

$$E_1(m) = \frac{E(m+1)}{E(m)} \qquad (4)$$

$E_1(m)$ stops increasing when m is greater than some value m_o. $E_1(m)$ increases slowly or

stops changing if m is significantly large and to overcome this CAO introduced another

quantity $E_2(m)$ which is given by:

$$E_2(m) = \frac{E^*(m+1)}{E^*(m)} \qquad (5)$$

Where

$$E^*(m) = \frac{1}{N - m\tau} \sum_{i=1}^{N-m\tau} |x_{i+m\tau} - x_{i+m\tau}^{nn}| \qquad (6)$$

Therefore, $E_1(m)$ is estimated to determine the minimum embedding dimension of time

series and $E_2(m)$ is used to distinguish the deterministic signals from stochastic signals.

3.2.4 Particle Swarm Optimization

Particle swarm optimization, a population based intelligent algorithm proposed

by Kennedy and Eberhart in 1995 is used to optimize SVM regression parameters [61].

PSO simulates the behavior of swarms in solving optimization problems iteratively

because of its simplicity, fast convergence and high performance. PSO is based on a set

of particles and their coordinates represent a potential solution of an optimization

problem. The position and velocity of ith particle in a population with N particles in a

d- dimensional space is given by $X_i(t) = \left(x_{i1}(t),\ x_{i2}(t), \dots, x_{iD}(t)\right)$ and $V_i(t) =$

$\left(v_{i1}(t),\ v_{i2}(t), \dots, v_{iD}(t)\right)$. PSO algorithm updates the velocity and position of the

particles at iteration $t+1$ using the following equations:

$$v_{id}(t + 1) = \omega v_{id}(t) + c_1 r_1 \big(p_{id}(t) - x_{id}(t)\big) + c_2 r_2 \Big(p_{gd}(t) - x_{id}(t)\Big) \qquad (7)$$

$$x_{id}(t + 1) = x_{id}(t) + v_{id}(t + 1) \qquad (8)$$

Where i = 1, 2, ..., N denotes particles of population size N

d= 1, 2, ..., D denotes dimension of search space with D dimensions

t = current iteration with the number of iterations T

ω = inertia weight to balance the local and global search abilities of particles

c_1, c_2 = learning factors

r_1, r_2 = random functions with uniform distribution of (0,1)

$v_{id}(t)$= velocity of the ith particle in t^{th} iteration

$x_{id}(t)$= position of the ith particle in t^{th} iteration

$p_{id}(t)$= p_best (local best) position of the ith particle

$p_{gd}(t)$= g_best (global best) position of the particle
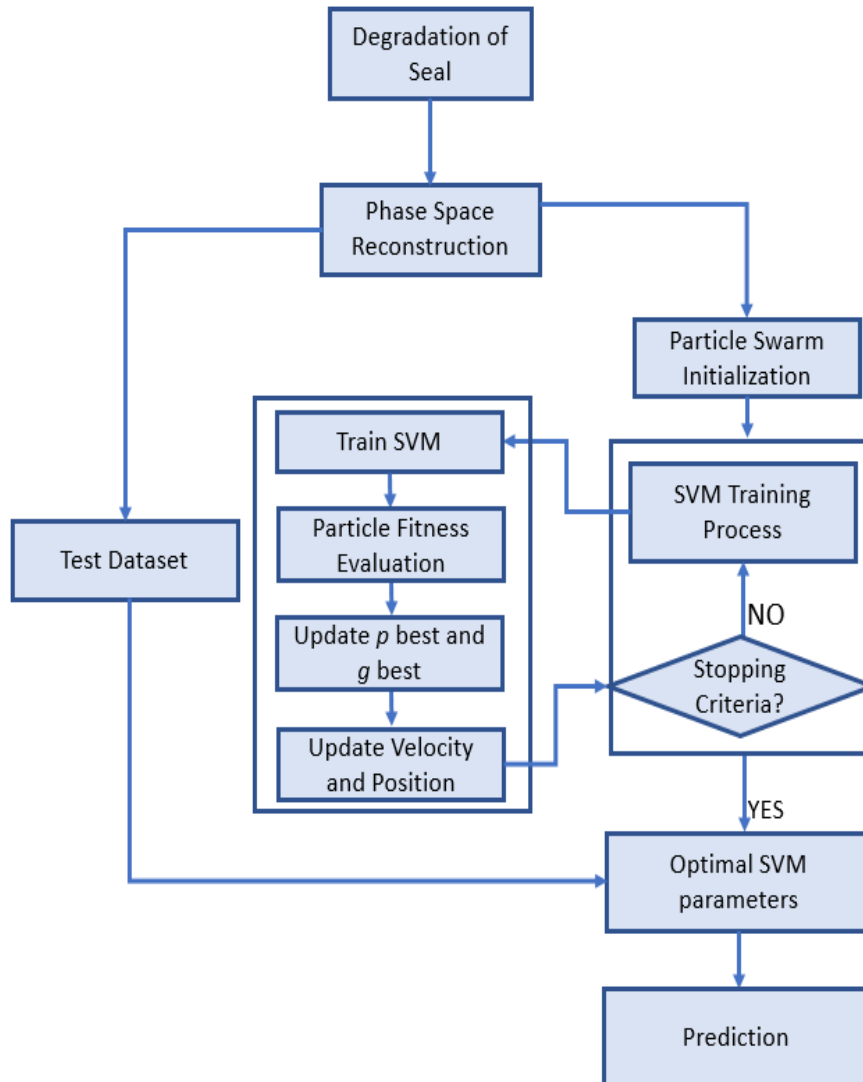
Figure 30: Flowchart Showing the PSO-SVM Procedure

The flowchart of optimizing SVM regression parameters: penalty factor C and kernel function parameter g based on PSO is shown in Figure 30 and the procedure is given below:

1. Randomly initialize population size, learning factors, inertia weight, random functions, position and velocity of each particle. Initialize the SVM regression parameters and set the termination condition.

2. SVM model is trained with the initialized parameters and the fitness value of each particle is calculated using the PSO fitness function given in Eq. (17)

3. The p_{best} and g_{best} values are adjusted based on the particle fitness value and the velocity and position of the particles are updated using the equation given in Eq. (7) and (8).

4. The SVM parameters are updated and the model is retrained is retrained using the PSO fitness function. Step 3 and step 4 is continued until the termination condition is satisfied.

5. When the termination condition is met, optimal parameters C and γ *of* SVM regression is found.

6. Retrain SVM regression with the optimal values and tested on the SVM regression.

3.2.5 Support Vector Regression

Support Vector Machine based on statistical learning theory is put forward by Vapnik in 1995. Given a set of training data $\{(X_1, y_1), (X_2, y_2), \ldots, (X_l, y_l)\}$, $X_i \in R^m$, $y_i \in R$, where y_i is the dependent variable for a given set of independent variable X_i, SVM generalization to Support Vector Regression (SVR) is performed by defining an ε-insensitive region, inside which errors are ignored. SVR formulates it as an optimization problem, where the objective is to find the flattest region (means to have a small ω) that contains most of the training instances while minimizing the prediction error (distance between the predicted and actual values). The regression in terms of constrained optimization problem can be written as:

$$\text{minimize} \quad \frac{1}{2} \|\mathcal{W}\|^2 + C \sum_{i=1}^{l} (\xi_i + \xi_i^*) \tag{9}$$

$$\textit{subject to} \quad y_i - \mathcal{W}x_i - b \leq \varepsilon + \xi_i \tag{10}$$

$$\mathcal{W}x_i + b - y_i \leq \varepsilon + \xi_i^* \tag{11}$$

$$\xi_i, \xi_i^* \geq 0 \tag{12}$$

where $\frac{1}{2}\|\mathcal{W}\|^2$ is the weight vector, y_i is the desired value and the tuneable parameter C

is the penalty factor that determines the trade-off between the flatness and the extent to

which deviations larger than ε are tolerated. The loss function defined is non-

differentiable due to the absolute value in function, so the positive slack variables ξ_i, ξ_i^*

are introduced to account for the errors in points that lie outside the ε-insensitive region.

Applying Lagrangian multiplier, this problem is converted into dual optimization

problem as follows:

$$\textit{maximize} \left[-\frac{1}{2} \sum_{i,j=1}^{n} (\alpha_i - \alpha_i^*)(\alpha_j - \alpha_j^*)(x_i, x_j) \right.$$

$$\left. - \varepsilon \sum_{i=1}^{n} (\alpha_i - \alpha_i^*) + \sum_{i=1}^{n} (\alpha_i - \alpha_i^*) \right] \tag{13}$$

$$\textit{subject to } \sum_{i=1}^{n} (\alpha_i - \alpha_i^*) = 0 \textit{ and } \alpha_i, \alpha_i^* \in [0, c] \tag{14}$$

Where α_i, α_i^* are lagrangian multipliers. For nonlinear regression, SVM uses a kernel

function. It performs by mapping the data X into a high dimensional feature space by

non-linear mapping and then performing regression in the feature space. Using the kernel function $K(x_i, x_j)$, the regression function is as follows:

$$f(x) = \sum_{i,j=1}^{n}(\alpha_i - \alpha_i^*)\left(\alpha_j - \alpha_j^*\right)K\left(x_i, x_j\right) + b \tag{15}$$

Where $K\left(x_i, x_j\right)$ is a kernel function. There are different kernel functions such as Linear, Polynomial, Radial Basis Function and Sigmoid. In this study, RBF function is utilized, and it is given by:

$$K\left(x_i, x_j\right) = \exp\left(-\gamma\|x_i - x_j\|^2\right), (\gamma > 0) \tag{16}$$

Where γ is the RBF kernel parameter.

3.2.6 Performance Criteria

The performance of the model is evaluated using Mean Square Error (MSE) and Mean Absolute Error (MAE). The MSE is defined as:

$$MSE = \frac{1}{N}\sum_{i=1}^{N}(p_i - y_i)^2 \tag{17}$$

$$MAE = \frac{1}{N}\sum_{i=1}^{N}|(p_i - y_i)| \tag{18}$$

where N is the total number of data points, y_i is the actual value and p_i is the predicted value of the model.

3.3 Results and Discussion

First, the entire time series is segmented into n segments and features are extracted from each segments of the time series. For example, length of seal-1 run-to-failure test is 60,372 and it is segmented into 774 segments (774 cycles). Main reason

for the reciprocating seal to fail is due to rolling, during which the friction increases leading to increased friction force and leakage.

As the seal degrades, compression peak: A*(maximum force during compression cycle) and tension peak: B (maximum force during tension cycle) shown in Figure 29 increases which results in significant leakage. The increase in tension peak can be observed in Figure 31. It was found that as the tension peak begins to increase and approach a force of 60 pound-force, a significant amount of leakage was observed.
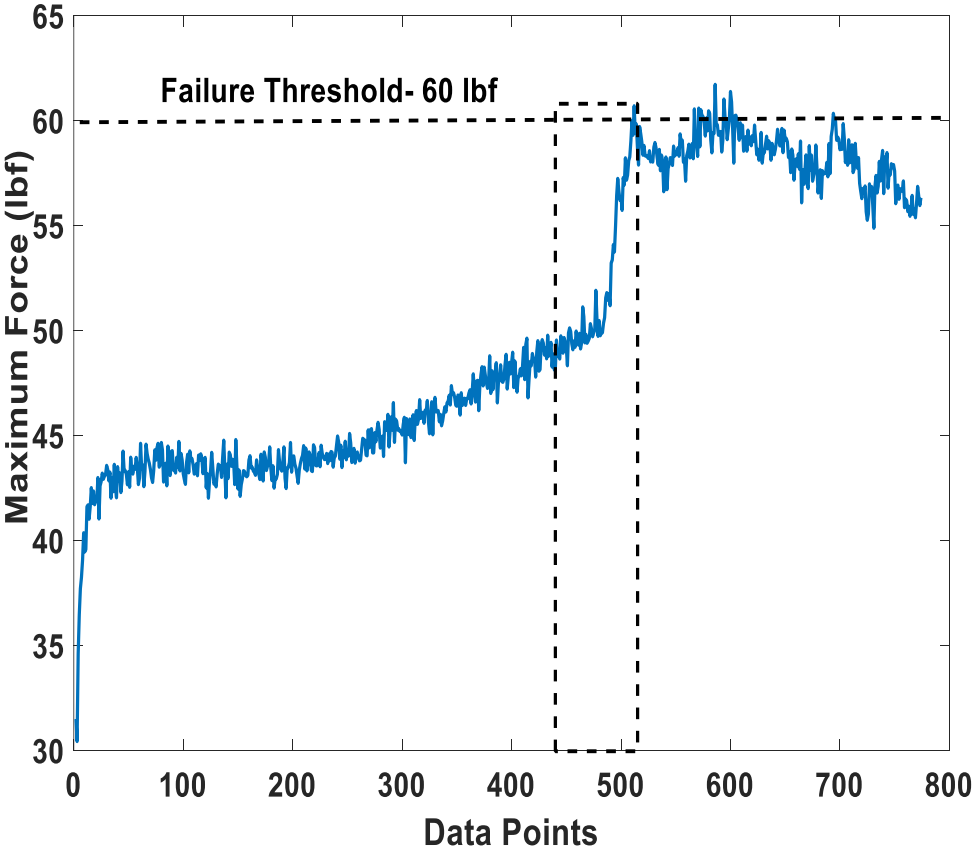
Figure 31: Degradation Trend Captured by Tension Peak with the Rectangular Box Showing the Degradation Region

This can be observed by comparing Figure 32 and 33 which shows the degradation region (data points 430-515) in terms of tension force and leakage. After the failure threshold, seals start leaking excessively (> 1 mL/cycle) and are labeled as failed. From Figure 29, we can see that the compression and tension regions are mirror image of each other and therefore, we decided to utilize tension peak to predict the degradation process of reciprocating seals. The tension peak value is extracted from every tension cycles of the raw force signal; this way we reduced the complexity of the raw data while also preserving the characteristics of the original data as much as possible.
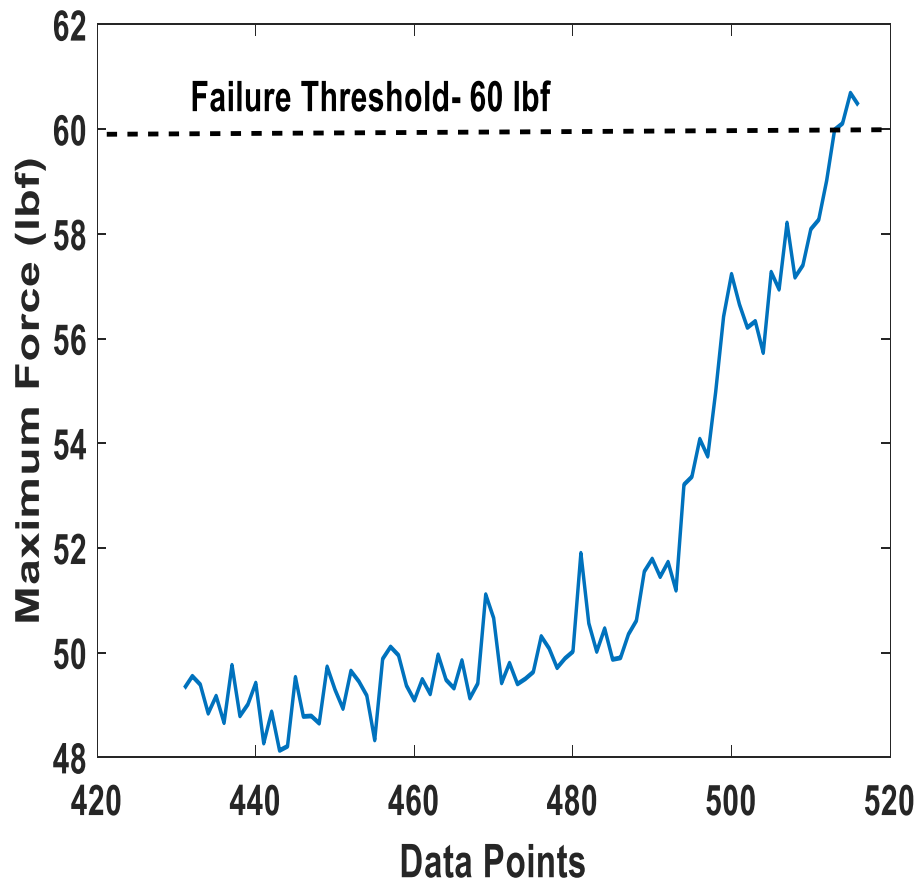
Figure 32: Degradation Region in Terms of Tension Peak
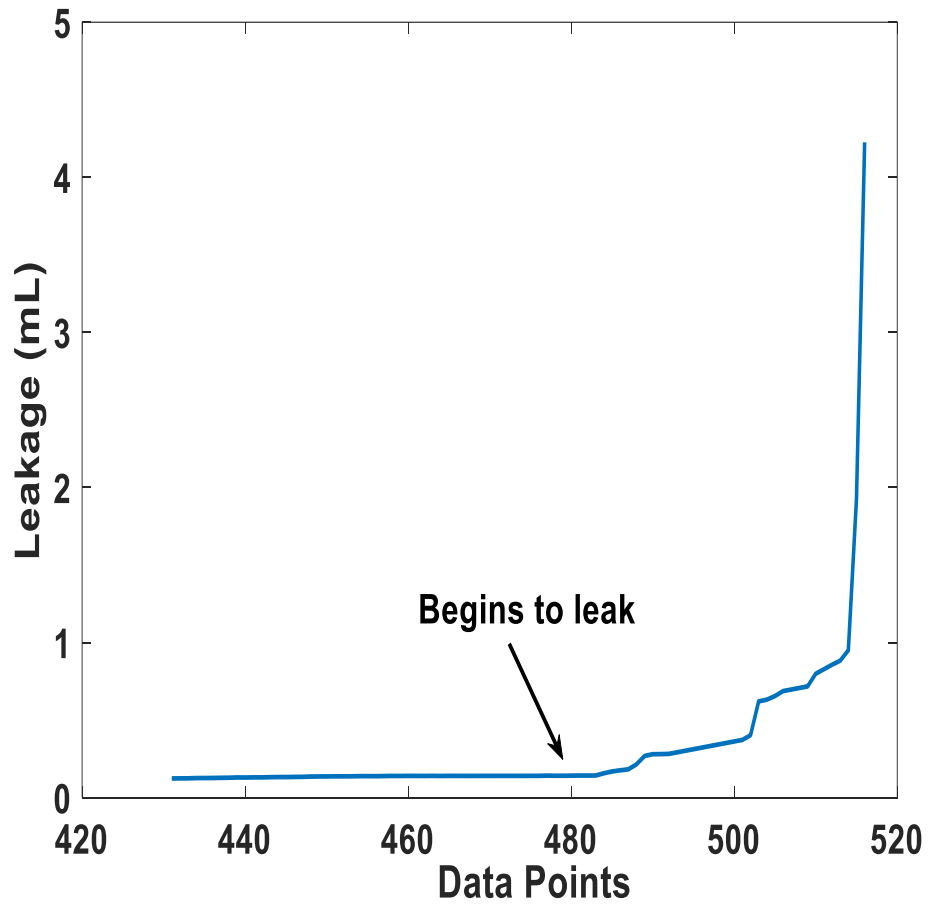
Figure 33: Degradation Region in Terms of Leakage

Out of eight run-to-failure tests, three tests (seal-1, seal-5, seal6) are used to develop the proposed model and the proposed model is tested on the rest. Figure 34 shows the normalized tension peak signal of run-to-failure tests.
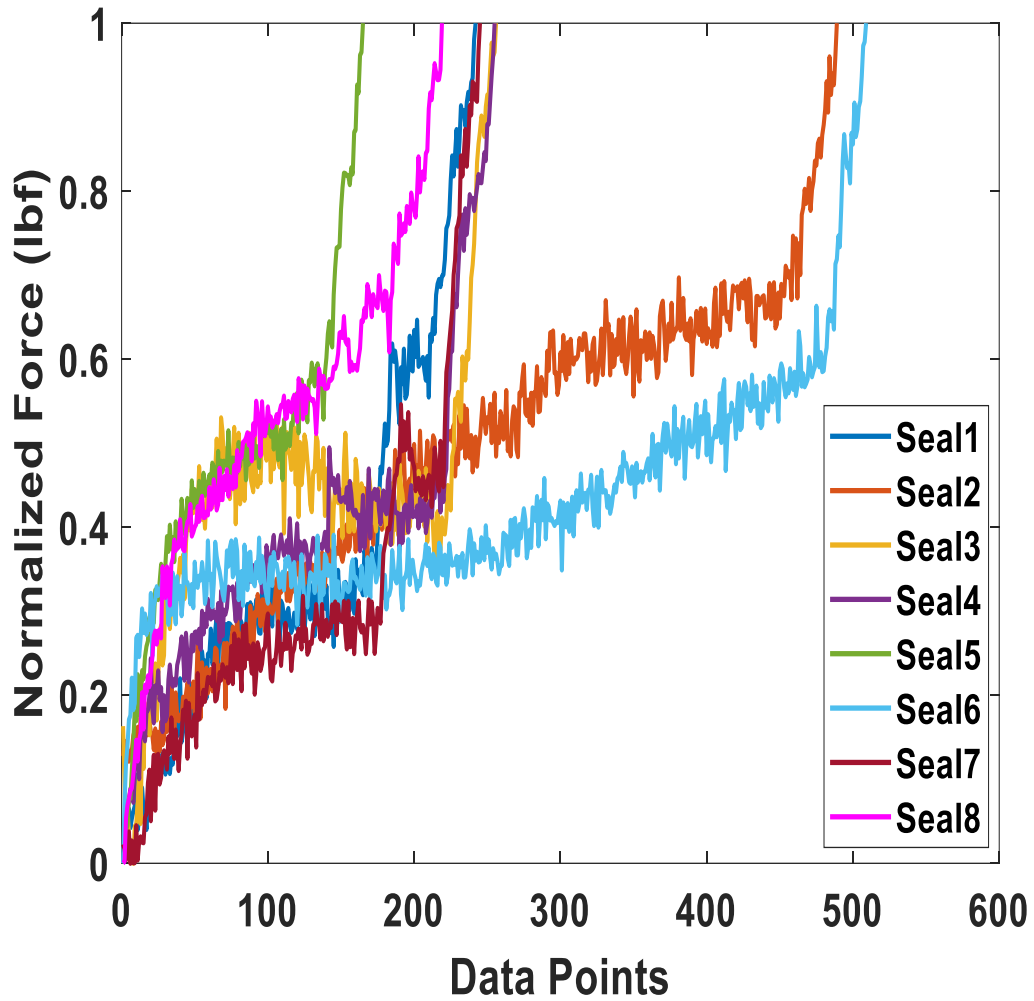
Figure 34: Normalized Tension Peak Signal of Run-to-Failure Tests

In order to verify if the tension peak feature would be an ideal indicator of reciprocating seal degradation, Spearman's rank correlation coefficient is used to assess the monotonic relationship between the tension peak and run-to-failure time duration of the test. The average correlation coefficient for the training samples is found to be 0.9592, which indicates tension peak to be a strong indicator of seals degradation process. Average mutual information method is used to estimate the time delay for the phase space reconstruction. It was found that the average mutual information function

value reached its first minimum when the time delay was 3 which can be observed in Figure 35. Then the embedding dimension is selected by the CAO method and Figure 36 shows the selection of the embedding dimension of tension force degradation signal and the optimal embedding dimension for the signal of interest is found to be 7.

Average Mutual Information (AMI)
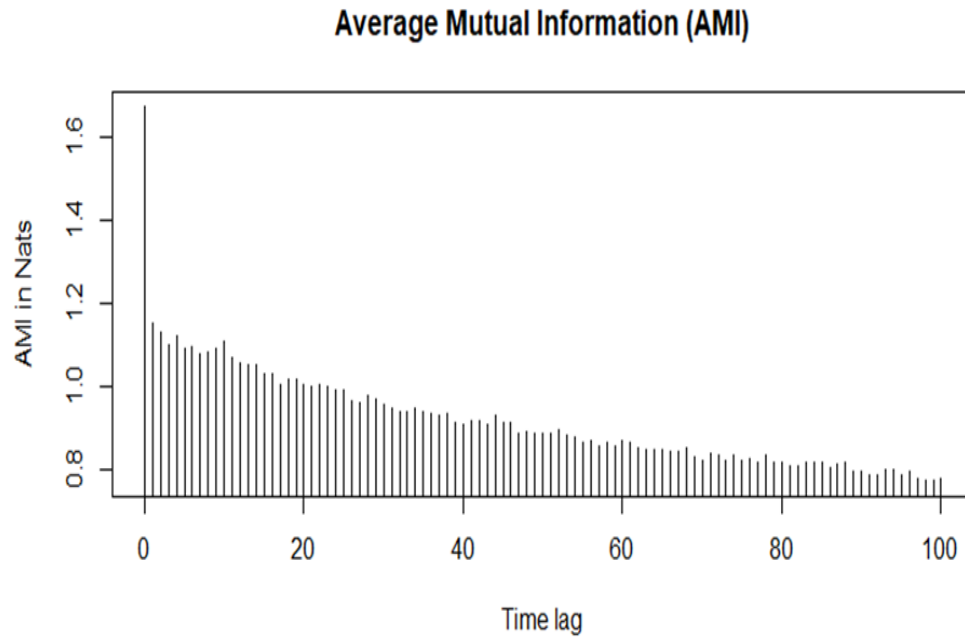
Figure 35: Time Delay Estimation Using Mutual Information Method

LIBSVM-3.1-Faruto ultimate 3.1 mode toolbox were used to implement SVM model. The performance of the SVM regression model depends on the penalty factor C and kernel parameter γ. In this study, an intelligent optimization algorithm: Particle Swarm Optimization was implemented to optimize the SVM parameters. Penalty factor C is an important parameter on which the accuracy of the regression model depends on. When the value of C is too large, the fitting of training samples will be very high, but the generalization ability of the model will be poor whereas when the value of C is too small, optimization process will take very long, and the search will be incomplete

66

leading to a model with poor fitting and low generalization ability. Therefore, the value

of *C* is usually between 0 and 100 to meet the requirements.
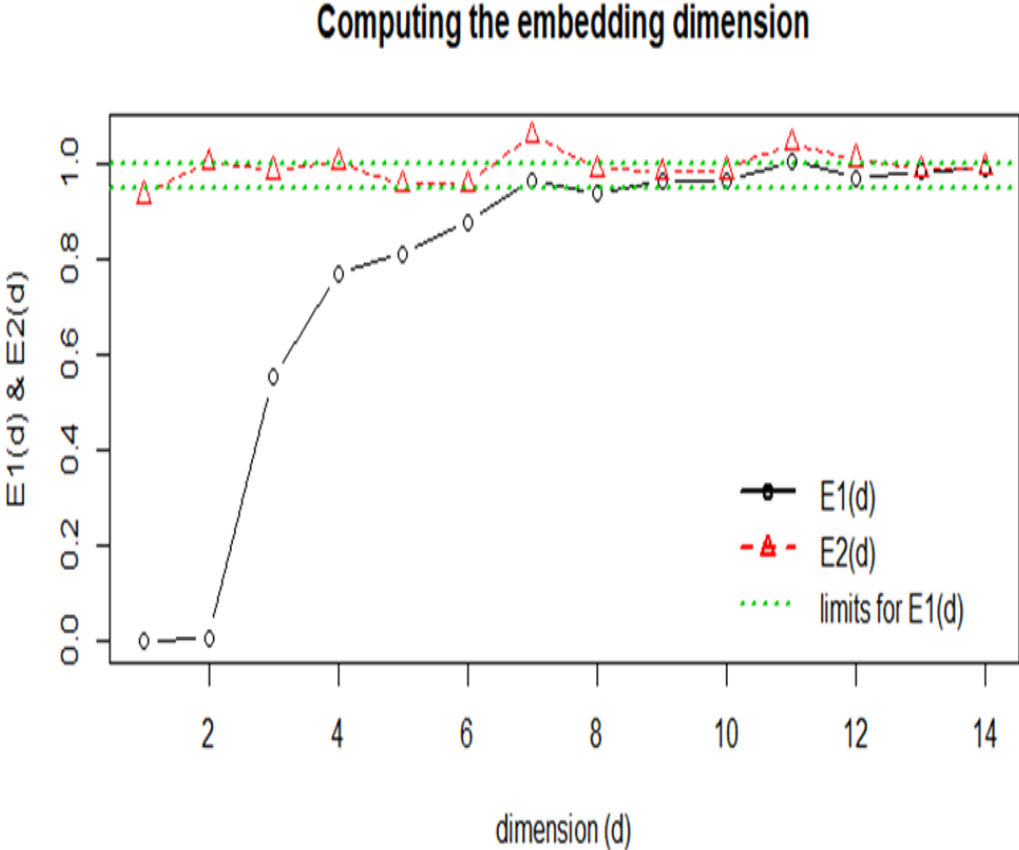
Figure 36: Embedding Dimension Estimation Using CAO Method

The initial parameters of PSO were set to $\omega = 0.6, C_1 = 1.5, C_2 = 1.7$,

maximum iteration was set to 100, population size was set to 20 and the penalty factor

was in the range of (0.1,100) and kernel parameter was in the range of (0.01, 1000).

When the termination condition was met the optimal parameters were found to be $C =$

15.8136 and $\gamma = 0.01$. The optimal SVM parameters are used to train the SVM model

and predict seals degradation. Three run-to-failure tests were used to train the optimized

SVM model and the model was tested on the remaining tests. We used the trained

model to predict the degradation region (the region before the seal approaches failure

threshold) of the remaining tests. The average test MSE of PSO-SVM model on the

unseen data was found to be 0.00206. Figure 37 shows the actual versus the predicted

trend of seal-2. It is obvious from Figure 37 that the predicted degradation trend is very

close to that of the actual trend.
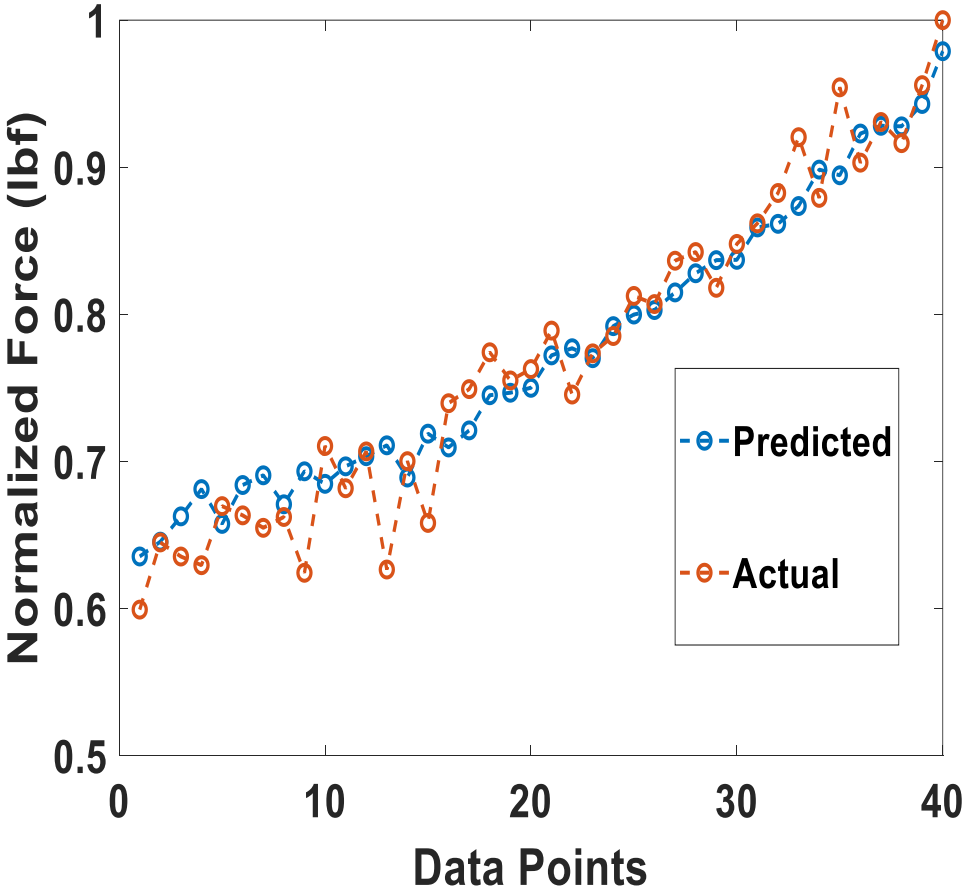
Figure 37: Actual Vs Predicted for Seal-2 Using Proposed Method

To validate the proposed approach, we used genetic algorithm to optimize SVM parameters and the optimized SVM model was tested on the unseen dataset. Also, we implemented an optimized distributed gradient boosting system: XGBoost to predict the degradation process of seals.

In addition to MSE, we also used Mean Absolute Error to compare the performance of different models. Table 5 shows the performance of the proposed approach compared to other machine learning algorithms ad it is found that the proposed method outperforms other methods used to validate our findings.

Table 5: Performance Comparison of PSO-SVM with Different Models

Failure Test	PSO-SVM		GA-SVM		XGBoost	
	MSE	**MAE**	**MSE**	**MAE**	**MSE**	**MAE**
Seal-2	**0.0010**	**0.0247**	0.0015	0.0283	0.0048	0.0575
Seal-3	**0.0029**	**0.0426**	0.0047	0.0563	0.0032	0.0480
Seal-4	**0.0017**	**0.0355**	0.0033	0.0510	0.0078	0.0791
Seal-7	**0.0031**	**0.0457**	0.0070	0.0726	0.0038	0.0517
Seal-8	**0.0015**	**0.0335**	0.0030	0.0468	0.0022	0.0369
Average	**0.0020**	**0.0364**	0.0039	0.0510	0.0043	0.05464

3.4 Summary

SVM has found to be effective in predicting the degradation of components such as batteries, bearings and other electronic components. There is little no research on the application of SVM in predicting the future running condition of polymeric components such as seals. In this study, we have presented a data-driven approach to predict the degradation process of reciprocating seals based on friction force using optimized SVM model. The most challenging aspect of tuning hyperparameters in SVM was carried out using particle swarm optimization. The proposed approach was validated using the data collected from an experimental test set-up dedicated to test reciprocating seals. This study finding shows that a hybrid approach of combining SVM model with PSO is effective in predicting the degradation process of reciprocating seal.

Chapter 4: Friction Force and Leakage Based Deep Neural Network for Predicting Remaining Useful Life of Reciprocating Seals

4.1 Introduction

Remaining Useful Life defined as "the length from the current time to the end of useful life" [62] aims to predict the remaining working time available before the seal fails. Therefore, accurate RUL is considered the most critical component in prognostics and health management since the maintenance decisions are made based on remaining useful life left in the component of interest. Although various performance related data like temperature, pressure, vibration and voltage could be collected to predict RUL of seals, friction force and leakage plays an important role in this task, which was discussed in Chapter 3.

4.1.1 Prognostic Health Indicators and Metrics for Assessment

Two important steps in developing an accurate RUL prediction is to: 1. Construct suitable indicators from friction force and leakage signal 2. Identify metrics to evaluate the suitability of constructed features for RUL prediction. RMS of the time domain vibration signal is the commonly used indicator to predict RUL of machinery. In [63], kurtosis and RMS was used to predict RUL of rolling bearing. RMS and peak values of wavelet coefficients was used in [64] to predict RUL of bearings. Spectral flatness [65] and entropy [66]of time domain signals are also used to predict RUL of bearings. To our knowledge, there is no previous work on the suitable indicators for RUL prediction of polymeric seals.

The next important step is to identify suitable features that can determine early degradation and can track the progression of degradation in seals. Degradation of components varies with time and the temporal information of degradation should be

beneficial in improving the RUL prediction [67]. Degradation of seals is assumed to be irreversible and the features reflecting the health of seals should possess a monotonically increasing or decreasing trend [68] and should correlate well with the progressively increasing degradation [38]. Also, they should be robust to noise and random fluctuation as the features with outliers would lead to poor prediction about RUL [69].

4.1.2 RUL Prediction Models

RUL prediction is categorized into physics-based and data-driven-based. The Paris-Erdogan is the commonly used physics-based model to study the RUL prediction of machinery in terms of crack growth [70]. Following the development of PE model, several other models including different versions of PE model such as empirical model [71] and state space model [72], other variants such as models based on Forman crack growth law [73], Norton law [74] and physical time-dependent crack growth model [75] have been developed to estimate RUL of different machineries including turbines, rotor shaft, turbo-propulsion systems, bearings, engines.

In recent years, deep neural network has emerged as one of the most effective methods for predicting remaining useful life. The multi-layer network can learn the complex non-linear relationships better than shallow ANN and are expected to perform better. Jia et al. [76] was the first to show the importance of DNN in fault diagnosis and health monitoring of rotating machinery. Ren et al. [77] built a DNN model using statistical time-frequency domain features to predict RUL of bearings. Deep Belief Network in addition to Convolutional Neural Network and autoencoder was used to

72

study faults in rolling bearings [78]. An integrated autoencoder with DNN was used for RUL prediction of lithium-ion battery [79].

In this chapter, DNN is used to predict RUL of reciprocating seals. Modes of reciprocating seal failure and the numerical models developed to study the degradation of this seals have been introduced in Chapter 3. Reciprocating test set-up and the run-to-failure test procedure to collect information on the performance degradation of reciprocating seals has been described in detail in Chapter 3.2.1 and 3.2.2. In the next section, construction of health indicators in terms of time and frequency domain features from force and leak signals and the metrics to evaluate the features for RUL prediction is explained in detailed, followed by DNN model for RUL prediction is presented. Results and discussion of the proposed approach is presented in results and discussion section and the study conclusions are summarized in summary section. Flowchart in Figure 38 shows the steps of this proposed approach.
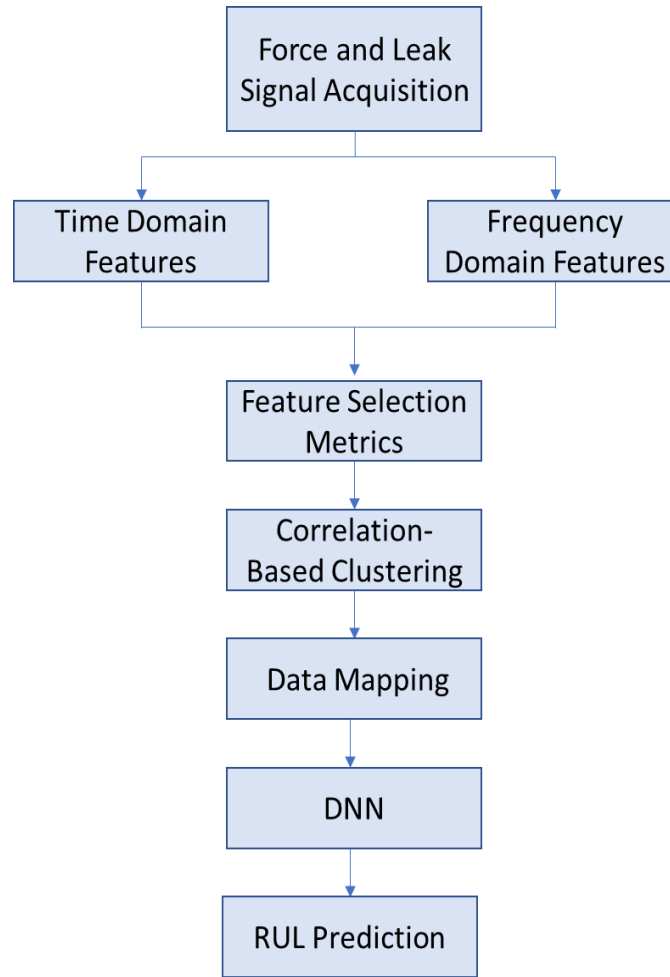
Figure 38: Flowchart Showing the Proposed RUL Approach

4.2 Methodology

4.2.1 Feature Extraction Methods

In this study, time domain features are extracted from the raw friction force signal obtained using reciprocating set-up. For time series x with a length of N, 11 different statistical features are calculated from raw signal. The most common time domain feature extraction method is to calculate the descriptive statistics, which measures the energy, amplitude and distribution of a signal over time [38, 40]. Table 6 shows the equation of time domain features (f_1-f_{12}) that are extracted from the force

signal and definitions can be found in [41]. Features f_1- f_3, f_7 & f_{12} show the change in

amplitude and energy of a signal over time while f_4- f_6 & f_8- f_{11} show the change in

distribution of a signal overtime with aging. In addition to time domain features, some

common statistical frequency domain features are also extracted from both force and

leakage signal. Table 6 shows the common statistical features in frequency domain that

are extracted from force (F_f_{13}-F_f_{15}) and leakage (L_f_{13}-L_f_{15}) signals. First, FFT is

applied to the raw data to transform time domain into its corresponding frequency

coefficients. Then, absolute values are calculated from the complex frequency

coefficients. Frequency domain features listed in Table 6 are extracted using the

absolute values which represent the strength of corresponding frequency coefficients in

the time domain data. In Table 6, $s(i)$ is a spectrum for $i= 1, 2, 3, ..., I$ where I is the

number of spectrum lines and f_i is the frequency value of the ith spectrum line. In

addition to frequency domain features extracted from leakage signal, the raw leakage

signal is aggregated by mean value to see how much the seals leak during ever cycle

(f_{16})

Table 6: Statistical Time and Frequency Domain Features from Force and Leakage Signals

Feature	Formula	Feature	Formula
Mean	$f_1 = \dfrac{1}{N}\sum_{i=1}^{N} x_i$	Standard Deviation	$f_9 = \sqrt{\dfrac{1}{N-1}\sum_{i=1}^{N}(x_i - \bar{x})^2}$
Root Mean Square (RMS)	$f_2 = \sqrt{\dfrac{1}{N}\sum_{i=1}^{N} |x_i|^2}$	Kurtosis	$f_{10} = \dfrac{\sum_{i=1}^{N}(x_i - \bar{x})^4}{(N-1)f_9^4}$
Maximum	$f_3 = max\{|x_i|\}$	Skewness	$f_{11} = \dfrac{1}{N}\sum_{i=1}^{N} \dfrac{(x_i - \bar{x})^3}{f_9^3}$
Impulse Factor	$f_4 = \dfrac{x_{max}}{|\bar{x}|}$	Minimum	$f_{12} = min\{|x_i|\}$
Crest Factor	$f_5 = \dfrac{x_{max}}{x_{rms}}$	Frequency Mean	$F\_f_{13}, L\_f_{13} = \dfrac{\sum_{i=1}^{N} s(i)}{N}$
Shape Factor	$f_6 = \dfrac{x_{rms}}{|\bar{x}|}$	Frequency RMS	F_f_{14}, L_f_{14} $= \sqrt{\dfrac{1}{N}\sum_{i=1}^{N} |s(i)|^2}$
Squared Mean Rooted Absolute Amplitude (SRA)	$f_7 = \left[\dfrac{1}{N}\sum_{i=1}^{N} \sqrt{|x_i|}\right]^2$	Frequency Standard Deviation	$F\_f_{15}, L\_f_{15} = \sqrt{\dfrac{\sum_{i=1}^{N} f_i^2 s(i)}{\sum_{i=1}^{N} s(i)}}$
Margin Factor	$f_8 = \dfrac{x_{rms}}{f_7}$	Leak Mean	$f_{16} = \dfrac{1}{N}\sum_{i=1}^{N} L_i$

4.2.2   Data Normalization

To eliminate the redundancy caused by features with different ranges of values,

features are transformed into same scale between 0 and 1 by the min-max normalization

method. This min-max normalization is given by:

$$\bar{x} = \frac{x - x_{min}}{x_{max} - x_{min}} \tag{1}$$

Where $\bar{x}$ is the normalized feature for feature x. This way each feature is given equal

importance in feature selection and in training phase.

4.2.3   Feature Selection Metrics

In chapter 2, we selected features based on their intraclass cohesiveness and

interclass separability for state-based prognostics and incase of remaining useful life

prognostics, it is important to evaluate the features based on their trending nature

reflecting degradation process effectively, robustness to outliers, etc. Three metrics

namely monotonicity, correlation and robustness are used to evaluate the capability of

the extracted features for RUL prediction and a weighted linear combination of the

three metrics is used to select the optimal features. The equations for calculating the

above-mentioned metrics are given below:

$$M(f_i) = \left| \frac{No\ of\ positives\ (\frac{d}{df_i} > 0)}{N - 1} - \frac{No\ of\ negatives\ (\frac{d}{df_i} < 0)}{N - 1} \right| \tag{2}$$

Where $M(f_i)$ refers to monotonicity which measures the increasing or decreasing trend information in the feature f_i. $\frac{d}{df_i}$ is the difference between two successive points in feature f_i and N is the length of the feature.

$$C(f_i, t_i) = \frac{Cov(f_i, t_i)}{\sigma_{f_i}, \sigma_{t_i}} \tag{3}$$

Where $C(f_i, t_i)$ refers to Pearson's correlation coefficient which measures the linearity between the feature f_i and degradation time t_i and $Cov(f_i, t_i)$ measures the covariance of the feature f_i with time t_i and σ is the standard deviation of the feature and time vector.

$$f_i = trend\ f_i - res\ f_i \tag{4}$$

$$R(f_i) = \frac{\sum_n^N exp\left(-\left|\frac{res\ f_i}{f_i}\right|\right)}{N} \tag{5}$$

Where $R(f_i)$ is a robustness metric which begins with the decomposition of a feature f_i into trend $(trend\ f_i)$ and residual $(res\ f_i)$ components. This measures the features' tolerance to noise and outliers which may be due to sensor noise, the stochasticity nature of bearing degradation or due to fluctuations in the operating conditions.

One metric is not enough to measure the capability of features for the RUL prediction and therefore multiple metrics are used in this study to evaluate features. A weighted linear combination of the three metrics is used to select the features [69]. This is formulated as a constrained optimization problem which is given as:

$$maximize\ Cri = \quad \omega_1 M(f_i) + \omega_2 C(f_i) + \omega_3 R(f_i) \tag{6}$$

$$subject\ to\ \sum_i \omega_i = 1, \quad i = 1,2,3 \tag{7}$$

$$\omega_i > 0 \tag{8}$$

Where Cri is the objective to be maximized and ω_i is the weights of the metrics. The objective function Cri is linearly and positively correlated with each metrics and their values range between 0 and 1. The feature with high Cri value is supposed to have a better predictive performance in estimating RUL of seals.

4.2.4   Correlation-Based Clustering

Features selected based on the hybrid metric might possess redundant information in terms of degradation trends of seal. To remove the redundancy, correlation-based clustering method is employed which consists of three steps: 1. normalizing data, 2. implementing clustering algorithm with an appropriate distance measure and 3. validating clustering algorithm's performance using a suitable clustering validation index.

Hierarchical clustering, a type of agglomerative clustering method is applied to repeatedly combine two nearest clusters into a largest cluster. This starts with each feature as a separate cluster and then identify two clusters that are similar and combine them into one large cluster until all the features are in a single cluster and the output of hierarchical clustering is represented by a dendrogram—a tree structure plot. The similarity between two features are measured in terms of Pearson's correlation coefficient which is calculated using:

$$Corr(u,v) = \frac{Cov(u,v,)}{\sigma_u, \sigma_v} \tag{9}$$

Where, $Corr(u,v)$ is the covariance of the feature u with feature v and σ is the standard deviation of the feature vector.

In clustering analysis, the distance between two features are measured in terms of dissimilarity instead of similarity, therefore 1 minus correlation coefficient is used to measure the distance and based on this, two features with a smaller distance is considered to have more similarity than the ones with larger distance. The distance between two features are given as:

$$dist(u,v) = 1 - Corr(u,v) \tag{10}$$

The inter-cluster distance between two clusters m and n are measured using the average linkage method which is given as:

$$dist(m,n) = \frac{\sum_{u=1}^{N_m}\sum_{v=1}^{N_n} dist(u,v)}{N_m N_n} \tag{11}$$

Where N_m is the number of features in cluster m and N_n is the number of features in cluster n. At each stage of clustering two nearest clusters are identified and merged as one single cluster.

Finally, the performance of the clustering algorithm is validated using Kelley Gardner Sutcliffe (KGS) penalty function, i.e. this function is used to select the optimal number of clusters [80]. This function compares the mean spread across all the clusters with the mean spread within cluster of dissimilarity measure. The objective of this

method is to maximize the spread between clusters and cohesiveness within clusters. It begins by calculating average spread value at each clustering level of dendrogram. At each stage of clustering, the spread of a cluster m containing N members is calculated using:

$$S_m = \frac{\sum_{i=1}^{N} \sum_{k=i+1}^{N} dist(i,k)}{N\,(N-1)/2} \tag{12}$$

Where i and k are members of cluster m and the average spread is given by:

$$AvgS_i = \frac{\sum_{m=1}^{\#N_i} S_m}{\#N_i} \tag{13}$$

Where $\#N_i$ is the number of clusters at each clustering stage i of the clustering.

Following that, the average spread value at each clustering stage i is normalized between 1 and N-1, where N is the number of structures in original dataset. This normalization is to give equal weightage to the number of clusters and average spread in the penalty function and it is as follows:

$$AvgS(norm)_i = \left(\frac{N-2}{Max(AvgS) - Min(AvgS)}\right)\left(AvgS_i - Min(AvgS)\right) + 1 \tag{14}$$

Where $Max(AvgS)$ and $Min(AvgS)$ are the maximum and minimum values of normalized average spread values. The penalty function value P$_i$ for each stage of clustering i is given using:

$$P_i = AvgS(norm)_i + \#N_i \qquad (15)$$

From the calculated penalty function value for each level, the level with minimum value $Min(P)$ is selected as the cut-off value in order to identify the consistent and distinct clusters. This is the level where there is a smaller spread within the members of the cluster.

$$P_{icut} = Min(P) \qquad (16)$$

4.2.5 Data Mapping

The next step towards building a RUL prediction model is to map y_i (RUL of seals) with the selected features x_i. The output of the model is predicted in terms of normalized remaining useful life percentage of seals which is calculated as follows:

$$y_i = \frac{N - i}{N} \qquad (17)$$

where N is the total number of strokes.

This way the selected features are mapped to the respective normalized life y_i before the training process. The seal is totally damaged when the y_i has reached 0.

4.2.6 Deep Neural Network

Deep Neural Network, a supervised learning model is used to predict RUL of reciprocating seals. DNN is stacked layers of neurons where neurons are connected layer by layer where as there is no connection between the neurons in the same layer. It consists of an input layer, output layer and a few hidden intermediate layers between them. Each hidden layer of DNN can be the output of non-linear transformation and

therefore DNN has more expressive capability than shallow neural network. The dimensionality of the input data and target decides the number of neurons in the input and output layer. Here neural network is a regressor, therefore output layer has single neuron. There is no fixed rule on the number of units in hidden layers but the optimal number is usually between the number of neurons in the input and output layers. Using a few neurons in hidden layers will result in underfitting where they do not adequately learn the degradation trend in the signals while having too many neurons will lead to overfitting where the network has increased processing capability and limited information in training is not enough to train all the neurons in the hidden layer. The non-linear relationships between the adjacent layers are given as:

$$x_j^m = \sigma(z_j^m) \tag{18}$$

$$z_j^m = \sum_i \omega_{ij} x_i^{m-1} + b_j^m \tag{19}$$

Where x_j^m is the activation of neuron j in layer m, z_j^m is defines the non-linear relationships between the adjacent layers. b_j^m is the bias vector of neuron j in layer m and ω_{ij} is the weight matrix between layer i and j.

In DNN, each of the intermediate hidden layer and output layer uses a non-linear activation function which is expressed as $\sigma(z)$. ReLu, tanh and sigmoid are some of the commonly used activation functions. DNN parameters such as weight and biases are randomly initialized and the output is calculated layer by layer for the given input and model parameters. We train the network and optimize the model parameters until the error (MSE) is minimized.

In order to evaluate the performance of DNN in predicting the RUL of

reciprocating seals, Mean Square Error (MSE) and Mean Absolute Error (MAE) are

used to assess the prediction accuracy and to compare the performance with other

models. Two different MSE and MAE, calculated using Eq. 20 and 21: 1. MSE and

MAE is calculated for prediction throughout seals life including early, mid and end life,

2. The prediction accuracy towards the end of seals life is more important than accurate

prediction during seals' early and mid-life as this will more likely affect the decision on

whether seals should be changed. Therefore, I compare the prediction performance of

the last 20 performance points before the failure to validate the approach.

$$MSE = \frac{1}{N} \sum_{i=1}^{N} (p_i - y_i)^2 \tag{20}$$

$$MAE = \frac{1}{N} \sum_{i=1}^{N} |(p_i - y_i)| \tag{21}$$

where N is the total number of data points, y_i is the actual value and p_i is the predicted

value of the model.

4.3 Results and Discussion

First, the entire time series is segmented into n segments and features are

extracted from each segments of the time series. For example, length of seal-1 run-to-

failure test is 60,372 and it is segmented into 774 segments (774 cycles). In this study,

19 different features in time and frequency domain are extracted from friction force and

leakage signals as listed in Table 6. One of the primary reasons for the reciprocating

seal to fail is due to rolling, during which the friction increases leading to increased friction force and leakage.

Typically two varying patterns are observed in these 19 features namely: monotonic increasing trend and features with no trend. As the seal degrades features such as the mean, RMS, maximum, standard deviation and minimum of force signal; frequency mean, frequency RMS, frequency standard deviation of force and leakage signal; and mean leakage signal are found to be monotonically increases with degradation. Figure 39 shows certain features extracted from force signal that shows monotonic trend and Figure 40 shows certain features extracted from leakage signal that exhibit monotonic trend. The rest of the features such as skewness margin factor, impulse factor, shape factor, etc. has no trend even after the seals begin to degrade. Figure 41 shows certain feature that has a weak /no trend.
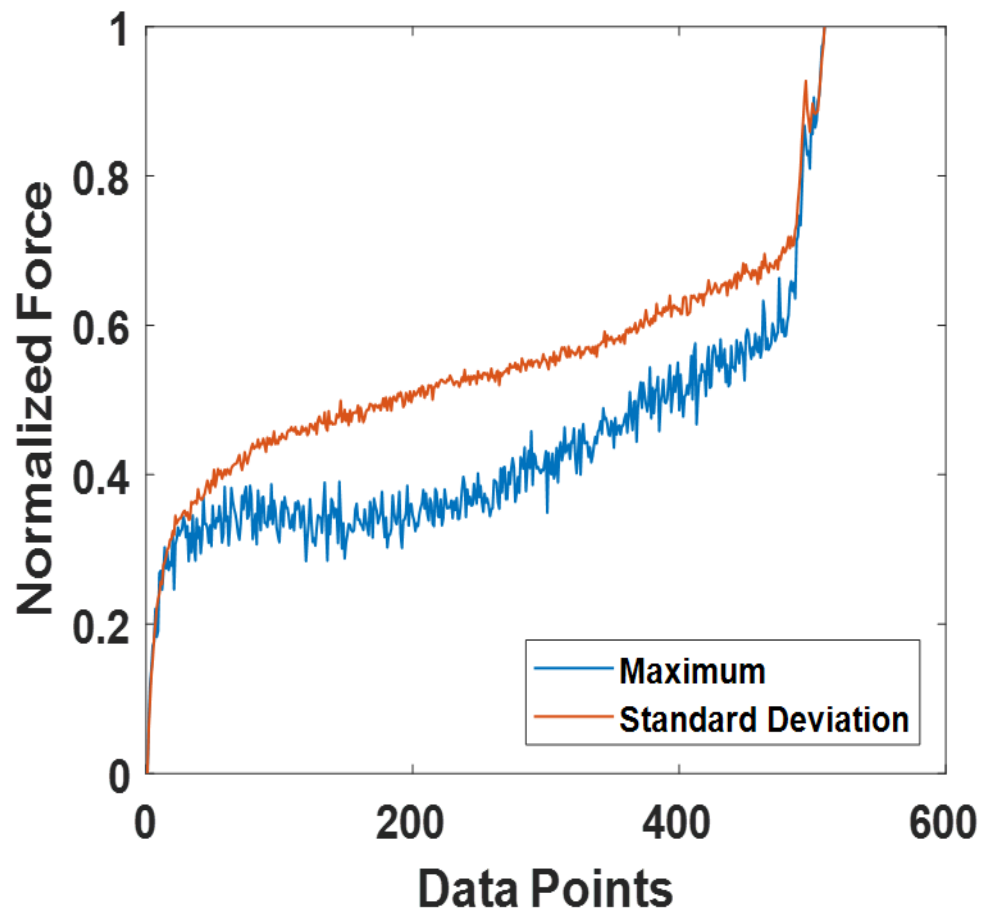
Figure 39: Monotonic Trend Exhibiting Features Extracted from Force Signal
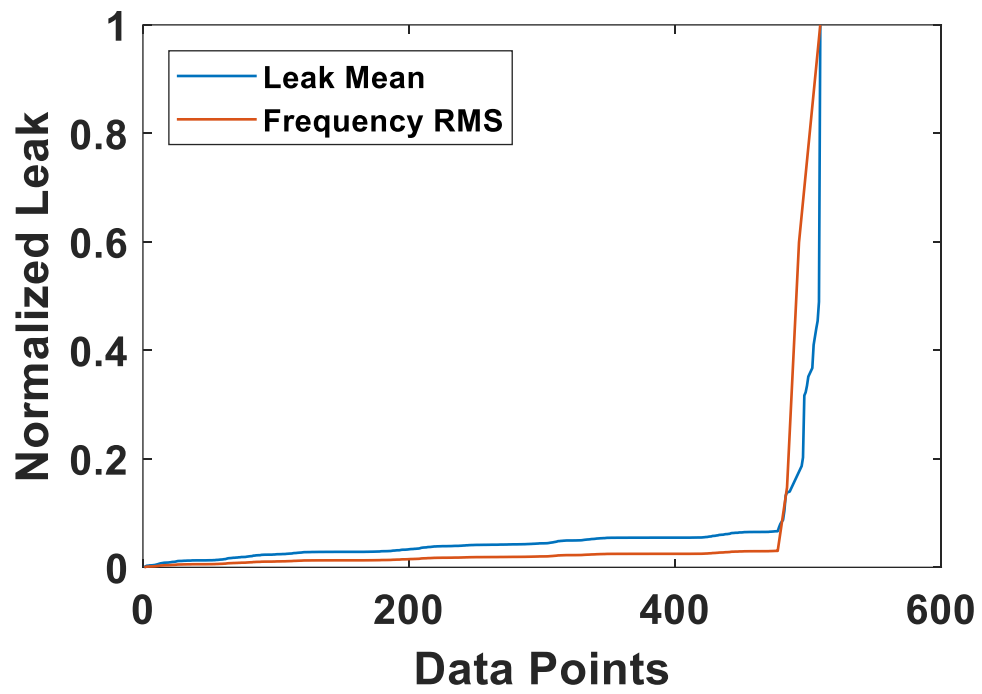
Figure 40: Monotonic Trend Exhibiting Features Extracted from Leakage Signal
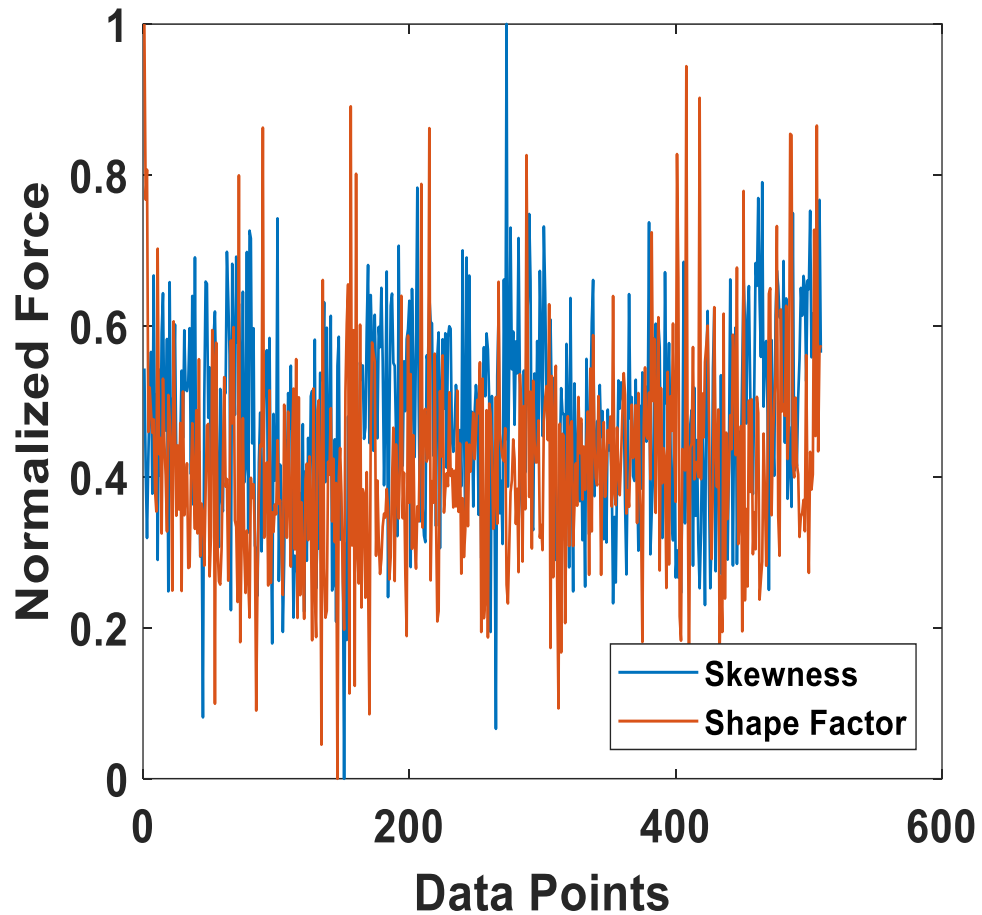
Figure 41: Features Exhibiting Weak/No Trend

After feature extraction, features are normalized using min-max normalization into [0,1] range. Monotonicity, correlation and robustness of each of the extracted features are calculated using Eq. (2-5) and a weighted linear combination of the three metrics is used to rank the features. Features with high monotonicity (i.e.) the one with increasing trend is more desired than the correlation and robustness metric of features. Based on this, 0.5, 0.3 and 0.2 weights are chosen for monotonicity robustness and correlation metrics to calculate the criteria using Eq. (6). The criteria based on the three metrics are calculated for the 19 original features and the features with the criteria value

greater than 0.5 are selected. It can be seen from Table 7, out of 19 features, 12
extracted features have their values greater than 0.5.

Table 7: Feature Selection Ranking Based on the Three Metrics

Features	Monotonicity	Correlation	Robustness	Cri
f_1	0.1842	0.9016	0.9824	**0.5672**
f_2	0.1875	0.9032	0.9839	**0.5696**
f_3	0.1181	0.8939	0.9522	**0.5235**
f_4	0.0283	0.4636	0.8453	0.3605
f_5	0.0332	0.4727	0.8495	0.3660
f_6	0.0299	0.2016	0.8139	0.2994
f_7	0.1262	0.8992	0.9763	**0.5358**
f_8	0.0191	0.4560	0.8431	0.3537
f_9	0.1929	0.9018	0.9840	**0.5720**
f_{10}	0.0337	0.2540	0.8513	0.3230
f_{11}	0.0144	0.1701	0.8162	0.2861
f_{12}	0.0804	0.8513	0.9514	0.4959
F_f_{13}	0.1264	0.8277	0.9710	**0.5200**
F_f_{14},	0.1908	0.9032	0.9849	**0.5715**
F_f_{15}	0.1927	0.9028	0.9827	**0.5718**
L_f_{13}	0.6860	0.6391	0.9747	**0.7632**
L_f_{14}	0.8000	0.6361	0.9856	**0.8229**
L_f_{15}	0.7848	0.6317	0.9861	**0.8146**
f_{16}	0.7405	0.6562	0.9729	**0.7933**

The redundancy in the selected features are eliminated using KGS penalty
function-based correlation-clustering algorithm. Correlation coefficient was used to as a
measure to cluster features using hierarchical clustering. At each stage of correlation-
based clustering algorithm identifies two nearest clusters and merge them as one single
cluster. Figure 42 shows the results of cluster analysis in the form of tree diagram called
a dendrogram. KGS penalty function was used to validate clustering algorithm's
performance. This function selected optimal number of clusters based on comparing the
mean spread across all the clusters with the mean spread within cluster dissimilarity

measure. This method applied at each clustering level and the level with a minimum penalty value is the optimal number of clusters. It can be seen from Figure 43 the penalty value is minimum for level with 5 clusters and the colored rectangular boxed in Figure 42 shows the optimal clusters. Therefore, one feature with maximum criteria from each cluster is selected to build a RUL prognostics model. In this study, I decided to use multiple features instead of single feature in order to avoid loss of any information that may be critical in assessing seal's degradation.
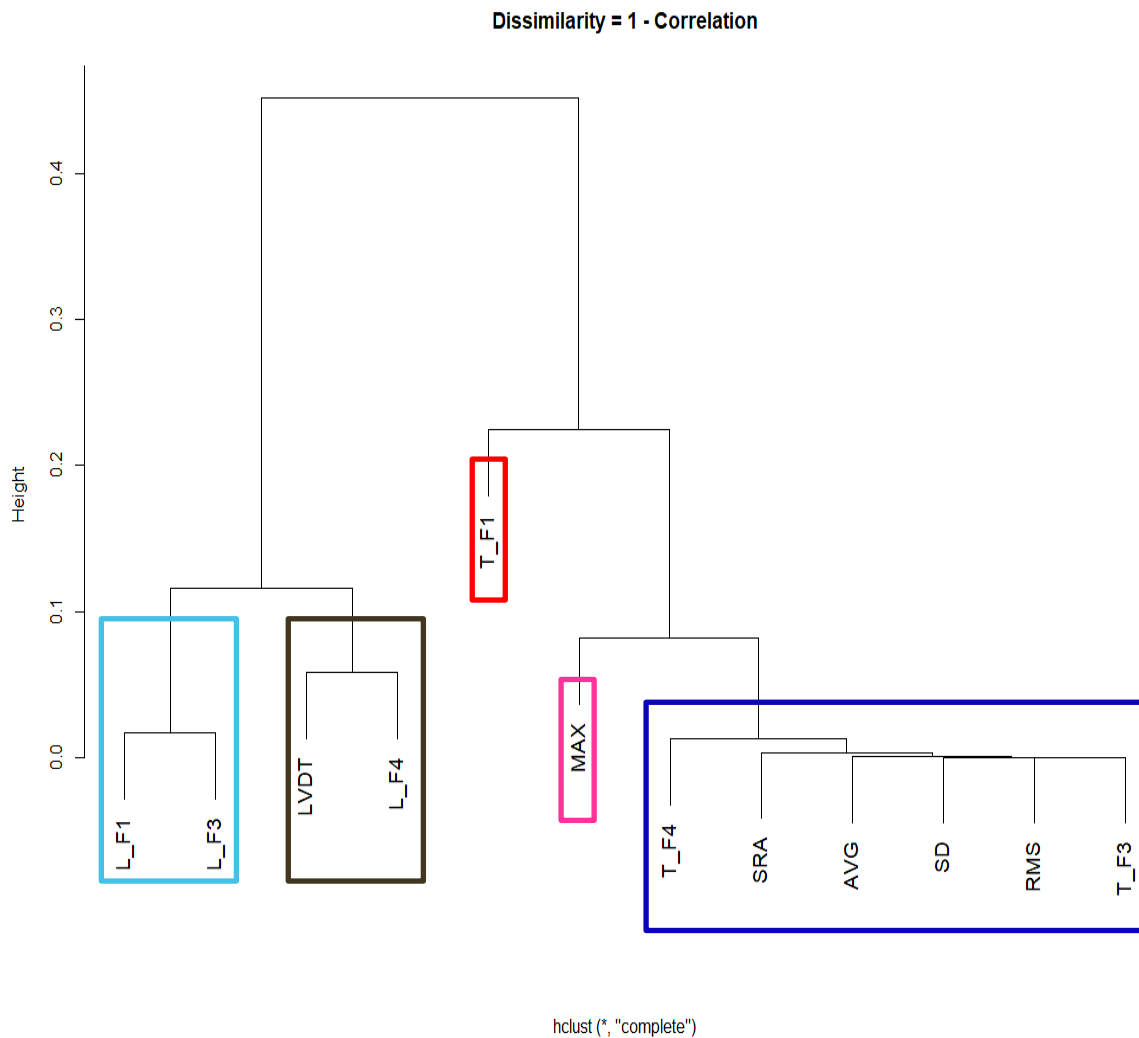
Figure 42: Clusters After Correlation-Based Clustering
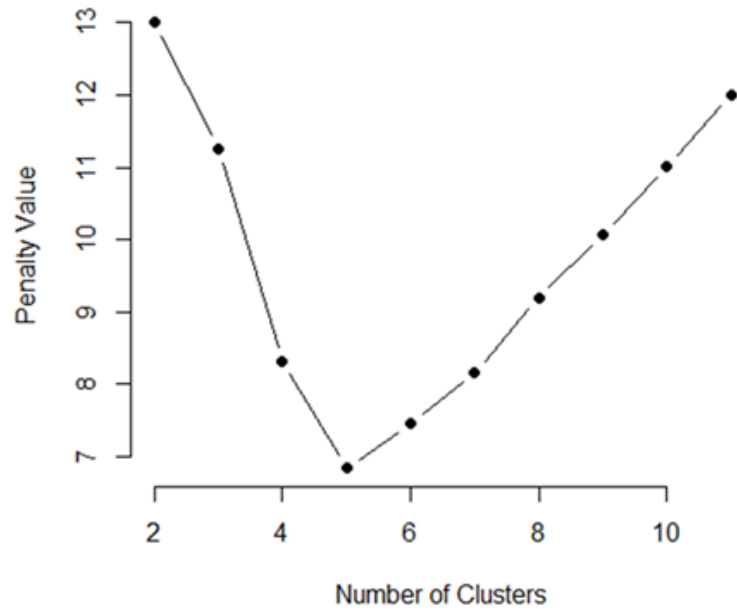
Figure 43: KGS Penalty Function Showing the Optimum Number of Clusters

The selected features are mapped with the respective y_i (remaining useful life) values before building the prognostics model. The normalized values of current (t) and previous (t-1) values were used as the input to train DNN parameters and remaining useful life is selected as the output of DNN model. The loss function was Mean Square Error (MSE) which estimates the accuracy of neural network in predicting the test data. Validation split was set to 0.2, where the model is trained on 80% of the data and tested on remaining 20% data. The trained model consisted of four fully connected layers with number of neurons of 10, 7, 6, 1 in each layer. The ReLu function was used as the activation function of intermediate hidden layer and sigmoid was used for he output layer. Optimization algorithm plays an important role in training deep neural network model to learn the locally optimal model variables. RMS prop was used as the optimization algorithm. The model is trained for 500 epochs with expectation that loss will decrease with each epoch and the prediction accuracy of the model improves

91

during the training. Early stopping condition was used to avoid overfitting by using cross-validation. The training was stopped when the MSE of validation set began to increase.

Three run-to-failure tests were used to train the DNN model and the trained model was tested on the remaining tests. The average test MSE of DNN model on the unseen data was found to be 0.0248 when tested on the entire life of seals whereas the average test MSE_{20} towards the end of seal life is 0.0007. Figure 44 and 45shows the actual versus the predicted trend of seal-2 and seal-8 It is obvious from Figure 44 and 45 that the predicted degradation trend is very close to that of the actual trend atleast towards the end of seal life than early and middle life.
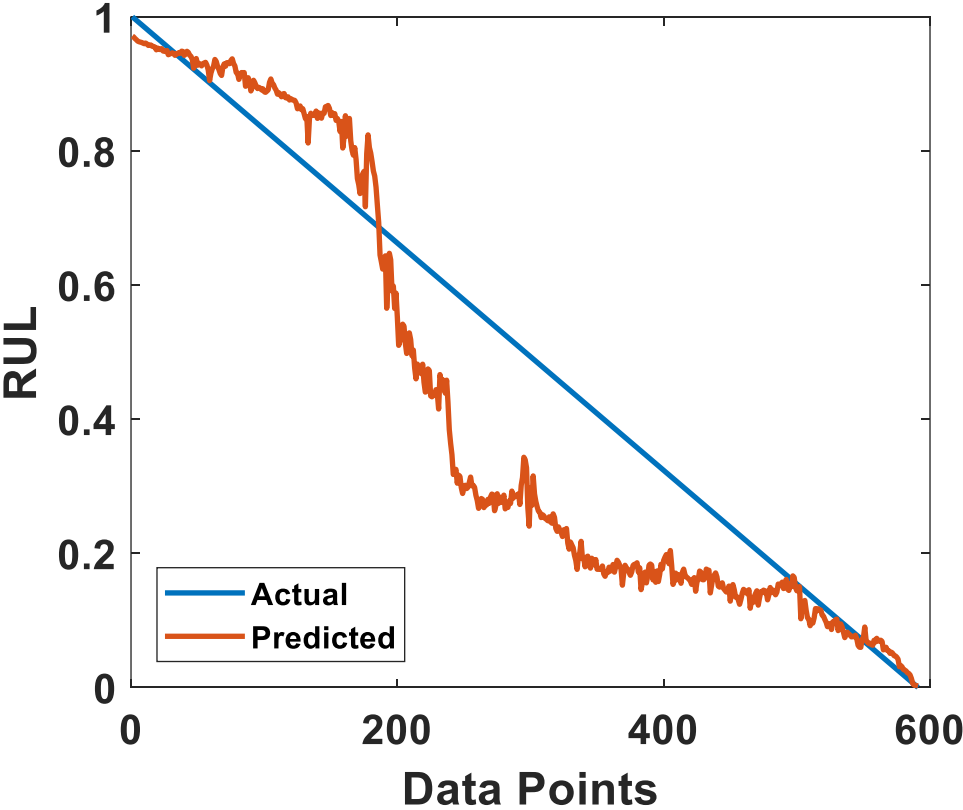
Figure 44: Actual Vs Predicted for Seal-2 Using Proposed Method

To validate the proposed approach, we used PSO to optimize SVM parameters and the optimized SVM model was tested on the unseen dataset. Also, we implemented an optimized distributed gradient boosting system: XGBoost to predict the degradation process of seals.

In addition to MSE, we also used Mean Absolute Error to compare the performance of different models. Table 8 and 9 shows the performance of the proposed approach compared to other machine learning algorithms and it is found that the proposed method outperforms other methods used to validate our findings.
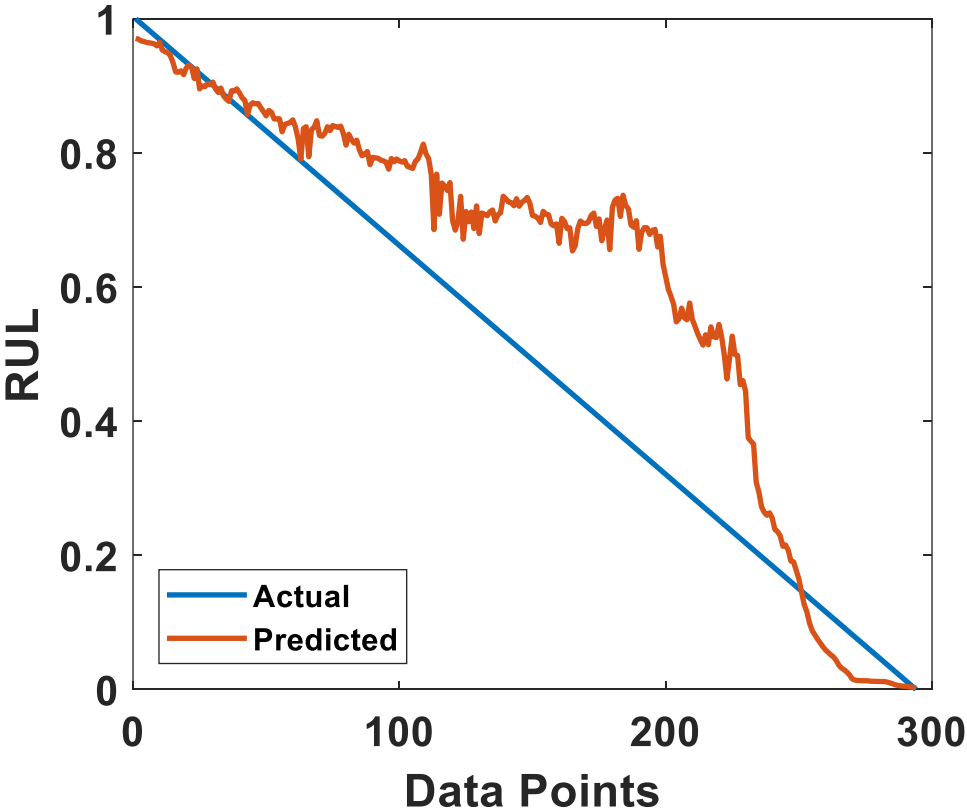
Figure 45: Actual Vs Predicted for Seal-8 Using Proposed Method

Table 8: Performance Comparison of DNN with Different Models Using All Predicted Values

Failure Test	PSO-SVM		XGBoost		DNN	
	MSE	MAE	MSE	MAE	MSE	MAE
Seal-2	0.0255	0.1315	0.0258	0.1398	**0.0185**	**0.1058**
Seal-3	0.0282	0.1288	0.0280	0.1517	**0.0278**	**0.1283**
Seal-4	0.0088	0.0805	0.0270	0.1477	**0.0059**	**0.0623**
Seal-7	0.0599	0.2114	0.0624	0.2175	**0.0597**	**0.2018**
Seal-8	0.0303	0.1480	0.0120	0.0887	**0.0119**	**0.0845**
Average	0.0305	0.1400	0.0310	0.1491	**0.0248**	**0.1166**

Table 9: Performance Comparison of DNN with Different Models Using Last 20 Predicted Values

Failure Test	PSO-SVM		XGBoost		DNN	
	MSE_{20}	MAE_{20}	MSE_{20}	MAE_{20}	MSE_{20}	MAE_{20}
Seal-2	0.0491	0.2145	0.0519	0.2275	**0.0001**	**0.009**
Seal-3	0.0136	0.1160	0.0491	0.2213	**0.0008**	**0.0242**
Seal-4	0.0178	0.1324	0.0437	0.2079	**0.0005**	**0.0188**
Seal-7	0.0158	0.1251	0.1369	0.3698	**0.0004**	**0.0161**
Seal-8	0.0301	0.1715	0.0408	0.2002	**0.0017**	**0.0345**
Average	0.0253	0.1519	0.0645	0.2454	**0.0007**	**0.0205**

4.4 Summary

In this chapter, remaining useful life prediction of reciprocating seal using deep neural network is presented. Two important aspects of RUL prediction is addressed in this chapter: 1. Extraction of features that reflect progression of seals degradation from performance signals, 2. Evaluation and selection the features that are suitable for RUL prediction. Time and frequency domain features are extracted from the friction force and leakage signals. Degradation of seals is assumed to be irreversible and the features reflecting the health of seals should possess a monotonically increasing or decreasing trend and should correlate well with the progressively increasing degradation. Also, they should be robust to noise and random fluctuation as the features with outliers would lead to poor prediction about RUL. Prognostic features with better monotonicity, high correlation with degradation time and more robust to outliers was selected and the redundancy information in the selected features is eliminated by clustering the similar features together using correlation-clustering algorithm. Then KGS penalty function value was used to select the optimal number of clusters and the feature with maximum trendability from each cluster are selected as the suitable features to build a DNN model to estimate the RUL of seals. Run-to-failure data collected from a reciprocating set-up was used to validate this approach. In addition to this, the performance of the model is compared with PSO-SVM and XGBoost regression.

Chapter 5: Conclusions, Implications and Possible Future Work

5.1 Conclusions

The oil & gas industry is capital-intensive, and it is important to keep the equipment in top operating condition to help maintain efficient process operations. The key aspects of prognostics include improving equipment availability by minimizing equipment downtime, preventing catastrophic failure, improving rate of return on equipment by predicting incidents before they happen, reducing operational risk of critical equipment and enabling appropriate timely and maintenance decisions. Prognostics and Health Management of polymeric seals from physics-based perspective often requires mechanical, material and seal related measurements to be made, which makes it hard on oil field operators to make these measurements between operations. The aim of this dissertation was to develop a data-driven prognostics model for dynamic seals such as rotary and reciprocating seals used in the oil & gas industry. The goal and associated tasks listed in Chapter 1.2 are accomplished by developing a multilayer perceptron model to differentiate the health state of rotary seals, a hybrid PSO-SVM model to assess the degradation of reciprocating seal from incipient state up until failure and a deep neural network model based on force and leakage signals to predict the remaining useful life of reciprocating seal. The dissertation conclusions, implications and possible future work are summarized below.

First, we have proposed a multi-sensor-based performance degradation assessment approach utilizing friction torque and leakage signals to classify the

96

running/health condition of rotary seals. To make the degradation pattern more obvious to the classifier, statistical time domain features were extracted from raw torque signals and change in fluid volume and frequency domain features were extracted from leakage signals. An optimal feature subset was selected using RFE with MLP neural network utilized as classification algorithm to best fit the relationship between the relevant features and the running condition of rotary seals. The proposed approach has shown that features extracted from torque and leakage lack a better discriminating power on its own in classifying the running condition of seals throughout its service life. Statistical features related to the amplitude of torque signal and the change in fluid volume every five minutes were found to be the optimal set of features using RFE search algorithm. The classifier built using optimal set of features from torque and leakage signals has resulted in a better classification accuracy when tested on an unseen data even at different temperature. Therefore, the implementation of multi-sensor based prognostic model results in the most reliable performance assessment of rotary seals.

SVM has found to be effective in predicting the degradation of components such as batteries, bearings and other electronic components. There is little no research on the application of SVM in predicting the future running condition of polymeric components such as seals. In this study, we have presented a data-driven approach to predict the degradation process of reciprocating seals based on friction force using optimized SVM model. The most challenging aspect of tuning hyperparameters in SVM was carried out using particle swarm optimization. The proposed approach was validated using data collected from an experimental test set-up dedicated to test reciprocating seals and also by comparing the performance of the trained model by testing the unseen data using

GA-SVM and XGBoost regression. This study finding shows that a hybrid approach of combining SVM model with PSO is effective in predicting the degradation process of reciprocating seal.

Finally, remaining useful life prediction of reciprocating seal using deep neural network is presented. Two important aspects of RUL prediction are addressed in chapter 4: 1. Extraction of features that reflect progression of seals degradation from performance signals, 2. Evaluation and selection the features that are suitable for RUL prediction. Time and frequency domain features are extracted from the friction force and leakage signals. Degradation of seals is assumed to be irreversible and the features reflecting the health of seals should possess a monotonically increasing or decreasing trend and should correlate well with the progressively increasing degradation. Also, they should be robust to noise and random fluctuation as the features with outliers would lead to poor prediction about RUL. Prognostic features with better monotonicity, high correlation with degradation time and more robust to outliers was selected and the redundancy information in the selected features was eliminated by clustering the similar features together using correlation-clustering algorithm. Then KGS penalty function value was used to select the optimal number of clusters and the feature with maximum trendability from each cluster are selected as the suitable features to build a DNN model to estimate the RUL of seals. Run-to-failure data collected from a reciprocating set-up was used to validate this approach. In addition to this, the performance of the model was compared with PSO-SVM and XGBoost regression and the proposed approach was found to be effective.

5.2 Implications

Till date, in oil & gas industry, maintenance decisions are made by the deep domain(subject-matter) expertise who has been operating these machineries in field for more than two-to-three decades. These decisions are mostly based on the observing the physical behavior of seals. This industry is now seeing a decline in the number of experienced experts and it is important to move into data-driven prognostics from the physics-based approach. The approach outlined in this dissertation would be a foundational in moving towards that direction.

In a rotating machinery, when a rotary seal fail, the contaminants from outside enter the cavity which will affect the performance of bearing that support the shaft in operating conditions. The performance degradation in bearing will result in excessive shaft run-out due to increased vibration which will be transferred to other components in the machinery resulting in costly downtime and large expenses. In the last decade, several studies have explored the vibration-based bearing prognostics and it has been shown to be effective in predicting the degradation of bearings. The torque and leakage-based prognostics method presented in this study could be implemented along with the vibration-based bearing prognostics to isolate and differentiate the defects in rotary machinery caused due to bearings and seals.

Data-driven prognostics has two phases: offline and online phase. The offline phase is where the performance related data from the component of interest are acquired, pre-processed and followed by feature engineering, model training and model evaluation. The developed models are then deployed online where the condition monitoring of seals take place in real time. This dissertation has addressed the offline

phase of the seal prognostics and has been foundational in developing an online

degradation assessment which would be of great interest to end users for making

maintenance decisions.

5.3 Possible Future work

The limitations of this dissertation open avenues for possible future work. First, this

research acquired data in a controlled environment where the operating conditions are

all fixed. In future, performance-related data could be acquired at variable operating

condition to compare the performance of the proposed approach. Second, seals make a

louder noise when they approach failure and an addition of an acoustic sensor to the test

set-up would be beneficial in comparing the diagnostic capability of the sensor with

torque/force and leakage signals. Third, performance of the developed data-driven

model could be compared with the physics-based methods found in the literature to

validate the efficiency of proposed data-driven approach in predicting the degradation

of dynamic seals. Finally, research could be extended to develop the architecture behind

online degradation assessment platform.

References

[1] Lou, W., Zhang, W., Liu, X., Dai, W., and Xu, D., 2017, "Degradation of hydrogenated nitrile rubber (HNBR) O-rings exposed to simulated servo system conditions," Polymer Degradation and Stability, 144, pp. 464-472.

[2] Liu, X., Zhang, W., Lou, W., Huang, Y., and Dai, W., 2017, "Investigation on thermal oxidative aging of nitrile rubber (NBR) O-rings under compression stress," Proc. IOP Conference Series: Materials Science and Engineering, IOP Publishing, p. 012003.

[3] Pazur, R., Cormier, J., and Korhan-Taymaz, K., 2014, "Service life determination of nitrile O-rings in hydraulic fluid," Rubber Chemistry and Technology, 87(2), pp. 239-249.

[4] Mosallam, A., Medjaher, K., and Zerhouni, N., 2016, "Data-driven prognostic method based on Bayesian approaches for direct remaining useful life prediction," Journal of Intelligent Manufacturing, 27(5), pp. 1037-1048.

[5] Guo, F., Jia, X., Lv, M., Wang, L., Salant, R. F., and Wang, Y., 2014, "The effect of aging in oil on the performance of a radial lip seal," Tribology International, 78, pp. 187-194.

[6] Guo, F., Jia, X., Huang, L., Salant, R. F., and Wang, Y., 2013, "The effect of aging during storage on the performance of a radial lip seal," Polymer degradation and stability, 98(11), pp. 2193-2200.

[7] Sharma, A., Amarnath, M., and Kankar, P., 2016, "Feature extraction and fault severity classification in ball bearings," Journal of Vibration and Control, 22(1), pp. 176-192.

[8] Dong, S., and Luo, T., 2013, "Bearing degradation process prediction based on the PCA and optimized LS-SVM model," Measurement, 46(9), pp. 3143-3152.

[9] Yu, JB., 2011, "Bearing performance degradation assessment using locality preserving projections," Expert Systems with Applications, 38(6), pp. 7440-7450.

[10] Guo, F., Jia, X., Longke, W., Salant, R. F., and Wang, Y., 2014, "The effect of wear on the performance of a rotary lip seal," Journal of tribology, 136(4), p. 041703.

[11] Jagger, E., 1957, "Study of the lubrication of synthetic rubber rotary shaft seals," Proceedings, Conference on Lubrication and Wear, pp. 409-415.

[12] Horve, L., 1992, "Understanding the sealing mechanism of the radial lip seal for rotating shafts," Fluid Sealing, Springer, pp. 5-19.

[13] Muller, H., 1987, "Concepts of sealing mechanism of rubber lip type rotary shaft seals," Proceedings, 11th International Conference Fluid Sealing, pp. 451-466.

[14] Horve, L., 1991, "The correlation of rotary shaft radial lip seal service reliability and pumping ability to wear track roughness and microasperity formation," SAE transactions, pp. 620-627.

[15] Horve, L., 1987, "A macroscopic view of the sealing phenomenon for radial lip oil seals," Proceedings, 11th International Conference on Fluid Sealing, pp. 710-731.

[16] Kawahara, Y., Abe, M., Hirabayashi, H., and Matsushima, A., 1978, "Effect of surface condition of lip on sealing phenomena of oil seals," No. 0148-7191, SAE Technical Paper.

[17] Nakamura, K., 1987, "Sealing mechanism of rotary shaft lip-type seals," Tribology International, 20(2), pp. 90-101.

[18] Nakamura, K., 1984 "An Investigation of Sealing Properties of Lip Seal through Observation of Sealing Surfaces under Dynamic Condition," Proceedings, 11th International Conference Fluid Sealing, pp. 87-105.

[19] Kawahara, Y., Abe, M., and Hirabayashi, H., 1980, "An analysis of sealing characteristics of oil seals," Asle Transactions, 23(1), pp. 93-102.

[20] Kuzma, D. C., 1969, "Theory of the mechanism of sealing with application to face seals," Journal of Lubrication Technology, 91(4), pp. 704-712.

[21] Kammüller, M., 1986, Zur Abdichtwirkung von Radial-Wellendichtringen," Dr. Ing. thesis, University of Stuttgart, Stuttgart.

[22] Gabelli, A., 1989, "Micro-elastohydrodynamic lubricant film formation in rotary lip seal contacts," Tribology Series, Elsevier, pp. 57-68.

[23] Gabelli, A., and Poll, G., 1992, "Formation of lubricant film in rotary sealing contacts: part I—lubricant film modeling," Journal of tribology, 114(2), pp. 280-287.

[24] Salant, R., 1992, "Numerical analysis of the flow field within lip seals containing microundulations," Journal of tribology, 114(3), pp. 485-491.

[25] Salant, R. F., and Flaherty, A. L., 1994, "Elastohydrodynamic analysis of reverse pumping in rotary lip seals with microundulations," Journal of tribology, 116(1), pp. 56-62.

[26] Salant, R. F., and Flaherty, A. L., 1995, "Elastohydrodynamic analysis of reverse pumping in rotary lip seals with microasperities," Journal of tribology, 117(1), pp. 53-59.

[27] Shi, F., and Salant, R. F., 2000, "A mixed soft elastohydrodynamic lubrication model with interasperity cavitation and surface shear deformation," Journal of tribology, 122(1), pp. 308-316.

[28] Shi, F., and Salant, R. F., 2001, "Numerical Study of a Rotary Lip Seal With a Quasi-Random Sealing Surface," Journal of Tribology, 123(3), p. 517.

[29] Whitaker, J., and EPM Inc, 2004, "The Seal Man's O-Ring Handbook," EPM, Inc-The Seal Man.

[30] Jennewein, B., and Frölich, D., 2012, "Simulation of the radial force of radial shaft seal rings at different temperatures and aging conditions," Proceedings of the 17th international sealing conference, Stuttgart, Germany, pp. 526-545.

[31] Salant, R. F., 2012, "Problems and Prospects for the Simulation of Dynamic Elastomeric Seal Wear and Life," Proceedings of the 17th International Sealing Conference, I, pp. 39-52.

[32] Caesarendra, W., and Tjahjowidodo, T., 2017, "A review of feature extraction methods in vibration-based condition monitoring and its application for degradation trend estimation of low-speed slew bearing," Machines, 5(4), p. 21.

[33] Seera, M., Wong, M. D., and Nandi, A. K., 2017, "Classification of ball bearing faults using a hybrid intelligent model," Applied Soft Computing, 57, pp. 427-435.

[34] Brzezinski, A., Wang, Y., Choi, D., Qiao, X., and Ni, J., 2008, "Feature-based tool condition monitoring in a gear shaving application," Proc. ASME 2008 International Manufacturing Science and Engineering Conference collocated with the 3rd JSME/ASME International Conference on Materials and Processing, American Society of Mechanical Engineers, pp. 65-74.

[35] Kowalski, C. T., and Orlowska-Kowalska, T., 2003, "Neural networks application for induction motor faults diagnosis," Mathematics and computers in simulation, 63(3-5), pp. 435-448.

[36] Lilo, M. A., Latiff, L., Abu, A. B. H., Al Mashhadany, Y. I., and Ilijan, A. K., 2015, "Gas Turbine bearing and vibration classification of using multi-layer Neural Network," Proceedings of Smart Sensors and Application (ICSSA), 2015 International Conference on, IEEE, pp. 20-23.

[37] Jin, C., Zhao, W., Liu, Z., Lee, J., and He, X., 2014, "A vibration-based approach for diesel engine fault diagnosis," Proceedings of Prognostics and Health Management (PHM), 2014 IEEE Conference on, IEEE, pp. 1-9.

[38] Yang, F., Habibullah, M. S., Zhang, T., Xu, Z., Lim, P., and Nadarajan, S., 2016, "Health index-based prognostics for remaining useful life predictions in electrical machines," IEEE Transactions on Industrial Electronics, 63(4), pp. 2633-2644.

[39] Wang, Y., Brzezinski, A. J., Qiao, X., and Ni, J., 2017, "Heuristic feature selection for shaving tool wear classification," Journal of Manufacturing Science and Engineering, 139(4), p. 041001.

[40] Wu, Q., Yang, X., and Zhou, Q., 2012, "Pattern recognition and its application in fault diagnosis of electromechanical system," Journal of Information & Computational Science, 9(8), pp. 2221-2228.

[41] Ramachandran, M., and Siddique, Z., 2018, "Statistical Time Domain Feature Based Approach to Assess the Performance Degradation of Rotary Seals," Proc. Proceedings of the ASME 2018 International Mechanical Engineering Conference & Exposition IMECE 2018, American Society of Mechanical Engineers.

[42] Kuhn, M., 2012, "Variable selection using the caret package," URL https://www.idg.pl/mirrors/CRAN/web/packages/caret/vignettes/caretSelection.pdf. Access date: 17, December 2018.

[43] Center, N. S. W., 1992, Handbook of reliability prediction procedures for mechanical equipment, Carderock Division, Naval Surface Warfare Center.

[44] Field, G., and Nau, B., 1975, "A theoretical study of the elastohydrodynamic lubrication of reciprocating rubber seals," ASLE TRANSACTIONS, 18(1), pp. 48-54.

[45] Kawahara, Y., Ohtake, Y., and Hirabayashi, H., 1981, "Oil film formation of oil seals for reciprocating motion," Proceedings of the ninth BHRA international conference on fluid sealing.

[46] Kanters, A., and Visscher, M., 1989, "Lubrication of reciprocating seals: experiments on the influence of surface roughness on friction and leakage," Tribology Series, Elsevier, pp. 69-77.

[47] Nikas, G., 2003, "Analytical study of the extrusion of rectangular elastomeric seals for linear hydraulic actuators," Proceedings of the Institution of Mechanical Engineers, Part J: Journal of Engineering Tribology, 217(5), pp. 365-373.

[48] Nikas, G. K., and Sayles, R. S., 2006, "Study of leakage and friction of flexible seals for steady motion via a numerical approximation method," Tribology International, 39(9), pp. 921-936.

[49] Nikas, G. K., 2002, "Elastohydrodynamics and mechanics of rectangular elastomeric seals for reciprocating piston rods," J. Trib., 125(1), pp. 60-69.

[50] Salant, R. F., Maser, N., and Yang, B., 2007, "Numerical model of a reciprocating hydraulic rod seal," Journal of Tribology, 129(1), pp. 91-97.

[51] Yang, B., and Salant, R. F., 2008, "A numerical model of a reciprocating rod seal with a secondary lip," Tribology Transactions, 51(2), pp. 119-127.

[52] Sun, C., Zhang, Z., and He, Z., 2011, "Research on bearing life prediction based on support vector machine and its application," Proceedings, Journal of Physics: Conference Series, IOP Publishing, p. 012028.

[53] Caesarendra, W., Widodo, A., and Yang, B.-S., 2011, "Combination of probability approach and support vector machine towards machine health prognostics," Probabilistic Engineering Mechanics, 26(2), pp. 165-173.

[54] Park, J. I., and Jeong, M. K., 2013, "Recursive support vector censored regression for nonparametric lifetime prediction using degradation paths and failure times in accelerated life tests," Citeseer.

[55] Guo, Y., Ma, J., Xiao, F., and Tian, T., 2012, "SVM with optimized parameters and its application to electronic system fault diagnosis," Proceedings of 2012 IEEE Conference on Prognostics and Health Management, IEEE, pp. 1-6.

[56] Xu, D., Wu, X.-X., Guo, L., and Hu, J.-B., 2010, "Method of residual life prediction for barrel of tank gun based on LS-SVM," Zhuangjiabing Gongcheng

Xueyuan Xuebao(Journal of Academy of Armored Force Engineering), 24(1), pp. 42-44.

[57] Huang, H.-Z., Wang, H.-K., Li, Y.-F., Zhang, L., and Liu, Z., 2015, "Support vector machine based estimation of remaining useful life: current research status and future trends," Journal of Mechanical Science and Technology, 29(1), pp. 151-163.

[58] Takens, F., 1981, "Detecting strange attractors in turbulence," Dynamical systems and turbulence, Warwick 1980, Springer, pp. 366-381.

[59] Fraser, A. M., and Swinney, H. L., 1986, "Independent coordinates for strange attractors from mutual information," Physical review A, 33(2), p. 1134.

[60] Cao, L., 1997, "Practical method for determining the minimum embedding dimension of a scalar time series," Physica D: Nonlinear Phenomena, 110(1-2), pp. 43-50.

[61] Eberhart, R., and Kennedy, J., 1995, "Particle swarm optimization," Proceedings of the IEEE international conference on neural networks, Citeseer, pp. 1942-1948.

[62] Si, X.-S., Wang, W., Hu, C.-H., and Zhou, D.-H., 2011, "Remaining useful life estimation–a review on the statistical data driven approaches," European journal of operational research, 213(1), pp. 1-14.

[63] Lei, Y., Li, N., and Lin, J., 2016, "A new method based on stochastic process models for machine remaining useful life prediction," IEEE Transactions on Instrumentation and Measurement, 65(12), pp. 2671-2684.

[64] Malhi, A., Yan, R., and Gao, R. X., 2011, "Prognosis of defect propagation based on recurrent neural networks," IEEE Transactions on Instrumentation and Measurement, 60(3), pp. 703-711.

[65] Loutas, T. H., Roulias, D., and Georgoulas, G., 2013, "Remaining useful life estimation in rolling bearings utilizing data-driven probabilistic e-support vectors regression," IEEE Transactions on Reliability, 62(4), pp. 821-832.

[66] Singleton, R. K., Strangas, E. G., and Aviyente, S., 2014, "Extended Kalman filtering for remaining-useful-life estimation of bearings," IEEE Transactions on Industrial Electronics, 62(3), pp. 1781-1790.

[67] Mao, W., He, J., Tang, J., and Li, Y., 2018, "Predicting remaining useful life of rolling bearings based on deep feature representation and long short-term memory neural network," Advances in Mechanical Engineering, 10(12), p. 1687814018817184.

[68] Javed, K., Gouriveau, R., Zerhouni, N., and Nectoux, P., 2014, "Enabling health monitoring approach based on vibration data for accurate prognostics," IEEE Transactions on Industrial Electronics, 62(1), pp. 647-656.

[69] Zhang, B., Zhang, L., and Xu, J., 2016, "Degradation feature selection for remaining useful life prediction of rolling element bearings," Quality and Reliability Engineering International, 32(2), pp. 547-554.

[70] Paris, P., and Erdogan, F., 1963, "A critical analysis of crack propagation laws," ASME J. Basic Eng., 85, pp. 528-533.

[71] Lei, Y., Li, N., Gontarz, S., Lin, J., Radkowski, S., and Dybala, J., 2016, "A model-based method for remaining useful life prediction of machinery," IEEE Transactions on Reliability, 65(3), pp. 1314-1326.

[72] Sun, J., Zuo, H., Wang, W., and Pecht, M. G., 2014, "Prognostics uncertainty reduction by fusing on-line monitoring data based on a state-space-based degradation model," Mechanical Systems and Signal Processing, 45(2), pp. 396-407.

[73] Ostachowicz, W., and Krawczuk, M., 1992, "Coupled torsional and bending vibrations of a rotor with an open crack," Archive of applied mechanics, 62(3), pp. 191-201.

[74] Baraldi, P., Mangili, F., and Zio, E., 2012, "A Kalman filter-based ensemble approach with application to turbine creep prognostics," IEEE Transactions on Reliability, 61(4), pp. 966-977.

[75] Chan, K. S., Enright, M. P., Moody, J. P., Hocking, B., and Fitch, S. H., 2012, "Life prediction for turbopropulsion systems under dwell fatigue conditions," Journal of Engineering for Gas Turbines and Power, 134(12), p. 122501.

[76] Jia, F., Lei, Y., Lin, J., Zhou, X., and Lu, N., 2016, "Deep neural networks: A promising tool for fault characteristic mining and intelligent diagnosis of rotating machinery with massive data," Mechanical Systems and Signal Processing, 72, pp. 303-315.

[77] Ren, L., Cui, J., Sun, Y., and Cheng, X., 2017, "Multi-bearing remaining useful life collaborative prediction: A deep learning approach," Journal of Manufacturing Systems, 43, pp. 248-256.

[78] Shao, H., Jiang, H., Zhang, H., and Liang, T., 2017, "Electric locomotive bearing fault diagnosis using a novel convolutional deep belief network," IEEE Transactions on Industrial Electronics, 65(3), pp. 2727-2736.

[79] Ren, L., Zhao, L., Hong, S., Zhao, S., Wang, H., and Zhang, L., 2018, "Remaining useful life prediction for lithium-ion battery: A deep learning approach," IEEE Access, 6, pp. 50587-50598.

[80] Kelley, L. A., Gardner, S. P., and Sutcliffe, M. J., 1996, "An automated approach for clustering an ensemble of NMR-derived protein structures into conformationally related subfamilies," Protein Engineering, Design and Selection, 9(11), pp. 1063-1065.